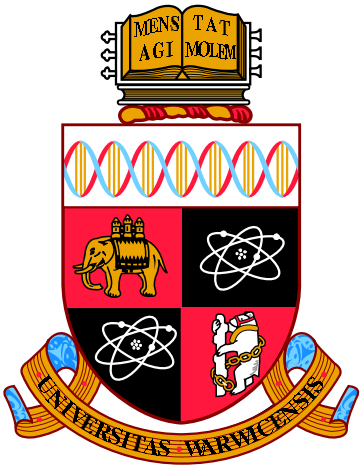

Single Molecule Mechanics of Kif15

by

Toni McHugh

Thesis

Submitted to the University of Warwick

for the degree of

Doctor of Philosophy

Systems Biology

October 2015

Contents

List of Tables

List of Figures

Acknowledgments

I would like to thank my supervisors Nick Carter and Matthew Turner for all their help, guidance and advice throughout my PhD. I would also like to thank Rob Cross for being a great source of ideas and for all the very helpful discussions over the past three years. I am very grateful to all three of them for being so understanding over the last couple of years, their support has helped immensely.

I would like to thank our collaborators Andrew McAinsh and Hauke Dreschler, not only for supplying many of the proteins used in my work but also for their feedback and comments and for useful discussions that have helped considerably in the interpretation of my data and the direction of my research. I also need to thank the members of my advisory panel, Andrew McAinsh, Stefan Grosskinsky and Masanori Mishima who helped to keep my project on track. I thank the EPSRC for providing my funding and the Systems Biology DTC and everyone at MCB, especially the hockey team and the members of the Cross Lab, for all their support.

I would like to thank Dr Arasaradnam and his team for all their efforts in diagnosing and treating me in order to get me back to health in time to finish my PhD, without their help this I would have struggled to finish this thesis.

Finally I would like to thank my family and friends for all of their support and encouragement. Special mention must go to my parents, for all the support that they have given me over the years, I haven't told them often enough how much I appreciate it. I must also mention Richard Westbrook, who has been a wonderful friend for my entire time at Warwick and who was the first person to attempt to read this thesis and who gave me many useful corrections. Most importantly I need to thank Dan Peet, he has been endlessly patient and caring and has made the past three years so enjoyable.

Declarations

This thesis is submitted to the University of Warwick in support of my application for the degree of Doctor of Philosophy. It has been composed by myself and has not been submitted in any previous application for any degree.

The work presented (including data generated and data analysis) was carried out by the author except where stated otherwise in the text.

Parts of this thesis have been published by the author: Parts of Chapter 3, Sections 1 to 5, and Chapter 4, Section 3, are presented in "Drechsler, H., McHugh, T., Singleton, M. R., Carter, N. J., McAinsh, A. D. (2014). The Kinesin-12 Kif15 is a processive track-switching tetramer. Elife, 3, e01724."

List of publications including submitted papers.

- Drechsler, H., McHugh, T., Singleton, M. R., Carter, N. J., McAinsh, A. D. (2014). The Kinesin-12 Kif15 is a processive track-switching tetramer. Elife, 3, e01724.

Abstract

Kinesin-12 is a motor protein that has a role in the processes of mitotic spindle formation and maintenance. The human Kinesin-12, Kif15, has been shown to have some functional redundancy with Eg5, a Kinesin-5 that plays key roles in the formation of the bipolar spindle and is a potential target for anti-cancer drugs. Eg5 is thought to contribute to spindle formation by cross-linking and sliding microtubules, however little is known about the mechanism of Kif15.

We have used laser tweezers to investigate the mechanical properties of Kif15 compared to those of kinesin-1. We have found that Kif15 is plus end directed and takes multiple steps along the microtubule without detaching. Full-length Kif15 walks faster and supports more load than full-length Eg5. Kif15 is less processive under load than kinesin-1, although it has a similar stall force. A second, diffusive, microtubule binding site in Kif15 supports processivity at zero load, and slows flyback following a detachment in the optical trap.

The microtubule-associated protein, Tpx2, is necessary for the localisation of Kif15 to spindle microtubules. We find that Tpx2 binding arrests the motion of Kif15 and creates a stable binding state that resists both assisting and hindering loads. We also find evidence of a tail-mediated auto-inhibitory mechanism that creates a stable MT binding state and causes pausing during processive runs. C-terminal truncation of the Kif15 tail relieves this inhibition leading to faster overall stepping and abrogates the effects of Tpx2.

We examined the detachment behaviour of Kif15 from microtubules, under assisting and hindering loads. We find that assisting loads cause single Kif15 and Kinesin-1 motors to detach from the microtubule more easily than hindering loads. Kif15 shows a much more asymmetric response to load in low levels of ATP than Kinesin-1, and both show more asymmetry than Eg5: previous work has shown that the behaviour of Eg5 does not change dramatically with differing loading directions. This has interesting implications for the roles of Kif15 and Eg5 motors in both parallel and anti-parallel microtubule bundles. Overall our data supports an *in vivo* mechanism for Kif15 that it distinct from that of Eg5.

We investigated the load-dependent detachment of Kinesin-1 and Kif15 in millimolar concentrations of ADP, AMPPNP and micromolar concentrations of ATP. Kinesin-1 in ADP detached at low loads, and in AMPPNP at two different loads, both higher than in ADP. These two AMPPNP states of Kinesin1 likely corresponding to single and double headed microtubule binding, as proposed by Ishiwata and colleagues. Kif15 behaved broadly similarly. At micromolar ATP concentrations and hindering loads, both Kinesin-1 and Kif15 again showed two different high load detachment states. This is inconsistent with the model proposed by Ishiwata and possible modifications are discussed.

Abbreviations

ADP	Adenosine Diphosphate
AOD	Acoustic Optical Deflector
ATP	Adenosine Triphosphate
ATPase	Enzyme that catalyses the hydrolysis of ATP to ADP and phosphate
AMP-PNP	Adenosine Triphosphate
DIC	Differential Interference Contrast Microscopy
EM	Electron Microscopy
GDP	Guanosine Diphosphate
GMM	Gaussian Mixture Model
GTP	Guanosine Triphosphate
K-Fibre	Kinetochore Fibre
Kif	Kinesin Family Protein
L5	Loop 5
LED	Light Emitting Diode
MAP	Microtubule Associated Protein
MT	Microtubule
MTOC	Microtubule Organising Centre
NEB	Nuclear Envelope Breakdown
P_i	Inorganic Phosphate
SAC	Spindle Assembly Checkpoint
SW1/2	Switch 1/2
TIRF	Total Internal Reflection Microscopy
UP Water	Ultra Pure Water

Chapter 1

Introduction

1.1 Microtubules, Motors and the Cytoskeleton

The cell cytoskeleton is a dynamic network composed of a variety of protein fibres which provide structure and organisation to the cell. One set of these cytoskeletal components is the microtubules, dynamic protein polymers that contribute to cellular shape, intracellular transport and cell division. Microtubules (MTs) are long tubular polymers composed of α and β tubulin subunits. These subunits form dimers of one α and one β tubulin, which bind end-to-end to form protofilaments. In a MT approximately 13 protofilaments bind laterally forming a polarised tube with β tubulin exposed at one end and α tubulin at the other, these are called the plus and minus ends respectively.

An important property of MTs is their ability to rapidly grow and shrink via a process called dynamic instability [1]. This allows the MT cytoskeleton to be rapidly disassembled and remodelled when necessary, for example upon entry to cell division. Tubulin dimers can be in two possible states, GTP bound or GDP bound. MTs grow when tubulin subunits bind to the MT ends in the GTP bound state. After incorporation into the MT the GTP can be hydrolysed to GDP. When the rate of hydrolysis is faster than GTP tubulin incorporation at the tip the MT loses its 'cap' of GTP tubulin, becomes unstable, and rapidly falls apart. This process of sudden switching from a period of growth to one of rapid shrinkage is called

catastrophe, Figure 1.1.

An equally important role of MTs is to act as a substrate for many of the molecular motors within the cell. These MT based motors; kinesins and dyneins, bind to the MT lattice and use the energy from hydrolysis of ATP to ADP and P_i to create directional forces [2]. Some of these motors have two MT binding domains and coordinate the cycling of ATP hydrolysis in each domain to make hand-over hand steps along MTs from one tubulin dimer to the next. In this way some motors are capable of moving distances of up to 1.5 microns along a MT without detaching [3, 4].

Cytoskeletal molecular motors acting on MTs as well as others acting on actin filaments fulfil many roles in cellular organisation. Some such as Kinesin-1, act as transporters actively moving cellular components around the cell [5]. Others such as the Kinesin-8, MCAK, act as regulators of MT dynamics [6] or, like Kinesin-5, create forces that aid in the organisation of the MT skeleton [7].

1.2 The Mitotic Spindle

During division, eukaryotic cells accurately segregate their duplicated chromosomes in to two separate daughter cells, this process is termed mitosis. The forces required for the mechanical separation of the chromosomes are largely mediated by MTs. During mitosis the MTs form a bipolar structure called the mitotic spindle. In this structure MTs emanating from two poles fan outwards towards the chromosomes that are grouped along the centre plane between the poles, forming the metaphase plate, Figure 1.2A [8]. The correct formation of the spindle structure is important as defects in the spindle can lead to incorrectly segregated chromosomes, which in turn lead to genetic defects or cell death.

The mechanisms of spindle formation are an active area of research in the hunt for new chemotherapy targets. Disruption of the spindle can potentially have a greater impact on rapidly dividing cancer cells over healthy cells. The spindle MTs are already successful chemotherapy targets with drugs such as paclitaxel and vinblastine acting to either over-stabilise or destabilise the spindle MTs respectively [9]. Drugs targeting other parts of the spindle machinery such as microtubule associated proteins (MAPs) and molecular motors

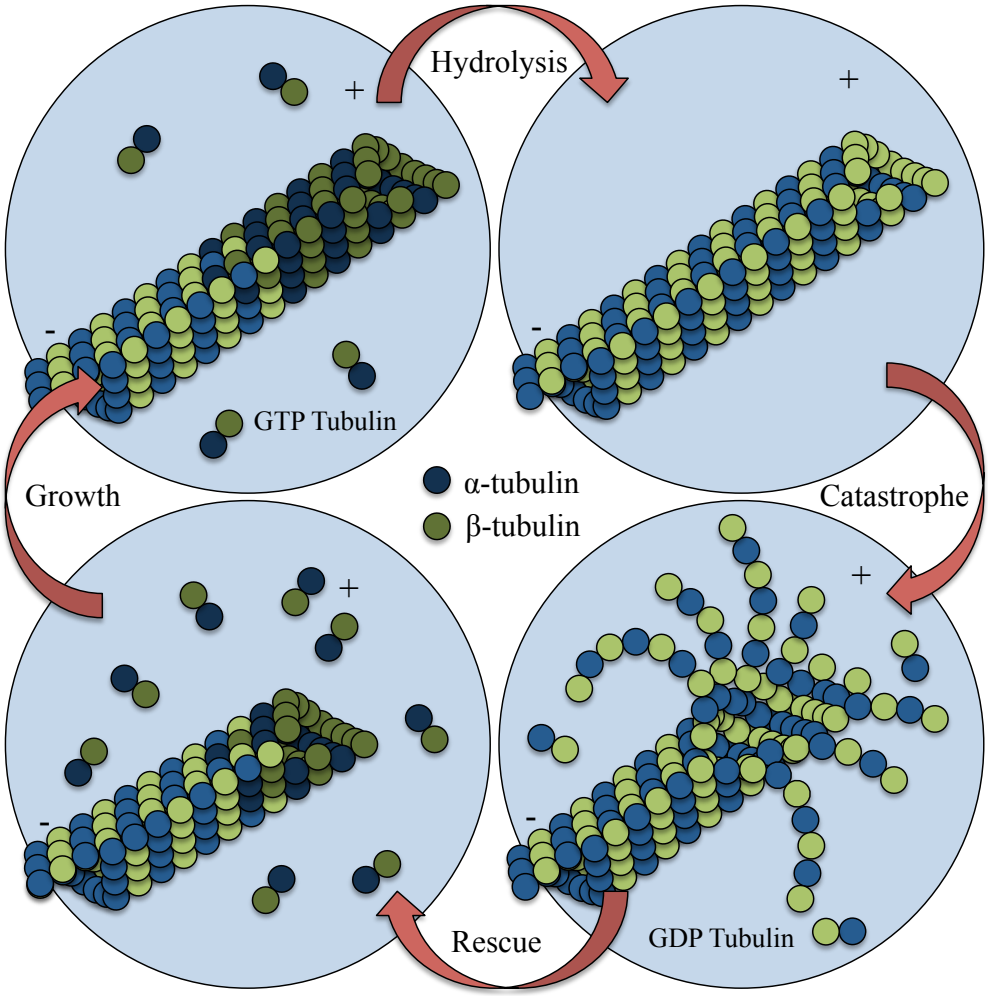

Figure 1.1: MT polymers are composed of tubulin dimers which can be in either the GTP bound or GDP bound state. MTs are dynamic structures, they grow by the addition of GTP tubulin at the tip. Once GTP tubulin is incorporated into the MT the GTP is hydrolysed to GDP. GDP tubulin forms a less stable polymer and once the GTP cap of the MT has gone the MT undergoes catastrophe and begins a period of rapid shrinkage. MTs can be rescued from this shrinkage by addition of GTP tubulin restoring the GTP cap and allowing the MT to resume growth.

are just starting to be developed. It is hoped that these drugs will be more mitosis specific than the MT based drugs, as unlike MTs many of the other key spindle proteins are inactive during interphase [10].

1.2.1 Components of the Mitotic Spindle

In the bipolar spindle there are several important structural elements, shown in Figure 1.2A. The spindle MTs can be divided into three categories [11]. Firstly K-fibre MTs exist in bundles connecting the chromosomes to the spindle poles. Interpolar MTs are found in the zone between the poles and overlap in the middle of the spindle, Finally astral MTs are directed outwards from the poles to the cell membrane. Each of these MT populations plays a distinct and important role in spindle stability, sizing and positioning.

Other components of the spindle include the chromosomes, each consisting of two identical sister chromatids. Each pair of chromatids is joined by a centromere, from which the the K-Fibre MTs attach to the chromosomes via kinetochores. Kinetochores are complex multi-protein structures, responsible for MT binding. They also play a significant role in cell signalling throughout mitosis. At the spindle poles the MTs focus at the MTOC (Microtubule Organising Centre). In eukaryotic cells this is the centrosome. In mitotic animal cells there are two centrosomes each of which contains a mother and daughter centriole along with a mass of protein termed the pericentriolar material which contains proteins required for MT nucleation and anchoring [8].

1.2.2 Spindle Formation

The process of spindle formation can be split into several stages, prophase, prometaphase and metaphase, Figure 1.2B. Firstly during prophase and before nuclear envelope breakdown (NEB), the cell separates its MTOCs to opposite sides of the cell [8]. After NEB, in prometaphase, the spindle MTs capture and begin to align the chromosomes whilst maintaining a correct separation of the poles and position of the spindle within the cell. During metaphase a balance is maintained between the inward and outward forces within the spindle to ensure correct attachment of the chromosomes to the K-fibre MTs via their kinetochores [11]. At this stage the spindle assembly checkpoint (SAC) must be satisfied to proceed with division. In order to turn off the SAC signalling each chromosome must be stably attached to two K-fibres from opposite poles. Once SAC signalling is turned off the cell proceeds to anaphase.

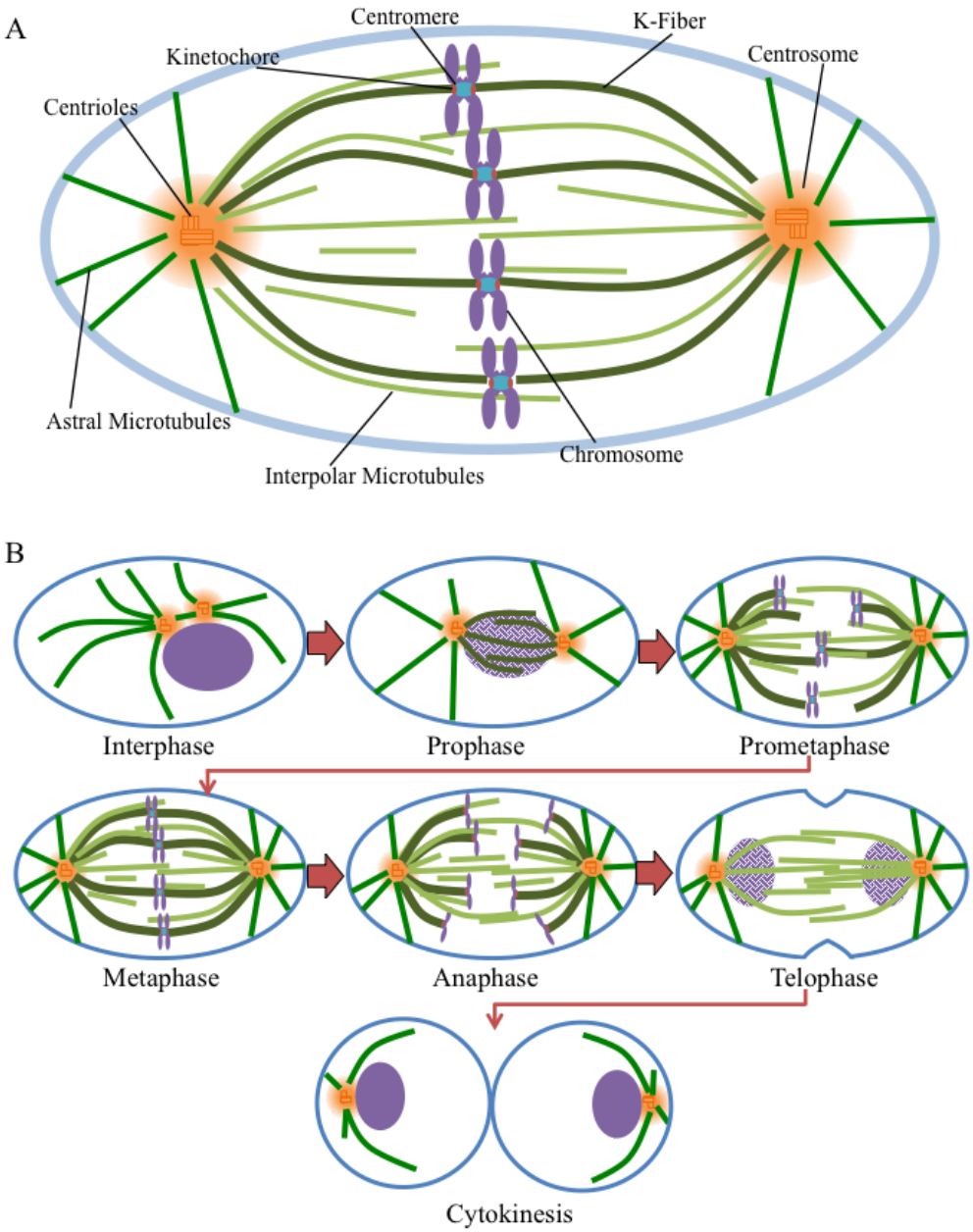

Figure 1.2: A) The components of a metaphase bipolar spindle, key structures are labeled. B) Stages of cell division, MTs are shown in green, centrosomes are shown in orange and DNA is shown in purple. The cell membrane is shown in blue.

The final stages in cell division are anaphase, telophase and cytokinesis. In anaphase the separated chromosomes move away from the metaphase plate towards the poles and the spindle is elongated. In telophase the chromosomes reach the spindle poles and the nuclear membrane starts to reform. The final stage, cytokinesis, is the process by which the cytoplasm of the cell is split to form two daughter cells. The forces involved in spindle formation and maintenance and chromosome segregation originate from the collective effects of MT dynamics and a large number of MAPs and motor proteins.

1.2.3 Microtubule Dynamics in the Spindle

MTs within the spindle are not static, they continue to undergo periods of growth and shrinkage. Each MT population is regulated differently leading to varying dynamics. Interpolar MTs are continuously being depolymerised from the poles and new MTs are nucleated throughout the spindle through a variety of mechanisms [12]. Astral MTs play a significant role in pole separation during prophase and create forces that are important for the correct positioning of the spindle in the centre of the cell [13]. The dynamics of astral MTs are similar to those of interpolar MTs.

K-fibre MTs are less dynamic than interpolar and astral MTs, they are parallel bundles of MTs which interact with the kinetochores at their plus ends. The minus ends of K-fibres undergo depolymerisation and interact with the spindle poles [14]. New MTs are incorporated in to the K-fibres through several different mechanisms, including capture of interpolar MTs and direct nucleation at the kinetochores [11].

Constant depolymerisation of MTs at the spindle poles leads to polar flux. As a result of polymerisation in the midzone and shrinkage at the poles there is a flux of MTs towards the poles. Motor proteins such as dynein (minus end directed) and Eg5 (plus end directed) also play a role in creating an overall poleward flux, with dynein transporting MTs poleward and Eg5 operating in the MT overlap to push MTs apart. MT dynamics are very important for the stability and formation of the spindle, dampening MT dynamics in cells by the application of MT stabilising compounds such as taxol causes major spindle defects and cell death [9].

1.2.4 MAPs and Motors in the Spindle

The detailed regulation of MTs within the spindle is dependent on a large number of MT associated proteins (MAPs) which bind MTs, affecting growth and catastrophe rates and forming MT bundles, whilst adjusting spindle morphology. These interactions form a complex network that is both spatially and temporally regulated. For example, the MAP Tpx2 plays a significant role in MT nucleation around the chromosomes [15]. The nucleation of MTs by Tpx2 is decreased by the binding of importin-α, which is dependent upon the RanGTP gradient. RanGTP is enriched at the chromosomes and decreases towards the spindle poles. RanGTP binds to importin-α sequestering it around the metaphase plate, allowing spatially regulated MT nucleation by Tpx2 to occur. Tpx2 is also responsible for cross linking MTs and regulates the activity of the Aurora A kinase [16] and the motor proteins Kinesin-5 [17] and Kinesin-12 [18]. The effect of Tpx2 on Kinesins 5 and 12 can only be felt after NEB, prior to this both are localised to the cytoplasm whereas Tpx2 has a nuclear localisation [19].

Motor proteins in the spindle can affect MT dynamics and bundling but they also provide active ATP driven forces of their own. They do this by walking in a stepwise manner along MTs to perform a variety of functions. Many motor proteins are active in the spindle, in human cells these include the Kinesins-7 (also known as CENP-E), -8 (Kif18a), -5 (Kif11 or Eg5), -13 (Kif2c or MCAK) and -12 (Kif15 or Hklp2) as well as dynein. Dynein is minus end directed and has a diverse range of functions depending on its localisation. At the cell cortex dynein is involved in creating the pulling forces used for correct spindle positioning [20], at the spindle poles it focuses the spindle MTs [21]. Dynein is also involved in the transport of MTs, MAPs and motor proteins to the spindle poles [22].

The kinesin motor proteins are involved in a variety of different processes and as such each is adapted to fulfil its specific role. Kinesin-7 is responsible for the congression of misaligned chromosomes, it is bound to the kinetochore and uses its motor domains to walk towards the plus ends of MTs pulling chromosomes in to alignment [23]. Kinesin-5 has a tetrameric structure, allowing it to bind to and walk along two MTs simultaneously, this property allows it to operate in the MT overlap between poles and aid spindle formation by

walking towards the plus ends of anti-parallel MTs, exerting an outward pushing force [24]. Kinesin-13 is a MT depolymerase that uses its motor activity to actively depolymerise MTs [6]. Kinesin-13 operates at the kinetochores and is necessary for the maintenance of good K-fibre attachements [25].

Many of the MAPs and motors involved in spindle formation and maintenance are potential anticancer targets. The MAP Tpx2 mentioned above has been found to be over-expressed in cancers and is a suggested marker for diagnosis and prognosis as well as being a potential drug target itself [26]. Drugs targeting the motor proteins Eg5 and CENP-E are already in development and the Kinesins-12 and 13 (Kif15 and MCAK) are being considered as potential candidates [10]. Drugs targeting the spindle formation role played by Eg5 have progressed to stage 2 clinical trails but have been only moderately successful. A possible reason for this is the partial overlap in function of Eg5 with the Kinesin-12, Kif15. This would allow Kif15 to compensate for the reduced Eg5 activity. In order to develop drugs targeting specific kinesin motor proteins an understanding of their structures, ATPase mechanisms and method of action is necessary.

1.3 Kinesin Motor Proteins

The Kinesin superfamily of proteins can be broken down into 14 families, Kinesins 1-14. Families 1-12 have a globular N-terminal ATPase (motor) domain followed by a tail domain, often consisting of coiled coil regions required for oligomerisation or regulatory regions. The Kinesin-14 family of motor proteins have a C-terminal motor domain whilst the Kinesin-13s have a more central motor domain with both N- and C-terminal tails. The mechanical properties of individual kinesin motors are influenced by small changes in their motor domains but also by the structure of their tail regions.

The best studied of the kinesins is conventional Kinesin-1 or Kinesin Heavy Chain (KHC) this motor forms a dimeric molecule with the two motor domains at one end. Kinesin-1 uses the hydrolysis of ATP by its MT bound motor regions to make co-ordinated directional steps along MTs towards the plus ends. Other motor proteins such as the Kinesin-7, CENP-E, and the Kinesin-5, Eg5, walk along MTs in a similar way but have different mechanical

properties such as stepping rate, and processivity (a measure of the number of consecutive steps made along a MT without detaching).

1.3.1 Kinesin Domain Organisation

Different kinesins exist in a variety of oligomerisation states, some such as Kif1A are monomeric whilst others such as the Kinesin-7, CENP-E are homodimeric. Some kinesins can also form heterodimeric or heterotrimeric complexes, for example Kif3A/3B/KAP3 [27]. The Kinesin-5 family form homotetrameric molecules. The tail regions of kinesin motors often contain additional MT binding sites or regulatory regions.

Different kinesins have distinct domain organisations, which allows for specialist functions to be fulfilled. The structures of the well characterised Kinesin-1 motor protein and the mitotic kinesins CENP-E (Kinesin-7), Eg5 (Kinesin-5), Kif15 (Kinesin-12) and MCAK (Kinesin-13) are described below;

Kinesin-1

The structure of Kinesin-1 is well studied and the terminology used to describe its different domains is often transferred to help describe other kinesin motors. Kinesin-1 has an N-terminal motor domain followed by a short disordered region termed the neck-linker. The neck-linker attaches the motor domain to a coiled coil region termed the neck, this is followed by a second coiled-coil region, termed the stalk, which is necessary for dimerisation, Figure 1.3. The stalk of Kinesin-1 is disrupted by a disordered region which acts as a hinge, this allows the protein to fold so that the globular C-terminal tail domains of Kinesin-1 can interact with its motor domains. The tail regions binds the motor domains and act to inhibit their MT binding and ATPase ability. The tail region is also able to bind to cargo molecules, relieving the inhibition of the motor [28].

CENP-E

Kinesin-7, CENP-E is another plus end directed dimeric motor protein, it also has N-terminal motor domains, followed by a neck-linker. The stalk of CENP-E is much longer

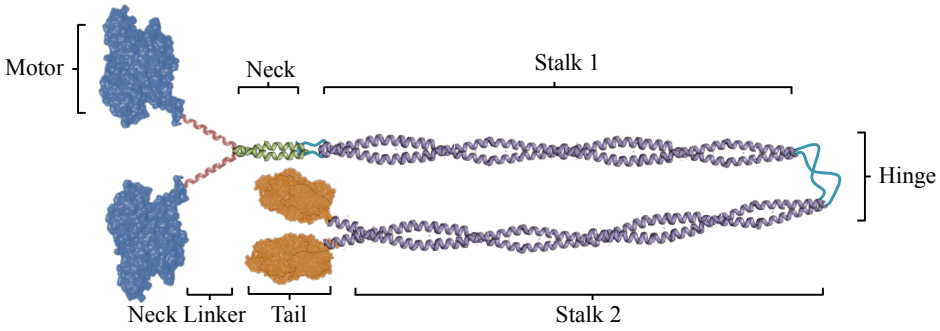

Figure 1.3: Diagram of the domain structure of Kinesin-1.

than other kinesin motor proteins, 230 nm compared to 80 nm for Kinesin-1, and is largely a flexible coiled coil [29]. CENP-E has two other regions of importance, firstly towards its C-terminal there is a kinetochore binding site [30]. Secondly the C-termins consists of a globular MT binding region, this region is also responsible for inhibiting ATPase activity of the motor domains [31].

Eg5

The Kinesin-5, Eg5 forms a short dumbbell shaped tetramer with two motor domains (heads) on either end. Eg5 like Kinesin-1 and CENP-E is a plus end directed motor protein with a second binding site at its C-terminal tail. The tails of Eg5 bind to MTs and act to aid the processivity of the motor [32]. Eg5 tails do not fold back on the motor heads, instead Eg5s anti-parallel arrangement of two dimers allows the tails of one dimer to bind the MT near to the heads of the other pair.

Kif15

The mitotic protein Kif15 has some functional overlap with Eg5 however structurally it differs significantly. It is unclear whether Kif15 forms a dimer or a tetramer as there are conflicting reports [33, 34]. Kif15 has an N-terminal motor domain followed by two coiled coil regions. It is suggested to have a second MT binding domain in its first coiled coil region [33]. The second coiled coil region is known to contain both an auto-inhibitory region [33]

and a binding site for the MAP Tpx2 [18]. Kif15 also contains sites enabling it to interact with Ki67 [35] and actin [36].

MCAK

The MT depolymerase, MCAK, is a Kinesin-13 motor protein, as such its structural organisation is different from Kinesins 1, 5, 7 and 12. The motor domain of MCAK is found roughly in the middle of the protein and has a highly charged N-terminal neck region. The N-terminal itself contains a globular domain required for correct sub-cellular localisation whilst the C-terminal is required for dimerisation. MCAK does not use its ATPase to walk along MTs but instead uses the hydrolysis of ATP to disassemble tubulin from MT tips [37]. MCAK can bind MTs in both the monomeric and dimeric states but is a more potent depolymerase as a dimer [38].

1.3.2 Motor Domain Structure

Despite the differences in their overall sequences and structures the motor domains of the kinesin superfamily are well conserved. The motor domains contain both a MT binding site and the catalytic pocket for ATP hydrolysis. The crystal structures of several kinesin motor domains have been solved showing that they share a conserved catalytic core [39, 40, 41, 42]. This core is also shared with the Myosin family of motor proteins which act upon actin filaments [39]. The core contains a layer of β-sheets sandwiched by 6 α-helices, as can be seen in Figure 1.4A. The MT binding site is on one side of the β-sheet and the active site for ATP-hydrolysis is on the other [39]. Differences between motors are often found in the flexible loop regions and it is these regions that are thought to be responsible for differences in the mechanochemical properties of the motor domains.

The motor domain is wedge shaped with the narrow end pointing towards the MT plus end when MT bound. The α4-helix sits at the interface of the α and β tubulin subunits, perpendicular to the MT axis. The catalytic pocket for ATP hydrolysis is situated on the top face of the motor domain towards the MT minus end (Figure 1.4C). The catalytic pocket (or active site) contains a highly conserved phosphate binding loop (P-loop), also found in

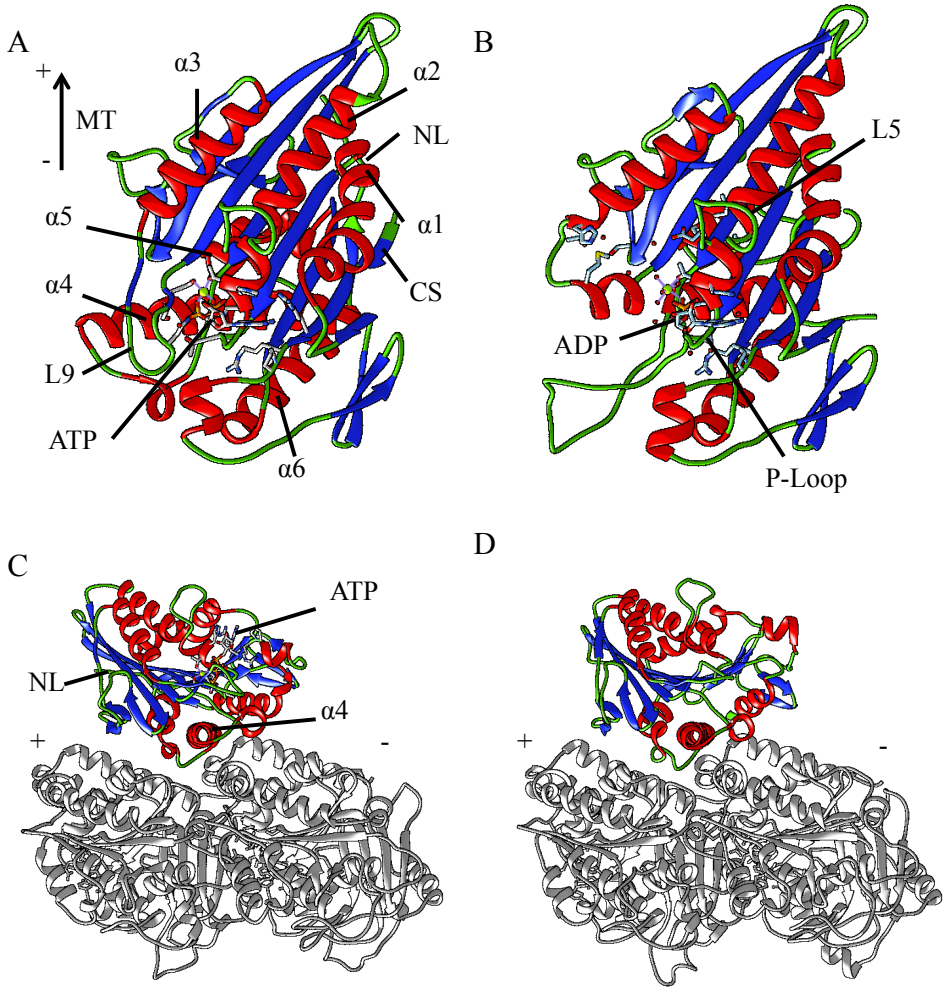

Figure 1.4: A) High-resolution structure of ATP analog-bound Kinesin-1 on microtubules (microtubule not shown), top view, 5 angstrom, Electron Microscopy Structure, PDBID:3j8y B) ADP bound Kinesin-1, 1.8 Angstrom, X-ray Diffraction Structure PDBID:1bg2. C)High-resolution structure of ATP analog-bound Kinesin-1 on microtubules, side view, 5 angstrom, Electron Microscopy Structure, PDBID:3j8y. D)High-resolution structure of no-nucleotide Kinesin-1 on microtubules, side view, 5 angstrom, Electron Microscopy structure, PDBID:3j8x.

myosin motor proteins and small G-proteins [43]. With ATP bound in the catalytic pocket the Switch 1 and Switch 2 (SW1 and SW2) regions adopt a closed conformation. In this conformation Switch 1 (loop-9) and Switch 2, consisting of the α4-helix, loop 12 and α5-helix, are joined by a salt bridge creating a tube that is catalytically active [44]. The closed or ATP-bound conformation shown in Figure 1.4A allows the neck-linker of the motor to

dock along the side of the motor oriented along the MT axis from the minus to the plus end.

The closing of the SW1 and SW2 regions around ATP catalyses the hydrolysis reaction; breaking ATP down to form ADP and P_i. The presence of a Mg^{2+} ion in the catalytic site is essential for this reaction. Upon phosphate release the motor enters the "ADP-like" or open state. Figure 1.4B shows the Kinesin-1 motor domain in its "ADP like" conformation, in this conformation the neck-linker is undocked and disordered and the motor affinity for MTs is reduced.

In solution kinesin motor domains need to have a nucleotide bound in the active site to avoid deformation. When MT bound it is possible for the motor to be in an nucleotide free or empty state, in fact it is a requirement of the motors ATPase cycle. With no nucleotide in its catalytic core the motor domain has a high MT affinity, as in the ATP bound state, however the neck linker is disordered and the catalytic pocket is not closed. Differences in MT affinity in different nucleotide states are due to changes in the conformation of the MT binding surface of the motor domain [45] (Figure 1.4D).

Structural Differences between Kinesin-1 and Kinesin-5 Motor Domains

Kinesin-1 and Kinesin-5 differ in both their cellular function and their mechanical properties. Eg5 is slower and less processive than kinesin-1 and responds differently to load [46]. Along with differences in domain organisation there are crucial differences in the structures of their motor domains. Two major differences can be found, the first is an extended neck linker in Eg5, this can reduce inter-head tension which is important for the co-ordination of the ATPase cycles of the heads during processive movement. The other major structural difference is in the size of loop 5 which interrupts α-helix 2, in Eg5 this loop is extended and can interfere with ATP binding in the catalytic pocket [47].

Loop 5 (L5) is a target site for small molecule Eg5 inhibitors such as monastrol. These drugs target L5 and change its positioning keeping the catalytic pocket in a 'closed' position, reducing the rate of the motors ATPase [48]. The loop structure of L5 in Eg5 is not a conserved structure even amongst other Kinesin-5 motor proteins, this leads to high

specificity in drugs targeting Eg5 via this mechanism.

1.3.3 Force Generation by Kinesins

The conformational changes of the kinesin motor domains are important in attempting to understand their mechanism of force production. As kinesin motors go through the ATP hydrolysis cycle they produce a directional force. The small conformational changes in the SW1 and SW2 regions, which couple to the state of the nucleotide in the active site, lead to larger conformational changes in the motor domain. These conformational changes create strain in the motor-MT connection. This strain is removed through movement of the motor molecule with respect to the MT substrate, this movement is termed a power stroke.

For kinesin the mechanochemical cycle has been found to go as follows;

- ADP-bound kinesin encounters a MT and binds weakly.
- ADP is released leading to tightly bound, nucleotide free kinesin.
- ATP binds creating a conformational change or 'power stroke'.
- Hydrolysis occurs and phosphate is released leaving the motor in an ADP-bound state.
- The weakly MT bound motor detaches from the MT.

Power Stroke

Evidence for the power stroke occurring upon ATP binding can be found by observing the structural changes that occur in the neck linker region of the motor upon ATP binding. The neck linker is the linkage joining the neck of the kinesin molecule to the motor domains. When ATP binds in the active site the neck linker changes from a disordered to an ordered conformation, docking along the side of the motor domain [49]. This conformational change upon ATP binding has been confirmed more recently by high resolution cryo-EM reconstructions showing the ATP bound and nucleotide free states of the MT bound motor domain [45].

The ATP dependent change had been reinforced by observations of the stepping of single kinesin molecules in mixed ATP and AMP-PNP (a slowly hydrolysable ATP analog) solu-

tions. In these experiments it was found that when AMP-PNP bound in the active site, the motor ceased stepping. This paused state was only relieved by a backwards step of the motor, releasing AMP-PNP and freeing the active site to bind ATP and continue processive movement. The coupling of AMP-PNP release to a mechanical step back indicates that it is the binding of the nucleotide and not its hydrolysis or subsequent steps of the cycle that triggers the stepping motion [50].

Crystallography of Kinesin-5 and Kinesin-1 motors at various stages of the stepping cycle have indicated that for these motors ATP binding causes a conformational change in the position of the cover strand as well as docking of the neck-linker [47, 40, 51]. The cover strand (the N-terminal of the motor) aligns parallel with the neck-linker upon ATP binding, forming a β-sheet termed the cover-neck bundle (CNB). Mutants lacking the cover strand show reduced processivity and a less effective power stroke [52].

Processive Movement

Processive kinesins take 8 nm steps along the MT from one tubulin subunit to the next. Kinesin motors do this in a hand over hand fashion [53], this means that from a two head bound state the rear head must be moved 16 nm to its next binding site in order to make a step. In this way kinesins are capable of stepping directionally pulling loads of up to 6 or 7 pN[54, 55]. The conformational change in the neck-linker is unlikely to be sufficient to cause this displacement as the neck linker is only about 12 amino acids long, so is not capable of moving the unbound head domain through a 16 nm distance independently. The size of the mechanical step of kinesin-1 upon ATP binding is estimated to be approximately 2.7nm [56].

Energy considerations also make it unlikely that the ATP induced neck-linker docking provides enough energy for the entire mechanical step. The energy gained from neck linker docking is not sufficient to account for the energy expended to making a forward step under load [57]. It is therefore likely that the 'power stroke' of kinesin is coupled with biased diffusion and a ratchet mechanism. In this scheme detachment of the rear bound head from the MT is more favourable than detachment of the front head. The MT bound front head then makes a small conformational change upon ATP binding which causes the unbound rear

head to be positioned favourably for diffusion to the forwards binding site [58, 57].

1.3.4 The ATPase cycle

As kinesins step along MTs in a processive manner they hydrolyse one ATP molecule per 8 nm step [59]. In order to remain MT bound through multiple steps the ATPase action of the heads must be well coordinated so that the rear head does not unbind before the front head is bound.

A simple scheme of kinesin-1 stepping is shown in Figure 1.5. In this scheme the kinesin starts its cycle with the first head MT bound and empty and the second head unbound with ADP in the active site [60, 61] . Upon ATP binding a conformational change in the first head allows the unbound second head to come into proximity with the MT. ATP hydrolyses to ADP and P_i in the first head and the second head releases ADP and binds the MT in a nucleotide free state. Finally the first head releases P_i and then, ADP bound, it unbinds the MT. The kinesin is now in the starting state but one 8 nm subunit closer to the MT plus end and with the opposite head binding the MT.

No mechanical sub-steps have been observed in the stepping of Kinesin for resolutions down to 30 μs [55]. This is true for both forwards and backwards steps. Kinesins make backwards steps, especially under load, however at low hindering loads the frequency of forwards steps is far higher than backwards steps. At high hindering loads it is possible to get a majority of backwards steps [55]. The mechanism of backwards stepping is unclear although it has been shown to be nucleotide dependent [55]. It is possible that a back step is a reversal of the forwards stepping cycle involving ATP synthesis. Alternately a backwards step could involve ATP hydrolysis or only require nucleotide binding to allow the step but involve no synthesis or hydrolysis.

For Kinesin-1 the stepping rate of both forwards and backwards steps are dependent on the ATP concentration, with a lower ATP concentration leading so a slower stepping rate under all loads. Interestingly although the stepping rate of Kinesin-1 can be slowed dramatically with hindering loads, assisting loads have little effect on the speed of the motor [55]. Even low assisting loads do however lead to a dramatic shortening of the run length of the motor

whilst hindering loads have a more gradual effect [62].

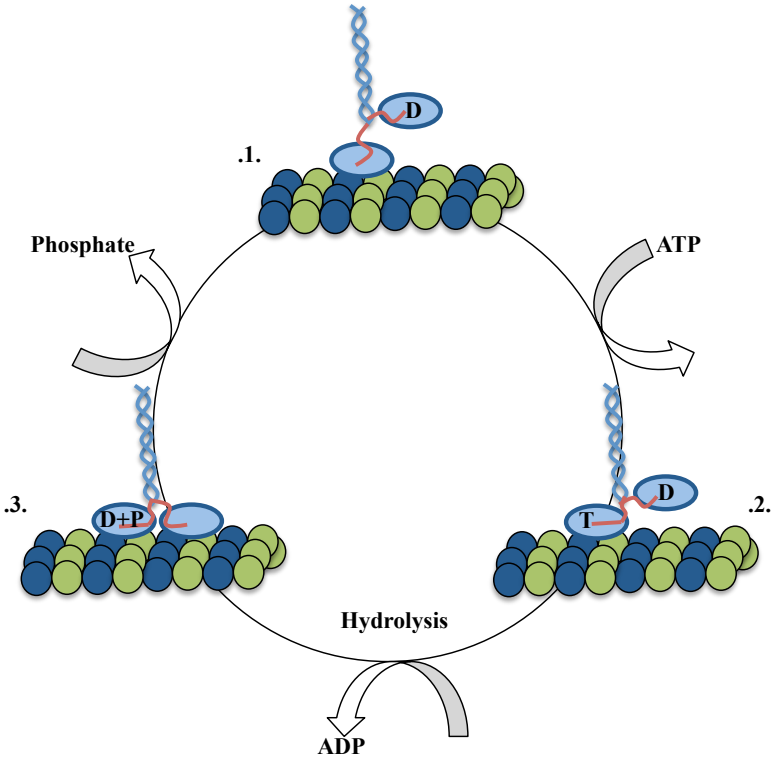

Figure 1.5: The ATPase cycle of Kinesin-1. 1) The motor is bound to the MT by one nucleotide free head, the other head is not MT bound and contains ADP. 1-2) ATP binds the MT bound head causing the motor to make a mechanical movement, bringing the second head into a position where it can bind the MT. 2-3) The motor releases ADP from the second head as it binds the MT, ATP in the first head is hydrolysed to ADP and P_i. 3-1) The motor releases P_i from the rear head and detaches from the MT in the ADP bound state.

Gating Mechanisms

In order to ensure the successful completion of a step several different gating mechanisms have been proposed. These mechanisms ensure that in a one head bound state the front head remains bound whilst the read head detaches and rebinds. In a two heads bound state gating promotes the unbinding of the rear head and maintains the attachment of the front. Gating acts through several different mechanisms to distinguish the forward from the backward head. Firstly inter-head strain can create differently directed loads on the heads.

Secondly differing neck-linker conformations again caused by the forwards and backwards positions of the motor domains can create differences between front and rear heads. Finally the nucleotide states of the motor domains can be responsible for gating.

Strain gating in the two heads-bound state can affect the ATP binding affinity of the front head, stopping ATP binding prior to release of the rear head. This is termed 'front head gating'. Strain gating can also affect the rear head, encouraging the weak MT binding ADP state and speeding MT release. This is termed 'rear head gating'. It is likely that both these methods are used to a greater or lesser extent in different situations and that different kinesins use different gating mechanisms [63].

Evidence for strain gating that occurs at the front head modulating ATP binding affinity was shown by Klumpp et al. [64]. The low binding rate of ATP to the front head whilst the rear head is MT bound reduces the chance of a futile ATP hydrolysis cycle. It has been shown recently that the binding of ATP is also gated by the neck-linker position, such that whilst there is backward strain on the neck linker, ATP binding is inhibited [65]. As mentioned, motors walking in mixtures of ATP and a non-hydrolysable analog pause upon binding of the analog and can only resume processive stepping after performing a backwards step. This indicates that the analog will exchange more easily when bound to the forwards head compared with the backwards head [50].

The direction of strain on a motor domain has also been shown to affect ADP affinity. ADP has a higher affinity for motor domains under assisting loads, such as the rear head in a dimer. This helps coordinate processive movement as the rear head is more likely to remain in the weakly MT bound ADP state and the front head is more likely to remain in the strong binding nucleotide free state [66].

Rear head gating allows the rear head of the motor to detach the MT before the forwards head. The strain applied to the motor domain has some effect on this as it has been shown that the load needed to detach a motor domain from the tightly bound (ATP or no nucleotide) state when forces are hindering motor movement is 45% more than under assisting loads [61]. These experiments are supported by Yildiz et al. [67] who show that artificially lengthened neck linkers cause a decrease in velocity as ATP hydrolysis and forward stepping are decoupled. In these constructs it is possible for motors under load to make proces-

sive runs in the absence of nucleotide however plus end directed loads induce shorter run lengths.

Nucleotide gating from the one head bound state has been demonstrated by Alonso et al. [68]. They show that binding of the tethered head to free tubulin is tightly regulated by ATP binding in the tubulin bound head. This is backed up by experiments showing that the two head binding state which can be detected via the motor unbinding force is far more transient in the nucleotide free state than the AMP-PNP bound state [69].

Recent experiments by the Block lab have found that although run lengths are independent of ATP concentration and hydrolysis rate, an increased phosphate concentration can increase processivity [62]. This effect is especially noticeable under assisting loads. This implies that there is some amount of gating at the stage of phosphate release. Milic et al. [62] suggest that this could be due to partial NL-docking upon ATP binding followed by more complete docking and binding of the second head upon hydrolysis.

1.3.5 Regulatory Mechanisms

Several methods of motor regulation have already been touched on, in particular the auto-inhibition of Kinesin-1 by its own tail domains. This type of inhibitory mechanism is reasonably common and is suggested as a mechanism of regulation for both CENP-E [31] and Kif15 [33]. The detailed mechanism of auto-inhibition for Kinesin-1 has been examined and crystal structures of dimeric Kinesin-1 in its inhibited state have been solved [70]. This structure shows that the tail locks the two motor heads together in manner that prevents the undocking of the neck-linkers and the release of ADP. This mechanism enables motors to be inactivated until either binding of cargo to the tail domain or, in the case of CENP-E, phosphorylation by a regulatory kinase.

The mitotic kinesin Eg5 also has a cargo sensing mechanism, in this case the cargo is a second MT. Molecules of Eg5 bound to a single MT show diffusive movement, however upon binding of a second MT to the other pair of head domains the motor switches to processive movement [24]. The initial binding and diffusion of Eg5 is not ATP dependent. Structures of the tetramerisation domain, the Bipolar Assembly (BASS) domain, in Eg5 indicate that the

two head domains might be rotated by 90 degrees to each other [71]. This would mean that when bound between two anti-parallel MTs torsion would be introduced in to the system. This could explain how the heads at opposite ends the molecule communicate switching from diffusional to directional movement. This might also explain the motors preference for anti-parallel over parallel MT bundles [24].

The localisation of Eg5 within the spindle is regulated by Tpx2 [17]. Tpx2 acts to increase the amount of Eg5 on the spindle MTs. Tpx2 also stops the motility of Eg5 by interacting with the motor directly [72]. Eg5 regulation is performed by chemical as well as mechanical means, for example, the tail of Eg5 is phosphorylated by CDK1 increasing MT localisation before spindle formation [73]. Phosphorylation in the tail region by either CDK1 or Mps1 also relieves auto-inhibition in CENP-E [31].

Motors are regulated within the spindle to recognise specific sub-cellular locations such as MT ends or the spindle mid zone. End Binding (EB) proteins play a key role in MT tip recognition and interact with various kinesin motors including the MT depolymerases Kif18b [74] and MCAK [75]. Motors such as Eg5 and Kif15 have also been shown to recognise MT tips in the absence of EB proteins, with *in vitro* experiments showing motors with extended dwell times at tips [24, 34]. PRC1 is a MT crosslinker that acts in the spindle midzone, it actively recruits the Kinesin-6 motors MKLP1 and MKLP2 [76]. As PRC1 works to form MT bundles its likely that its action also leads to the recruitment of motors such as Eg5 or Kif15 which recognise these structures [33].

1.4 Spindle Organisation and Maintenance

Two of the key motor proteins involved in mitotic MT reorganisation in human cells are the Kinesin-5, Eg5 and Dynein. These are required for separation of the centrosomes before NEB and formation of the spindle in prometaphase. They also contribute to the maintenance of the bipolar structure in metaphase. A third motor protein, Kinesin-12, known as Hklp2/Kif15 in humans, is also involved in spindle maintenance and has some overlap of function with Eg5. The extent of this functional redundancy is particularly of interest as Eg5 is being developed as an anticancer drug target and an overlap could lead to increased likelihood of drug resistance developing in the cancer.

1.4.1 Force Balance Model

In order to form the bipolar spindle the centrosomes must be separated. In vertebrate cells, which undergo "open" mitosis, this usually happens during prophase about 1hr before NEB. The centrosomes migrate along the nuclear envelope until they reach opposite sides of the nucleus. MT motors play an important role in this process, in particular Kinesin-5 has been shown in many organisms to be essential for centrosome separation before NEB [77].

One model for the process of centrosome separation and in particular the maintenance of the spindle is the balance of forces. In this model the action of the plus end directed motor Kinesin-5, and to some extent Kinesin-12, creates outwards forces that are balanced by minus end directed dynein and the Kinesin-14, HSET [78]. In the force balance model centrosome separation occurs by the combined efforts of cortical dynein pulling the spindle poles apart and Eg5 pushing them apart in the overlap region, Figure 1.6. Once the centrosomes are separated in prometaphase then the outwards pushing forces of Eg5 become counteracted by the pole focussing inwards forces of dynein also working in the overlap region. Evidence for this balance comes from depletion of Eg5 during spindle formation leading to monopolar spindles with unseparated centrosomes. Depletion of dynein in addition to Eg5 restores spindle bipolarity [79].

This effect is clearest in immature spindles prior to NEB. However even in metaphase

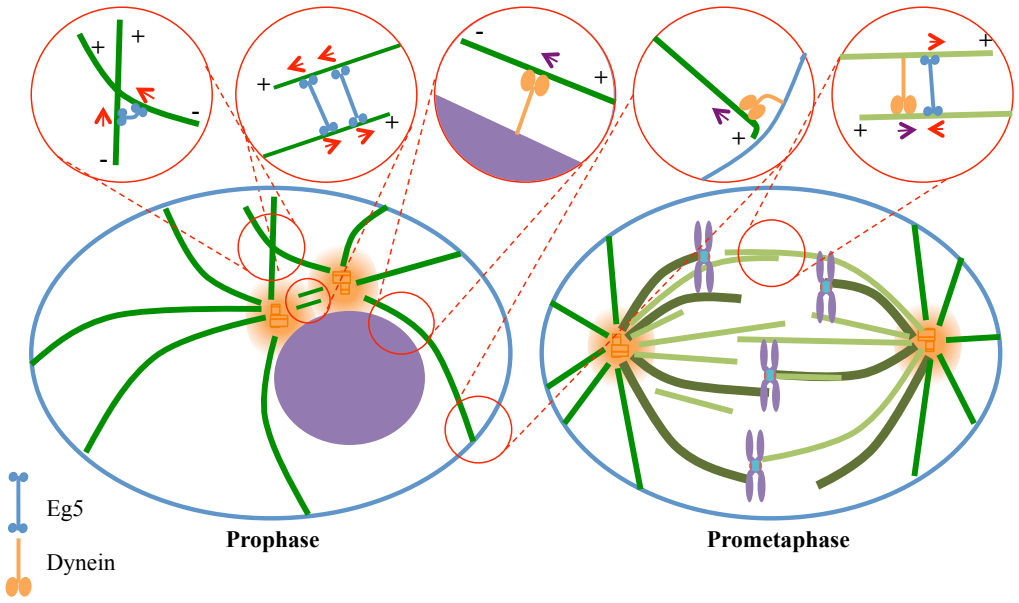

Figure 1.6: Roles of Eg5 and Dynein in spindle formation and maintenance. In prophase Eg5 operates in the spindle overlap creating outwards pushing forces whilst Dynein operates at the nuclear envelope and cell cortex creating outwards pulling forces. In prometaphase Eg5 and Dynein both operate in the MT overlap region creating opposing forces and a balance of forces.

spindles Eg5 inhibition leads to spindle shortening by 30% as a result of an excess of inwards force. Meanwhile dynein inhibition creates 30% longer spindles due to a force imbalance in favour of outwards Eg5 dependent forces [80]. The ability of the spindle to both form and maintain its bipolar shape in the absence of either Eg5 or dynein motors indicates that other force producing motors must be at work. These motors are suggested to be the plus end directed Kinesin-12, Kif15 and the minus end directed Kinesin-14, HSET.

The involvement of Kif15 in spindle maintenance was investigated by Tanenbaum et al. [19] and Vanneste et al. [35] in 2009. They showed that Kif15 depletion sensitised cells to Eg5 inhibition during metaphase. In the absence of both plus end directed motors the bipolar spindle collapses to a monopolar state. However if dynein were inhibited in these cells then spindle bipolarity is retained, albeit with a loss of chromosome alignment [21]. This loss of chromosomal alignment sheds some light on the purpose of these seemingly redundant motors, their action is necessary in order to maintain stable Kinetochore-MT

attachments.

1.4.2 Kif15 Dependent Forces

The action of Eg5 as a plus-end directed tetramer working in the MT overlap to create outwards forces on anti-parallel MTs is well established. Several studies have suggested that Kif15 might work in a similar manner to Eg5. However little is known about the single molecule properties of Kif15 and the mechanism behind the outwards force generation of Kif15 is unclear.

Localisations

Eg5 and Kif15 have different spatial and temporal localisation patterns during prophase and metaphase whilst the spindle is formed and the chromosomes are aligned. Association of Eg5 with MTs is dependent on cell cycle regulated phosphorylation [77]. Eg5 accumulates around the centrosomes at mitosis onset and remains enriched at the spindle poles during metaphase [19, 35]. Kif15 is not recruited to the spindles until after nuclear envelope breakdown and is uniformly distributed on spindle microtubules in metaphase cells. The localisation of Kif15 to spindle microtubules is dependent on Tpx2, a microtubule associated protein that is localised to the nucleus during interphase and to the spindle MTs after NEB. Tpx2 is enriched on K-fibre MTs [19, 81], and Kif15 has been shown to preferentially bind to K-fibres [82] whilst Eg5 localises equally to both K-fibre MTs and interpolar MTs [77].

Kif15 localises to the cytoplasm during interphase and to both the spindle microtubules and the chromosomes after nuclear envelope breakdown. The chromosomal localisation of Kif15 is dependent on interaction with chromosomal protein Ki67. In Ki67 silenced cells chromosomal localisation of Kif15 is decreased. In contrast to the shortened spindles caused by global Kif15 depletion, these cells display on average slightly longer spindles and also slight alignment defects of chromosomes [83].

Kif15 Dependent Spindle Formation

In the absence of Eg5, Kif15, expressed at normal levels, is not sufficient to rescue spindle formation although it is enough to maintain a preformed spindle. However cells either over expressing Kif15 [19] or with inhibited Eg5 and dynein function [21] are capable of assembling a functional bipolar spindle. In both these circumstances the mechanism of spindle formation is different from the usual Eg5 dependent route. In the absence of Eg5 function the centrosomes fail to separate prior to NEB, instead a monoastral bipolar spindle is formed. This spindle has unseparated centrosomes with the MTs fanning out to one side attaching to the chromosomes. The centrosome separate after NEB via a 'jack knife' movement where the spindle poles appear to pivot around the chromosomes to form a bipolar spindle. In cell lines developed to function without Eg5 this mechanism of spindle formation is also used and their division is dependent upon Kif15 [82, 84].

K-Fibre Mediated Forces

Kif15 localises primarily to K-fibres and has been shown to increase K-fibre length and stability [82]. It is therefore likely that some Kif15 dependent forces are mediated through the K-Fibres. In support of this Gayek and Ohi [85] have shown that not all human cell types are unaffected by Eg5 inhibition at metaphase. Those with less stable K-fibres collapse upon inhibition of Eg5 regardless of the presence of Kif15. It would seem that the maintenance of the bipolar spindle requires either outward pushing forces of Eg5 on the interpolar MTs or the increased stability of K-fibres provided by Kif15.

In cells lines developed to be resistant to Eg5 inhibition, or when Kif15 is over expressed, Kif15 localises to the non-K-fibre MTs [82]. It has been suggested that it is this mis-localisation that enables the functional overlap with Eg5 allowing Kif15 to work in centrosome separation. Kif15 appears to bundle MTs and might either cause mechanical strain through the sliding of parallel MTs or by affecting MT polymerisation. Strain induced by the interaction of Kif15 on parallel MT bundles could cause the jack-knifing effect [82].

The effects of Kif15 and Eg5 aren't always in support of each other, due to their different mechanisms they have been shown to operate antagonistically. In prophase Kif15 in K-fibres

moderates Eg5 dependent pole separation. The presence of Kif15 slows spindle pole separation leading to a continuous lengthening. In the absence of Kif15 the poles snap rapidly apart, overshooting the stable metaphase spindle length before under going contraction [82]. As already mentioned the effect of removing the interaction of Kif15 with the chromosomes via Ki67 leads to shorter and not longer spindles [83]. This antagonism is also seen in the effect of Eg5 and Kif15 on chromosome oscillations in metaphase. Whilst Eg5 inhibition leads to loss of chromosome oscillations consequent depletion of Kif15 partially restores them [86].

Conclusions

The motor protein Kif15 contributes to the balance of forces within the spindle, creating outwards forces in metaphase. This function it shares with the Kinesin-5, Eg5. Kif15 is also necessary for the formation of the spindle in the absence of Eg5 in which case either Kif15 over expression or dynein under expression are also required. As such Kif15 has a substantial over lap of function with Eg5 giving it the potential to compensate for loss of Eg5 activity. Eg5 is a target for anticancer drugs, however this functional overlap is likely to cause Eg5 inhibiting drugs to be less effective. As Kif15 itself has the potential to become a drug target [87], it is therefore necessary to investigate the method of action of Kif15 more thoroughly.

From the research to date it appears that Kif15 mainly acts to produce outwards forces in the spindle via the K-Fibres. This is different from Eg5 which acts on both K-Fibres and interpolar MTs. The method by which Kif15 forms spindles also differs to Eg5, going by way of a monopolar intermediate. Kif15 and Eg5 despite their similarity in function therefore appear to operate via distinct mechanisms. The cross-link and slide mechanism of Eg5 is well established but the manner of Kif15 operation is still unclear. In order to gain a better understanding of the method by which Kif15 operates it is necessary to look more closely at the force generating properties of single Kif15 molecules.

1.5 Non-Mitotic Functions of Kinesin-12

Aside from their role in cell division many mitotic motor proteins have been shown to act in the development of neurones. Both Kif15 and Eg5 have been shown to have inhibitory effects on axon growth, again suggesting a similar mechanism of action. The role of Eg5 and Kif15 in axons is to act as a balance against dynein dependent axon lengthening forces. However in axons as well as mitosis the functions of Eg5 and Kif15 appear to diverge. Kif15 depletion reduces the size of the growth cone and axonal branching whilst Eg5 depletion increases these properties [88]. It has been suggested that these additional functions of Kif15 are due to an actin binding site which would allow the motor to link the microtubule and actin networks. Due to the effects of Kif15 and Eg5 depletion on axonal growth recent experiments have investigated the possibility of targeting these motors to improve the regeneration of injured axons with some success, indicating a potential secondary use for inhibitors of these proteins [89, 90].

Another role for Kif15 has been recently discovered in the regulation of the integrin $\alpha 2$ [91]. Integrins are transmembrane adhesion proteins and are involved in cell-cell adhesion and attachment to the extra cellular matrix (ECM) [8]. An siRNA screen found that Kif15 acts as an inhibitor of the endocytic trafficking of $\alpha 2$ integrin. Eskova et al. [91] suggest that Kif15 plays a role in localising the alternative clathrin adaptor Dab2 to the plasma membrane.

1.6 The Mechanical Properties of Kinesin-1, Eg5 and Kif15

By examining motor proteins in an *in vitro* environment much can be learnt about the properties of teams or individual motors. This information can then be used to inform models of the mechanism of mitosis. Kinesin-1 and Kinesin-5 motor proteins have been extensively studied *in vitro* and much is known about their structure and force generating properties. The majority of work on Kinesin-5 has focused on either the full-length *Xenopus*

Kinesin-5, Eg5 or a truncated human Kinesin-5 Eg5-513-5His.

1.6.1 *In vitro* Experiments for Examining Kinesin Motor Proteins

There are several key types of *in vitro* experiments that are performed with motor proteins. The first of these is the gliding assay, in these assays motor proteins are bound to the surface of a glass slide, fluorescently labelled MTs in solution then land on this surface and are bound by the motors. In the presence of ATP the motors walk along the MT, gliding them across the surface. The movement of the MTs is recorded and information on the velocity and directionality of the motors can be established. The second type of assay is a single molecule assay, in these experiments MTs are bound to the surface of the slide and fluorescently labelled motors in solution bind and move along the MTs. These experiments track the movement of individual motor molecules and can provide data on the individual motors velocity, its processivity (a measure of the motors ability to make consecutive steps on the MT without detachment) and any diffusive or pausing behaviour.

A final type of experiment looks at the ability of motors to walk under load. These experiments use a technique called optical trapping or laser tweezers to capture and apply load to small beads. When motors are bound to these beads in a flow cell and then allowed to walk along a MT the motors velocity and run length under a varying loads can be determined.

1.6.2 Biophysical properties of Kinesin-1 and Eg5

Kinesin-1 and Kinesin-5 motors play very different roles *in vivo* and this is reflected in their differing mechanical capabilities, Table 4.1. As a transport motor protein Kinesin-1 is fast and processive, this makes it ideal for rapid transport over long distances. In contrast Eg5 is significantly less processive and moves more slowly [46]. Under load Eg5 maintains a much more steady velocity than Kinesin-1, this could enable it to work well in crowded environments with externally imposed loads. In contrast Kinesin-1 slows significantly under applied loads [55], this may be beneficial when its cargo encounters an obstacle.

Similarly to the velocity, the run length of Eg5 is only mildly sensitive to load [92], whereas

for Kinesin-1 the run length falls rapidly especially under assisting loads. This again indicates that Eg5 is more likely to be consistent in its force generation under the externally imposed loads that it will encounter in the spindle where as Kinesin-1 will alter its behaviour in adverse conditions. The lower sensitivity of Eg5 to load can be explained by a model which predicts a shorter characteristic distance of the load-dependent transition state, 1.9 nm as opposed to 2.7 nm [46].

Observations of a dimeric human Eg5 construct under load show that the run length remains fairly constant. However full-length tetrameric *Xenopus* Eg5 was shown to detach from MTs at hindering loads above 3pN [93]. The tetramer showed similar velocity dependence to the dimer and did not slow significantly before release. This suggests that the behaviour of the dimeric motor domains of Eg5 is likely to be affected by tetramerisation *in vivo*.

The randomness of both Eg5 and Kinesin-1 at saturating ATP conditions are similar. The randomness parameter is a measure of the stochasticity of stepping. A constant step time would give a randomness value of zero whilst an exponentially distributed poisson process would give a value of one. With decreasing ATP concentration the randomness parameter for both Kinesin-1 and Eg5 tends to one as the rate limiting step is ATP binding which is a stochastic process.

	Kinesin-1	Eg5
Velocity (Unloaded)	800 nm/s [55]	96 nm/s
Run Length	1.4 μm [3]	67 nm
Stall Force	6-7 pN [55]	>7 pN
Randomness	0.38 [56]	0.4

Table 1.1: Biophysical Values for Eg5 and Kinesin-1. Values for Eg5 are for the dimeric Eg5-513-5His construct taken from Valentine et al. [46] . Kinesin-1 values are for *Drosophila* Kinesin-1 [55] or *Loligo pealei* [56, 3].

The stepping cycle of Eg5 appears to be different to Kinesin-1 [94], upon first encounter with the MT Eg5 releases ADP from both its heads. The first ADP unbinds rapidly followed by slow release of the second ADP. The motor then starts its processive run from a 2 head bound state. During its processive run ATP hydrolysis is the rate limiting step [95], for

Kinesin-1 this is phosphate release [64]. The reason for the low processivity of Eg5 is not completely clear. Because of its ability to bind both heads to the MT without ATP binding in the rear head Eg5 may struggle to keep its motor domains well coordinated. Alternately the gating at other points in the cycle may be weaker making it more likely for ADP to bind creating a two heads weakly bound state.

From these results it is clear that there are questions remaining as to the manner in which full length human Eg5 motors move on microtubules. The human dimeric constructs are capable of stepping against forces up to 7 pN, where as the tetrameric *Xenopus* Eg5 is limited to pulling only 3 pN of load. If the tail regions supply a slip-clutch type mechanism allowing the motor to detach at prematurely low loads as described by Korneev et al. [93] this could be an important mechanism to aid the multi motor dynamics when teams of Eg5 motors crosslink and slide MTs. The binding of both pairs of motor domains to two antiparallel MTs appears to increase processivity although it is not clear whether this would allow Eg5 to sustain longer runs under load.

1.6.3 Biophysical Properties of Kif15

In contrast to Kinesin-1 and Eg5 the Kinesin-12, Kif15 has not been well studied *in vitro*, this makes interpretation of its *in vivo* method of function difficult. It has been suggested that Kif15 act in a manner similar to Eg5, crosslinking and sliding MTs in the spindle overlap. In this case it would seem likely that Kif15 and Eg5 might display similar mechanical properties. However there is some evidence that Kif15 produces outwards forces in the spindle via a different mechanism.

Recent work on Kif15 by Drechsler et al. [34] and also by Sturgill et al. [33] has shed some light on the behaviour of single Kif15 molecules. The groups agree that Kif15 is processive, capable of walking distances of over 1μm along a MT without detaching. Kif15 is also slow with an unloaded velocity of around 150nm/s. There is disagreement however as to the oligomerisation state of Kif15 with Drechsler et al. [34] finding a tetrameric motor and Sturgill et al. [33] finding a dimeric motor.

Sturgill et al. [33] show that Kif15 has a regulatory C-terminal coil similar to those of

Kinesin-1 and CENP-E which is capable of inhibiting motor movement. They also suggest that Kif15 has a second MT binding site. Drechsler et al. [34] find that Kif15 can display a variety of modes of movements including long plus end directed movement, short minus end directed runs and diffusive movement.

These papers along with a structural and biochemical study by Klejnot et al. [42] have been published since the start of this project. Work from this project contributed to the Kif15 paper by Drechsler et al. [34]. The structure of Kif15 has been shown to be similar to that of Eg5 and of Kinesin-1, importantly loop L5 in Kif15 is different to that in Eg5 explaining why Eg5 inhibitors which target this loop are ineffective for Kif15.

1.7 Conclusions

Kinesin motor proteins play an important role in spindle formation, through the use of ATP hydrolysis they create essential forces within the spindle. They do this by binding to the MT cytoskeleton and walking along MTs in a directed hand-over-hand manner. The stepping of kinesins is a highly coordinated process ensuring that the motors remain attached to the MT whilst making each step. The structure and subsequent biochemistry of different motors provide them each with unique biophysical properties adapting them to their particular *in vivo* functions.

The Kinesin-5, Eg5, has been shown to be essential for spindle pole separation and important in spindle maintenance in many cell types. This makes Eg5 an attractive target for anti-mitotic cancer drugs and Eg5 inhibitors have shown promise in clinical trials. However in human cells Eg5 is functionally redundant in its spindle maintenance role with the Kinesin-12, Kif15. It has been shown that Kif15 is also capable of supporting spindle formation in the absence of Eg5 in some circumstances. This overlap of function could allow cells to develop resistance to Eg5 inhibiting drugs. It is therefore important to discover how Kif15 is capable of performing its mitotic function.

The mechanism of action and mechanical behaviour of Eg5 are well characterised. Single molecules have been shown to be capable of cross-linking and sliding MTs. They produce spindle pole separation forces by sliding apart anti-parallel MTs in the region of overlap between the poles. The mechanical behaviour of Eg5 differs from that of transport motor proteins such as Kinesin-1 making it better adapted for its role in spindle formation. Eg5 has a much shorter run length, is slower and is less sensitive to applied loads. In contrast to Eg5, Kif15 is poorly characterised with little known about its biophysical properties or method of action within the spindle.

1.8 Project Outline

This project investigates the load dependent behaviour of single Kif15 molecules. This is done using an optical trap to apply loads to motors as they walk along MTs. From optical trapping records it is possible to examine the velocity of the motor under varying loads. It is also possible to examine the number of forward and backward steps taken and determine a stall force, the load at which the motor ceases to make net forwards progress. Load dependent properties of Kif15 are compared to those of *Drosophila* Kinesin-1, which is well characterised, as a control. This biophysical characterisation of Kif15 will help to narrow down the possible mechanisms through which Kif15 creates forces within the spindle.

Possible regulatory mechanisms of Kif15 are examined and the effect of the MAP Tpx2 on Kif15 stepping is studied. Tpx2 is known to be important for the *in vivo* localisation of Kif15. Truncated Kif15 constructs are used in order to begin investigating the effects of regulatory regions of Kif15. Based on the behaviour of Kif15 in previous experiments, an asymmetry in unbinding of the motors, dependent on the direction of applied load, is investigated. This may affect the behaviour of Kif15 if the motor is to work in teams. This asymmetry is again compared to a Kinesin-1 control and the effects of regulatory regions and Tpx2 on the unbinding loads is tested.

Chapter 2

Methods

2.1 Introduction

The human Kinesin-12, Kif15, is a motor protein that has a role in the process of spindle assembly and maintenance. Little is known about the properties of single Kif15 molecules, it has been the aim of this project to investigate the single molecule mechanics of the motor. Since we wish to know the mechanical behaviour of Kif15 under a variety of opposing and assisting loads an optical trap has been used. The optical trap allows load to be applied to motors and the movement of single motor proteins to be tracked.

Optical traps use a highly focused laser beam to trap a small (300-1000 nm diameter) polystyrene bead, Figure 2.1. By moving the stage with piezoelectric motors and adjusting the focus point of the laser beam it is possible to precisely position a bead. In our experiments kinesin motors are bound to the beads, the bead is then positioned over a surface bound microtubule. The motor is allowed to bind to the MT. When the motor binds to the MT in the presence of ATP it can begin processive 'hand-over-hand' movement along the MT pulling the bead out of the trap. As the bead is moved from the trap centre the restoring force increases in a linear manner; the further the motor has walked along the MT the greater the load it has to pull against. The position of the bead is measured as it is pulled out of the trap.

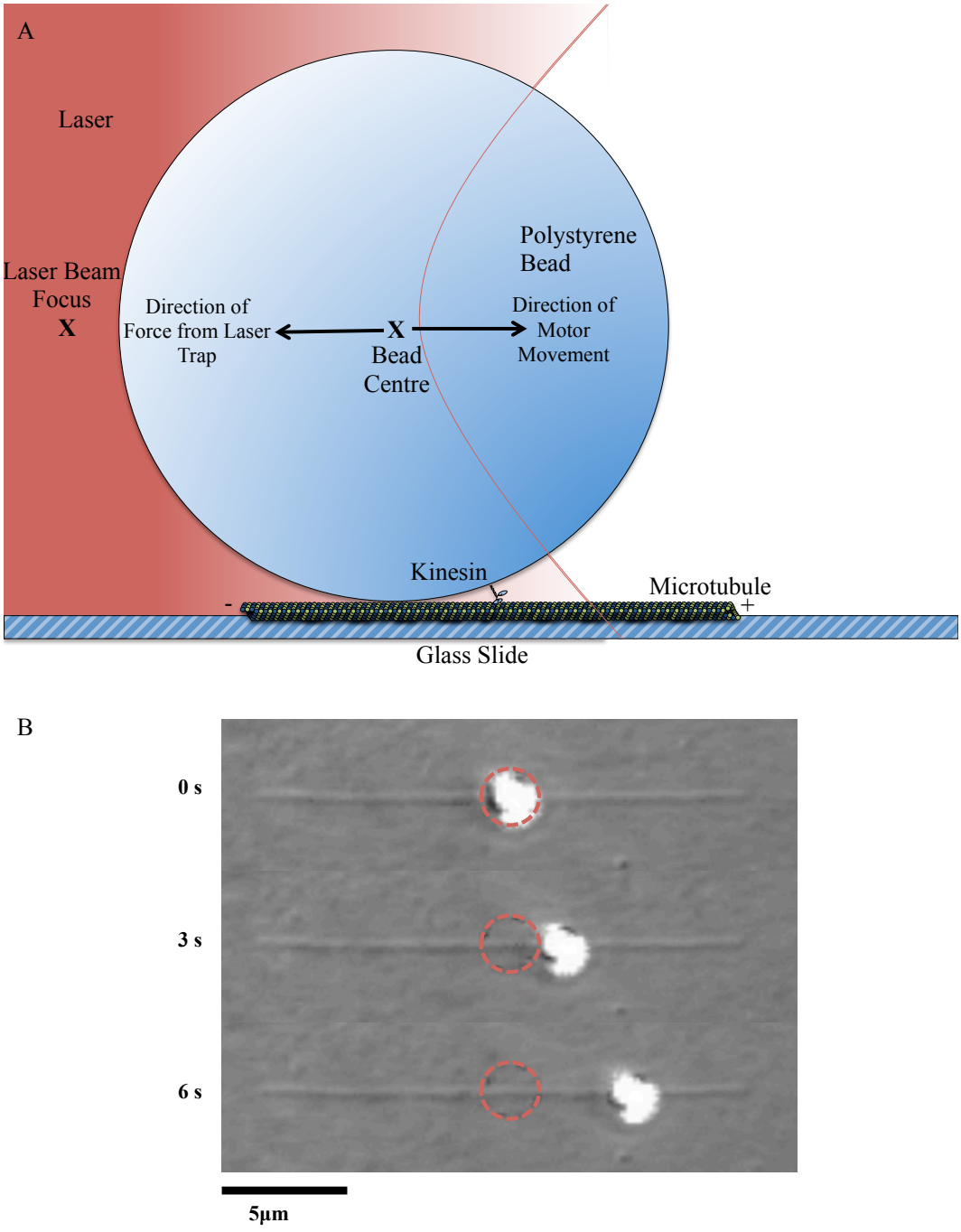

Figure 2.1: A) Experimental set up (to scale). As the Kinesin motor walks along the microtubule the bead will be pulled out of the centre of the trap. The beads lateral position relative to the trap centre is recorded. Distance from the trap centre is linearly related to the restoring force acting towards the trap centre. B)DIC (Differential Interference Contrast) Images of a 560 nm diameter polystyrene bead with a kinesin motor attached as it moves along a microtubule away from the trap (red circle).

2.2 Materials

Unless otherwise stated all reagents are supplied by Sigma Aldrich.

2.2.1 Buffers

Buffer A/A20;

- 80 mM K.PIPES (Potassium piperazine-N,N'-bis(2-ethanesulfonic acid), 20 mM K.PIPES, pH 7.0
- 2mM $MgSO_4$
- 1mM EGTA (Ethylene Glycol Tetra Acetic Acid)
- 1mM DTT (Dithiothreitol)
- 3mg/ml D-Glucose

1 ml aliquots stored at -20°C

Buffer B1/B120:

- Buffer A, Buffer A20
- 1mg/ml α-casein from bovine milk

Filtered though a 0.2μm minisart syringe filter before storing in 0.5 ml aliquots at -20°C. Centrifuged for 10 minutes at 4°C and 14,000rpm before use.

GOC (Glucose Oxidase/Catalayse);

- 50% Glycerol
- 45% Buffer A
- 5 mg/ml Glucose Oxidase from *Aspergillus Niger* (lyophlised powder, 147.9 unit/mg)
- 1 mg/ml Catalase 47000 unit/mg

Filtered though a 0.2μm minisart syringe filter before centrifuging 850μL at 4°C and 20 krcf for 10 minutes. Stored in 7.5μL aliquots at -20°C.

10mM Taxol;

- 0.58 ml DMSO (Dimethyl sulfoxide)

- 5mg Paclitaxel, from *Taxus brevifolia*, =95% (HLPC), powder

5μL aliquots stored at -20°C

100mM ATP;

- 20mM K.PIPES
- 100mM Adenosine 5?-triphosphate disodium salt hydrate, ATP (Sigma A7699-1G)
- 100mM $MgCL_2$

Na.ATP added slowly to K.PIPES solution whilst maintaining pH 7.0 by addition of small amounts of 10M KOH. Stored in 5 μL aliquots at -20 °C.

100mM ADP;

- 100mM Adenosine 5'-diphosphate sodium salt, ADP (Sigma A2754)
- 100mM K.PIPES, pH 6.9

Stored in 5μL aliquots at -20 °C.

100mM AMP-PNP;

- 100mM Adenosine 5'-(β,γ-imido)triphosphate lithium salt, AMP-PNP (Sigma A2647)
- 100mM K.PIPES, pH 6.9

Stored in 5μL aliquots at -80 °C.

2.2.2 Beads

560 nm diameter, 1.0% Polystyrene Microspheres in water (Polysciences). Non-functionalised, monodisperse, polystyrene microspheres containing a slight anionic charge from sulfate ester.

2.2.3 Coverslips and Coverslip Cleaning

22 x 22 mm and 22 x 50 mm, thickness Number 1.5 (170μm) (Menzel-Gläzer or Corning)

Coverslips in metal racks were cleaned using hot detergent and sonication with in a 600W ultrasonic bath (Ultrawave Ltd.). Racks of coverslips were first sonicated in hot (>80°C) ultra pure(UP),18.2 Ω resistance, water for 15 minutes. The coversliips were rinsed and then sonicated in 1% Neutracon (Decon Laboratories Limited) again at >80°C for 15 minutes. After the sonication with detergent, six rounds of rinsing interspersed with 10 minutes sonication in hot UP water were performed. The coverslips were then dried in an oven at 180°C for an hour before plasma cleaning for 5 minutes (with room air).

2.2.4 Microtubule Polymerisation and Stabilisation

15 μL aliquots of 60 μM pig brain tubulin purified as described in Katsuki et al. [96] and stored in liquid nitrogen were provided by the Cross Lab. Initial buffer conditions were; 100 mM K-PIPES (pH 6.9), 1 mM $MgSO_4$, 2 mM EGTA and 20 μM GDP.

1mM GTP and 1mM $MgSO_4$ were added to the tubulin which was then incubated at 37°C for 60 minutes to allow MTs to polymerise. Taxol was then added at 20 μM and mixed slowly, the MTs were left for a further 60 minutes at 37°C. The polymerised MTs were then spun down in the AirFuge (Beckman Coulter, A110-Rotor) at ∼80,000 rpm for 20 minutes. The supernatant was then drawn off and the pellet was resuspended in 60 μL of buffer A with 0.2 μL of 10mM Taxol. The MTs were left on the bench and used for 2-3 weeks at 2-8% dilution (depending on surface binding rates) in buffer A and 10 μM Taxol.

2.2.5 Antibodies

Antibodies used;

- Anti Hklp2 Antibody (Category Number AKIN13) from Cytoskeleton; Affinity purified rabbit polyclonal specific for Kinesin Hklp2.

2.2.6 Protein Constructs

In these experiments several different motor proteins and MAPs were used, Figure 2.2;

- Full length Drosophila Kinesin-1

- Full length Human Kif15 with N-terminal His-tags
- Full length Human Kif15 with N-terminal His-tags and C-terminal GFP
- Truncated Human Kif15-1293 with N-terminal His-tags
- Full-length Human Tpx2
- Full-length Human Eg5

The Kinesin-1 protein was purified by M.Braun as described in Braun et al. [97]. The Kif15 and Eg5 motor proteins and the Tpx2 were purified by H.Dreschler as described in Drechsler et al. [34]. Proteins were stored in liquid nitrogen at -196°C and were not refrozen after thawing.

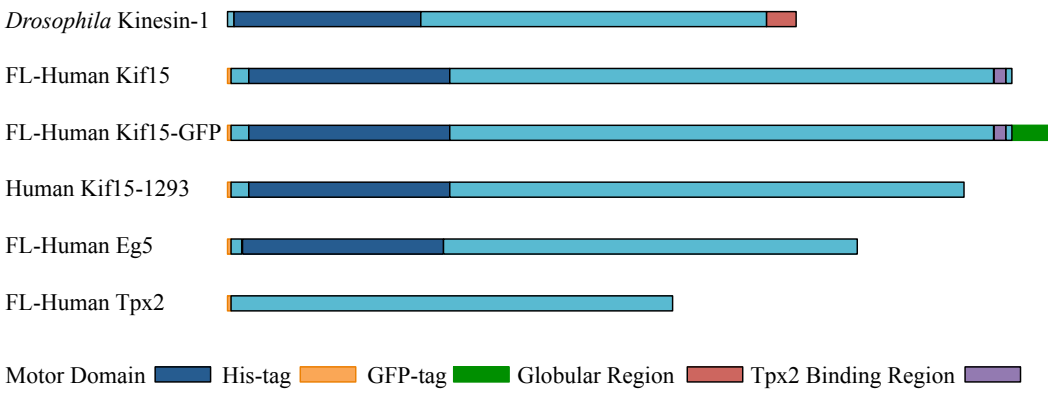

Figure 2.2: 6 different proteins have been used in these experiments; Full length Kinesin-1, full length hKif15 with N-terminal His-tags, with and without C-Terminal GFP label, C-terminal truncated hKif15-1293, full length hEg5 and full length hTpx2.

2.3 Sample Preparation

560nm Polystyrene beads and motors were incubated together in a solution containing buffer A, 0.2mg/ml casein and 1 μM ATP. The concentration of motor was decreased until most beads did not bind the microtubule so as to increase the likelihood that single molecule behaviour was observed, see Section 3.1. When higher ionic strengths were used for bead incubation the motors were incubated in high salt (buffer A + 380 mM NaCl) for 30 minutes prior to incubation with beads, also in a high salt buffer, see Section 3.8 on motor

tetramerisation.

Flow cells were constructed using sonicator and plasma cleaned coverslips and Dow Corning High Vacuum Grease. Two lines of grease were applied to the base coverslip (22 x 50 mm) using a syringe, the top coverslip (22 x 22 mm) was then pressed in to place, forming a flow cell of approximately 8μL volume. Pig brain microtubules were diluted in buffer A (as above), with 10 μM taxol to stabilise them. The microtubules were introduced to the flow cell and allowed to adsorb on to the surface. Before addition to the flow cell, 0.2 μl of the incubated bead-motor solutions were diluted in 20 μl of assay buffer, composed of buffer A20, 1mM ATP, 0.4 mg/ml casein, 10 μM taxol and 0.4 μl of the glucose oxidase/catalase described above. The beads were then introduced to the cell using capillary action to draw the solution through. The cell was sealed and the sample was viewed immediately.

2.4 Instrumentation and Data Collection

The details of the optical trap used have been previously described by Carter and Cross [55]. The optical trap uses a Nd-YAG laser which emits light with 1064 nm wavelength, the laser power output can be modulated between 20 and 2000 mW. The laser passes through a pair of AODs (acoustic optical deflectors), which allow the laser beam to be rapidly repositioned, these are used for fine scale trap positioning.

The laser is focused on to the sample enabling it to capture polystyrene beads with motors attached. A captured bead is then positioned over a microtubule by moving the stage with piezoelectric positioning motors (Physik Instrumente (PI) 50μm x 50μm XY piezoelectric translation stage). The stage is controlled by a 12 bit DAC (Digital to Analog Converter) which allows the 50μm stage to be stepped in 12.2 nm movements in both the x and y directions, giving coarse positional control. The laser is then focused to the surface of the coverslip bringing the motor within range of the microtubule. The slide is illuminated by a white LED and is imaged using differential interference contrast (DIC) microscopy. This allows the polystyrene beads and surface bound MTs to be imaged.

For data collection the microtubule position and orientation were marked and the bead image was moved to the quadrant photodiode detector, which detects the position of the

bead in the trap. When using the photodiode detector both polarisers are removed from the optical pathway, allowing a bright field image to be focused on the detector. The microscope software collects data at 80-100 kHz, this is sampled down before storage to 45 kHz whilst performing calibrations and to 22kHz whilst collecting motor stepping data, allowing longer traces to be collected.

2.4.1 Quadrant Photodiode Detector Calibration

In order to calibrate the positional sensitivity of the quadrant detector the AODs are first calibrated. This is done with the microscope in DIC by moving a bead a known distance of 2μm with the AODs and visually checking the correct distance is moved.

The quadrant detector is calibrated by moving the bead $+/-$ 30% of the bead diameter in both the X and Y axes using the AODs. The quadrant is calibrated by dividing the known distance moved by the number of units moved, as registered by the detector.

2.4.2 Trap Stiffness Calibration Methods

Three different methods were used to calibrate the X-Y trap stiffness, the stiffness of the trap in the z-direction is unknown. Each of these methods has a different degree of sensitivity to the accuracy of the predicted bead radius and the quality of the quadrant calibration. By comparing the trap stiffnesses calculated by each of these methods we get a more reliable estimation. These comparisons allow bad calibrations due to inaccuracies in the given bead radius or poor quadrant calibrations to be addressed. For the instrument and laser powers used for these experiments trap stiffnesses are in the range of 0.01 - 0.3 pN/nm.

Equipartition

The thermal fluctuations of the trapped bead can be used to estimate the trap stiffness by applying equipartition theory [98]. The equipartition theory relates the mean distance of the bead from the trap centre to the trap stiffness and thus relies on an accurate distance calibration. For an objected trapped in a harmonic potential with stiffness κ the variance

of the distance x is given by;

$$\frac{1}{2}\kappa\langle x^2\rangle = \frac{1}{2}k_bT \tag{2.1}$$

Where k_b is the Boltzmann constant and T is the absolute temperature. For this method of calibration an accurate bead diameter is not necessary.

Power Spectrum

If the bead diameter is known then the trap stiffness can be found by looking at the power spectrum of the bead fluctuations due to thermal noise [98]. The one sided power spectrum of a bead of known diameter can be fit with a Lorentzian function using a least squares fit. From this function the rolloff frequency f_0 is given by $f_0 = \kappa(2\pi\beta)^{-1}$. κ is the trap stiffness and β is the drag coefficient. The viscosity of the solution is known and the value of beta is given by β=$6\pi\eta r$, where η is the viscosity of the solution. Since this calibration method relies only on the frequencies seen in the thermal motion of the bead a good distance calibration is unnecessary.

Stokes

The Stokes calibration requires both an accurate bead size and a good distance calibration. In this method of calibration the stage is moved in a saw-tooth pattern causing the bead to move though the buffer at a constant speed v in alternating directions. The drag forces acting on the bead, $F = 6\pi\eta r v$, cause the bead to be offset from the trap centre. The size of this offset, x, is measured and along with the drag force which we can calculate from the bead radius and the velocity of stage movement. The trap stiffness can then be calculated using Hookes law, $F = -\kappa x$. When using this calibration method an accurate bead radius is needed to calculate the magnitude of the drag forces, whilst a good positional calibration is necessary to accurately report the offset of the bead.

2.5 Data Analysis

Steps in the data were found using an automated step-finder algorithm. The technique used to find steps in the data in Chapters 3 and 4 was a moving window t-test algorithm [55]. The data in a window of set size before and after each point was compared to assess the probability of a step having occurred at that point. A t-test is performed comparing the the two windows of data points, when the t-test returns a value above a defined threshold a step is scored. From these steps, those above an upper size limit of 12nm were discounted to avoid scoring detachments and rapid double steps. The size of the window and the threshold value over which a step is scored is varied by the user depending on the data being analysed. A smaller window size allows faster steps to be distinguished in the data however it also leaves the algorithm more susceptible to noise.

Dwell times measure the amount of time between steps. In order for a dwell time to be calculated both the preceding and current steps need to fit the criteria of the step finder above. The end point of the preceding step and the start point of the current step must not be more than 4nm apart, this reduces the chance of incorrectly scoring long dwell times where steps are not resolved. Due to the high positional noise close to the center of the trap, steps that occur below 1.5 pN are not included.

The step detection software is also used to calculate the loads at which the motors detach from the MT. These detachments result in rapid returns towards the trap centre. In order to detect these fly backs the upper size limit of the steps is raised to over 120 nm. The threshold for scoring steps is increased so that only large detachments are detected.

2.6 Backpulls

In order to gain an insight into the behaviour of the motor proteins at high loads it was necessary to perform 'Backpulls'. In a Backpull the stage is moved, forcing the motor to loads above stall force. This stage movement is triggered when the motor has walked to a set load of 4pN. At this trigger point the stage is moved so that the trap centre is shifted towards

the MT minus end, this imposes a greater backwards load upon the motor, a backpull. The load that is imposed on the motor is also set, usually at 8 or 10pN. At these loads motors make mostly backwards steps and so without the stage movements these loads would not be observed. It is possible to use the same mechanism to study the stepping of motors under forwards loads by moving the stage so the trap centre is displaced towards the MT minus end. Examples of traces from Kinesin-1 with backwards pulls are shown in Figure 2.3

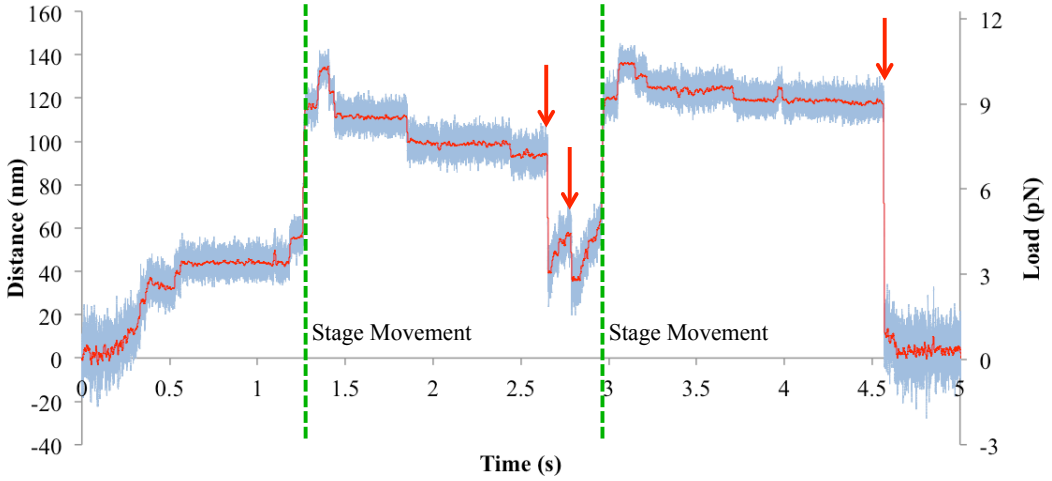

Figure 2.3: Example data from a Kinesin-1 backwards pulling experiment. Green dashed lines show the positions at which the stage movement was triggered, pulling the bead to 10 pN backwards load. The motor then steps backward towards the trap centre before detaching (red arrows). Raw data at 22kHz is shown in blue, a 200 point moving average in red.

2.7 Single Molecule Flow Through

In 'flow through' experiments the initial set up was as in Section 2.3 but the flow cell was not sealed. Once a bead with active motor was found and recorded a further 3-4 cell volumes of assay buffer with 18 nM dimeric Tpx2 was passed through the cell whilst retaining the bead in the trap, recordings were again made before a further 3-4 cell volumes of assay buffer without Tpx2 were passed through the flow cell. In this way the behaviour of the same single motor molecule could be observed in varying conditions.

In order to keep the bead in the trap centre during the flow through its was necessary to keep the bead close to the imaging surface. This was for two reasons, firstly due to boundary layer effects the buffer flows past more slowly close to the surface, making it less likely to drag the bead out of the trap. This means that a lower trap stiffness can be used reducing the chance that other beads flowing past in solution get caught in the trap. The second reason is because of the trap geometry, items above the laser focus in solution get pushed up and away from the trap whereas items below the laser focus in solution get pulled up into the trap. By keeping the focus as near to the lower surface as possible the number of beads that could potentially get caught in the trap is reduced.

2.8 Unbinding Loads

In Chapter 5 a series of experiments to discover the unbinding loads of motors under a variety of conditions are described. In these experiments a bead with a bound motor is moved along a MT at a constant rate, the motor will occasionally bind to the MT and the bead will be dragged out of the trap centre [99]. The load at which the motor unbinds from the MT and the bead returns to trap centre is recorded, Figure 2.4A. This process is performed pulling the bead towards both the plus and minus ends of the MT.

2.8.1 Stage Movement

The unbinding load experiments require the motor to move past the MT at a constant rate. The microscope software was altered to make it possible to drag a bead along a MT in either direction whilst recording the bead position relative to the trap centre on the quadrant detector. Since the quadrant has a small linear region the laser itself is not moved.

As in usual data collection a microtubule was found and marked, the stage was then moved, dragging the motor along the microtubule. The stage of the optical trap can be moved using piezoelectric stepper motors, these motors are capable of moving the stage in 12.2 nm steps. This means that load is applied to a MT bound bead in a stepwise motion. An example reading from a surface bound bead is shown in red in Figure 2.4B along with an example

reading from a Kinesin-1 motor binding and releasing a MT in blue.

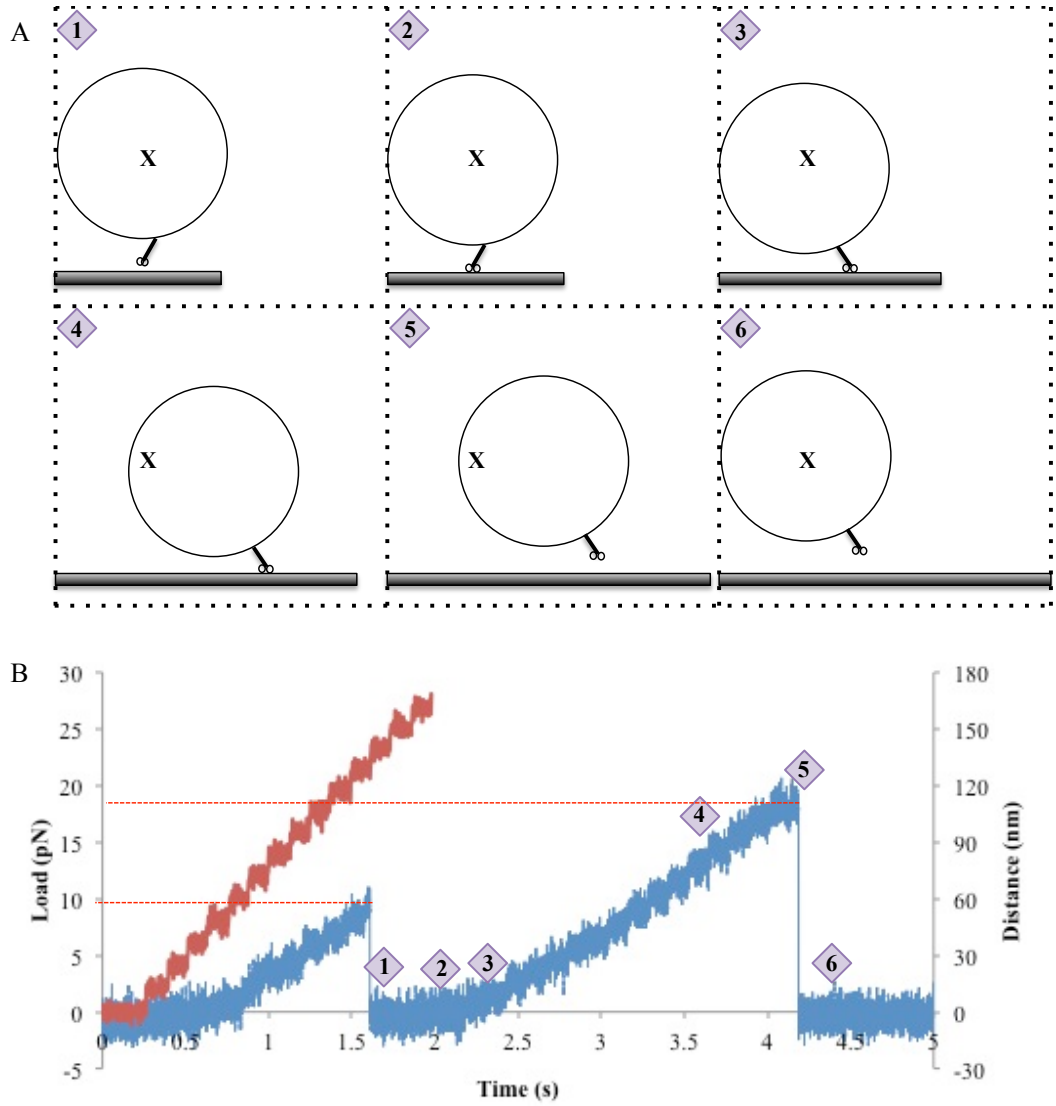

Figure 2.4: A) Cartoon showing the stages in an unbinding load experiment. 1, Bead in trap centre and motor not MT bound; 2, Motor binds to moving MT; 3, MT moves with the motor attached;. 4, MT continues moving with motor attached pulling the bead away from the trap centre; 5, Motor detaches from the MT; 6, Bead and motor return to trap centre, MT continues moving. B) Example traces from a surface bound bead in red an a Kinesin-1 motor in blue, traces were collected at 22kHz. The gradient of the Kinesin-1 bound bead is shallower due to compliance in the linkages between the slide and the bead. The Unbinding loads for this trace are measured as 10 pN and 18 pN (red dashed lines). Positions on the trace given by purple diamonds correspond to stages in the motor binding experiment as depicted above.

2.8.2 Loading Rates

The rate at which load is applied can make a large difference in the distribution of the unbinding loads. The load dependent unbinding of the motors can be given by;

$$\tau(F) = \tau(0) \exp^{-Fd/k_bT} \tag{2.2}$$

Where τ is the load dependent lifetime of the motor-MT binding, F is the backwards load, d is a characteristic distance and $\tau(0)$ is the unloaded lifetime of MT binding. T is the temperature and k_b is the boltzmann constant. Since we are applying load at a constant rate then in our experiments $F = \alpha t$. If the loading rate, α, is not kept constant the load at which the motor unbinds will change, with faster loading rates leading to higher unbinding loads.

The easiest way to vary the loading rate is to change the speed of stage movement. It is not possible to vary the trap stiffness significantly as high trap stiffnesses of 0.1-0.2 pN/nm are required for detachments to occur within the linear range of the detector. Several different speeds of stage movement were investigated, however it was found that high stage velocities led to a greater range of loading velocities due to variation in the stiffness of the linkages between the bead and the surface of the slide, Figure 2.5A.

The variation in loading rate for Kinesin-1 with 5μM ATP and 100 nm/s stage movement is uniformly distributed from 1 - 15 pN/s, Figure 2.5B . As can be seen from Figure 2.5C this leads to a smearing of the detachment rates. The faster loading rates give a higher load distribution of unbinding forces. For this reason data was collected from stage movements of 100 nm/s and then windowed to include only a small range of loading rates.

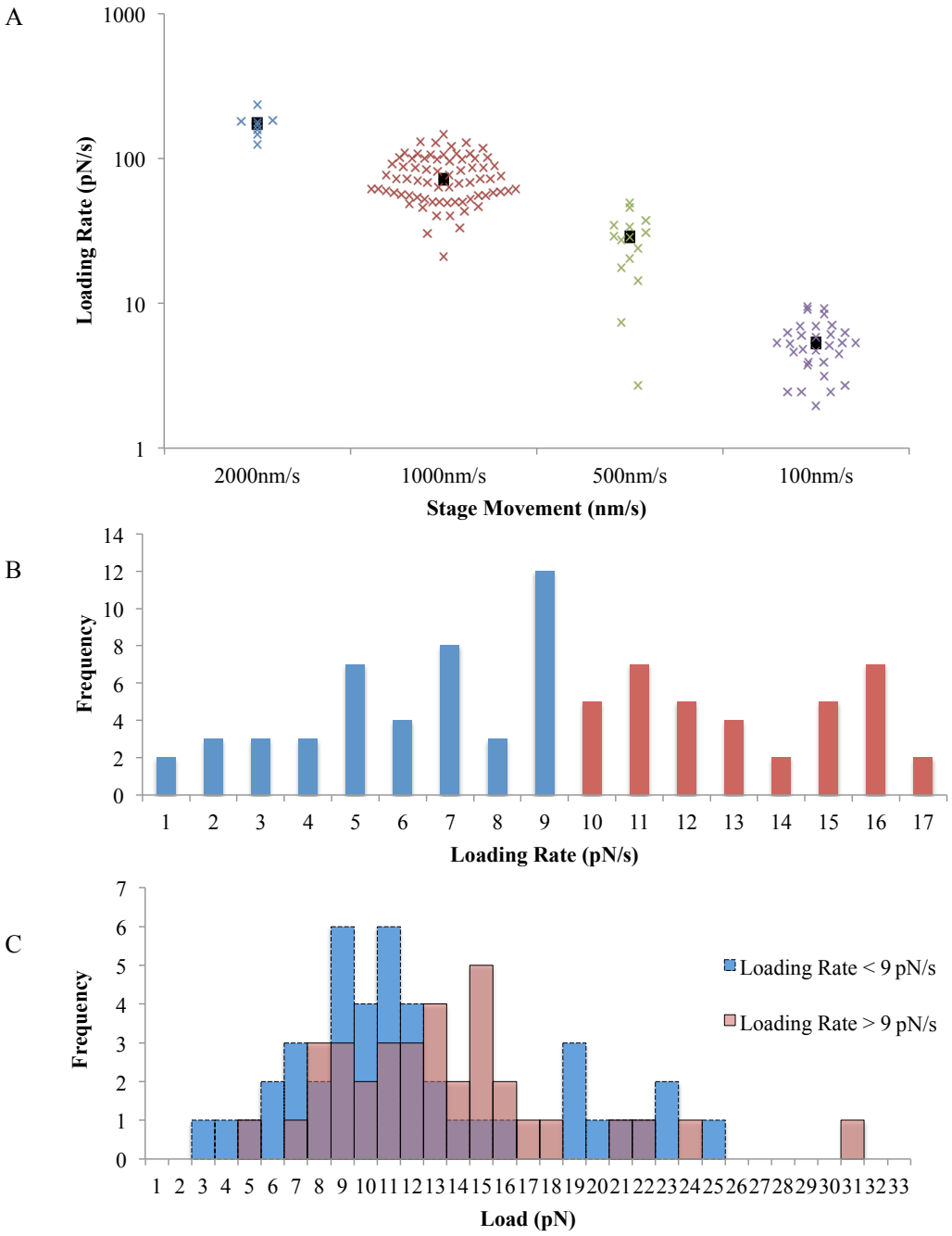

Figure 2.5: A) Loading rate distributions for 4 different stage movement velocities. Faster stage movements have a larger range of loading rates. B) Loading rates from Kinesin-1 with 5μM ATP, gathered using the 100nm/s stage movement. Loading rates are grouped in to 1pN bins, values below (blue) and above (red) 9pN are marked. C) Unbinding loads for Kif15-1293 with 5μM ATP split in to data gathered with minus end directed loading rates below 9 pN/s (blue with dashed line) and above 9 pN/s (red with undashed line).

2.8.3 Data Analysis

The data from the unbinding experiments were recorded from on-screen values. For each trace the load at detachment and the average loading rate in the 450 ms before detachment were recorded, Figure 2.4B. When comparing data sets the data was cropped so that for each set of data the loading rates were similar and only a small range of loading rates was used. The loading rate depends on several variables, the rate of stage movement, the stiffness of the optical trap, and the stiffness of the motor and MT linkage. The loading rate can vary over a single recording as different parts of the same MT are bound to the surface with different stiffnesses. If the motor is able to step along the MT to either end then this might also affect the loading rate. In cases where the bead does not return to the trap centre after a detachment (a backward slip greater than 16nm) the second detachment is discounted.

Chapter 3

Results: Full Length Kif15 Single Molecule Mechanics

The single molecule properties of the Kinesin-12 motor protein, Kif15, have previously been unknown, making interpretation of its *in vivo* function difficult. Using full-length His-hKif15 (Kif15) molecules and an optical trap the single molecule mechanics of Kif15 motors under load have been examined. Optical trapping allows us to collect data on the stepping behaviour of molecular motors under varying loads. Data on the better characterised Kinesin-1 was also collected for comparison purposes. These experiments demonstrate that Kif15 is a processive kinesin motor protein capable of moving at velocities of approximately 140 nm/s and moving forwards under loads of up to 6 pN. These experiments were performed alongside single molecule TIRF and MT gliding assays performed by H.Drechsler [34].

3.1 Confirmation of Single Molecule Conditions

An important first step in performing single molecule experiments using the optical trap is to calibrate the concentration of motor necessary to achieve a high likelihood that motile beads will be bound by only one motor. For this purpose the fraction of beads, which show MT binding is evaluated at varying concentrations of motor. If a first order Poisson curve can

be fit to these data points this indicates that one motor bound to a bead is sufficient for MT binding. The forms of the first and second order Poisson equations are given below;

$$\rho(C > 0) = 1 - \exp(-\lambda_1 C) \tag{3.1}$$

$$\rho(C > 1) = 1 - \exp(-\lambda_2 C) - \lambda_2 C \exp(-\lambda_2 C) \tag{3.2}$$

C is the number of motors per bead and λ is the binding coefficient. The value of λ gives a measure of the affinity of the motors for the beads, a higher value corresponds to greater affinity. When fewer than 30% of beads bind to the MT and the data are best fit by a first order Poisson curve, Equation 3.1, the probability that we are observing the behaviour of a single molecule from a bead is 95%. If we assume that motors will bind uniformly and randomly to the beads then the probability that two motors bind to the MT simultaneously is decreased still further as it is unlikely given the large bead size in comparison with motor tether length (See Appendix) that two motors will be bound close enough to simultaneously bind the MT.

As can be seen from the data in Figure 3.1 and the fits in Table 3.1, a first order Poisson fit is the best description for the binding of both Kinesin-1 and Kif15 motors. The first order

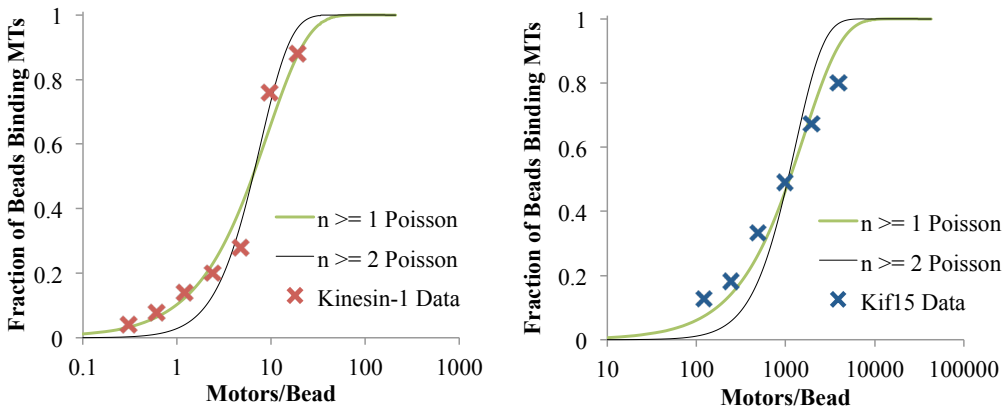

Figure 3.1: Fits of 1st order (green) and second order (black) Poisson curves to data from Kinesin-1 (left, red) and Kif15 (right, blue) bead binding experiments. For both Kinesin-1 and Kif15 the first order curve is a better fit indicating that only one motor is necessary to bind a bead to the MT.

	λ_1	λ_2	RSS1	RSS2
Kinesin-1	0.11	0.26	0.029	0.033
Kif15	0.00063	0.0016	0.024	0.11

Table 3.1: Poisson fit coefficients and corresponding Residual Sum of Squares for the fits to the data shown in Figure 3.1. The first order equation gives a lower RSS value for both Kif15 and Kinesin-1 data.

binding coefficient λ_1 for Kinesin-1 is 1700 times that for Kif15. As such Kinesin-1 has a 1700 times greater affinity for the polystyrene beads than Kif15. The importance of this will be seen in the next section.

For the rest of the experiments performed in this section the concentration of Kif15 incubated with beads was such that less than one third of beads bound to the MTs, ensuring that the majority of motility seen on these beads was the result of only one molecular motor. Since Kif15 has been shown to be a tetramer at the ionic strengths used in these experiments it is not clear whether any movement seen is the result of one or two pairs of heads interacting with the MT.

3.2 Kif15 and Kinesin-1 Unloaded Velocities

A first step in examining the single molecule mechanics of Kif15 was to investigate the velocities of unloaded beads along MTs. The initial results for both Kif15 and Kinesin-1 are shown in Figure 3.2A. As expected Kinesin-1 velocities are fast and distributed around a mean of 670±22 nm/s, Kif15 however shows two populations of velocities. The lower Kif15 population has a mean velocity of 140±12 nm/s, whilst the second, higher velocity population has a mean of 738±11 nm/s, Figure 3.2A. The velocity of the slower population of Kif15 corresponds to those seen in single molecule TIRF experiments [34], however in these fluorescence experiments no faster motors were seen.

As can be seen in Figure 3.2B. Kif15 beads show a variety of behaviours upon MT binding. At all motor concentrations more beads bind without moving than move either quickly or slowly along the MT. At concentrations where fast motility is seen there are more slow than

fast moving motors. Kif15 motors often pause at MT tips, and are capable of sustaining load whilst bound there, a behaviour not seen for Kinesin-1. Pausing behaviour, both on the lattice and at MT plus tips, is also seen in TIRF data along with diffusional movement along the MT. Diffusional movement is not easily seen in the trap, when a load is applied the bead will not be able to move from the trap centre. For unloaded beads diffusion of the motor over short distances would be indistinguishable from the brownian motion of the bead itself.

There are several possible explanations for the discrepancy between the TIRF and trapping data. Firstly the higher velocity Kif15 population could be the result of an alternative regulation state of Kif15 in the bead assay, possibly induced by conformational changes of the motor when binding to the beads. A second explanation is that the high velocity motors represent a low level Kinesin-1 contamination from the insect cells used in the expression of the Kif15 protein. Given the substantially higher affinity of Kinesin-1 for polystyrene beads this is a possibility. If this were the case then a ratio of one Kinesin-1 molecule to every 2500 Kif15 molecules would account for the proportion of faster motors. Using polyacrylamide gel electrophoresis, contaminations at this level could not be detected.

3.3 Kif15 Displays Two Populations of Motor Velocities

The high velocity Kif15 population not only displays Kinesin-1 like velocities but has a load bearing ability very similar to Kinesin-1, Figure 3.3A. These high velocity beads step rapidly away from the trap centre and slow to stall at around 6pN where clear forwards and backwards steps can be seen. This is strikingly different to the load bearing ability of the lower velocity traces in Figure 3.3B. In this trace the trap stiffness is higher than in the Fast Kif15 trace so a similar load is equivalent to a shorter distance . These motors make much shorter excursions from the trap centre, indicating that they are either less processive or more sensitive to load. The slower moving motors rarely reach loads of greater than 5pN even at high trap stiffnesses.

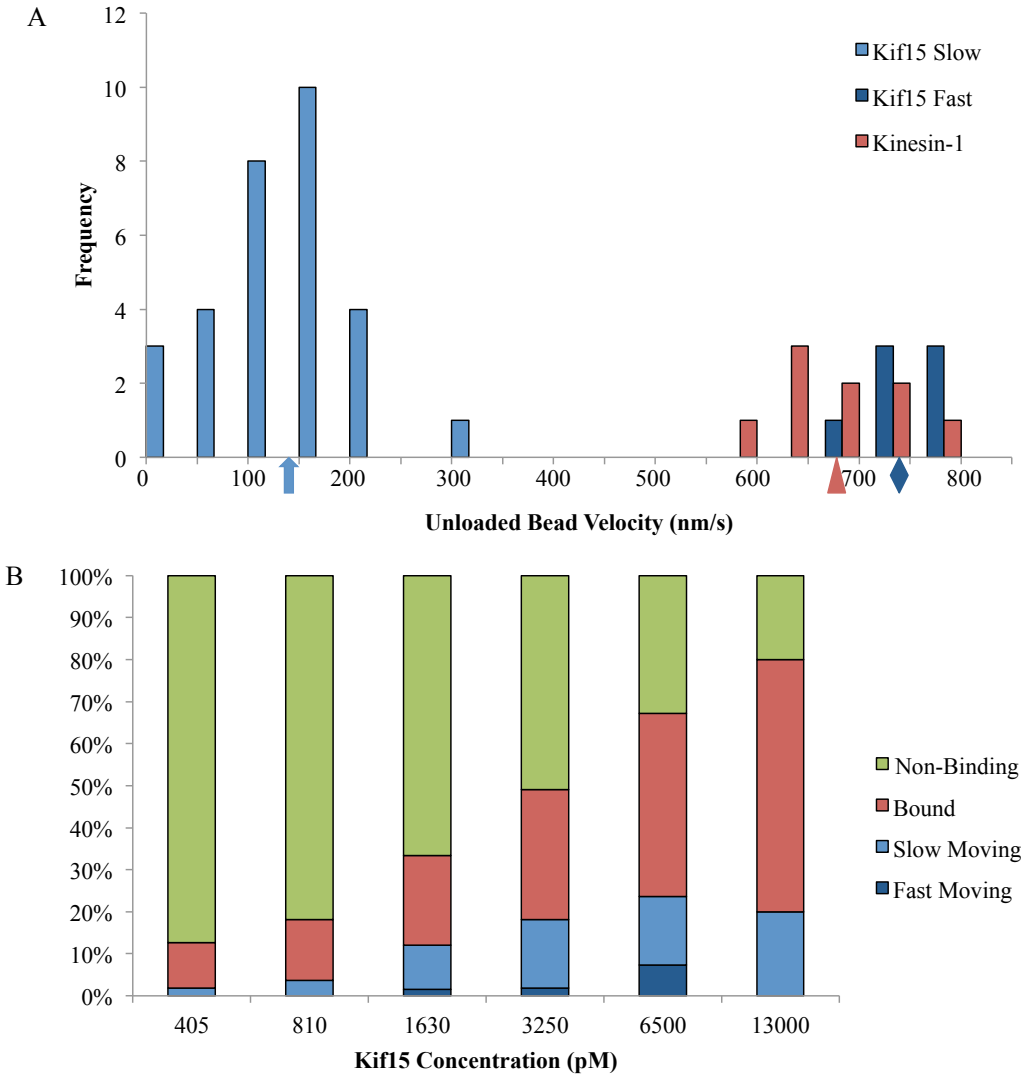

Figure 3.2: A) Distribution of unloaded bead velocities for beads coated with Kif15 (blue) and Kinesin-1 (red), 50nm bins. The Kif15 distribution is split into two populations. Inset) The lower velocity population has a mean velocity of 140±12 nm/s (blue arrow). The high velocity Kif15 population has a mean of 738±11 nm/s (blue diamond) similar to Kinesin-1 at 670±22 nm/s (red triangle). B) Frequency of the outcome of Kif15 coated beads introduced to the MT (>= 2 MTs for 30s) over a range if Kif15 concentrations. A significant proportion of beads that bind the MT do not show motility. At all motor concentrations more beads move slowly than quickly along the MT. For motor concentrations below 13000pM $n > 50$, for 13000pM n=30.

We attempted to distinguish whether the fast moving motors represented an alternative regulation state of Kif15 or if they were a contamination of Kinesin-1 incurred during the

purification process. If the former were true then it is unlikely that the proportion of differently binding/alternately-regulated motors would change from experiment to experiment. With this in mind Kif15 from two different protein preparations were compared. As can be seen in Figure 3.4A no statistically significant difference in the ratio of fast to slow moving motors across the two protein preparations was found, however the sample size was small for both experiments.

A second approach was to attempt to deplete a solution of GFP-hKif15 using anti-GFP antibodies to pull down the GFP-hKif15 protein and then check for the presence or absence of fast motors in the depleted solution. The results shown in Figure 3.4B show that the GFP-Kif15 solution had a high proportion of fast motors, however depletion of GFP-Kif15 in this solution made no significant difference. Both the GFP-Kif15 and anti-body depleted conditions had a much higher proportion of fast motors compared to the His-hKif15. When the GFP-Kif15 was examined by H.Dreschler using TIRF microscopy very few active motors could be seen. This lends support to the theory of contamination. If the GFP tagged motors in the GFP-Kif15 are inactive then it is likely that the fast moving motors in the bead experiments are unlabelled contaminants.

It is not possible from the data above to entirely rule out either explanation for the two Kif15 populations, however it is clear from agreement with single molecule fluorescence experiments that slow moving, low load bearing beads represent the movement of Kif15 motors and it is this population that are focused on in the following experiments and analysis.

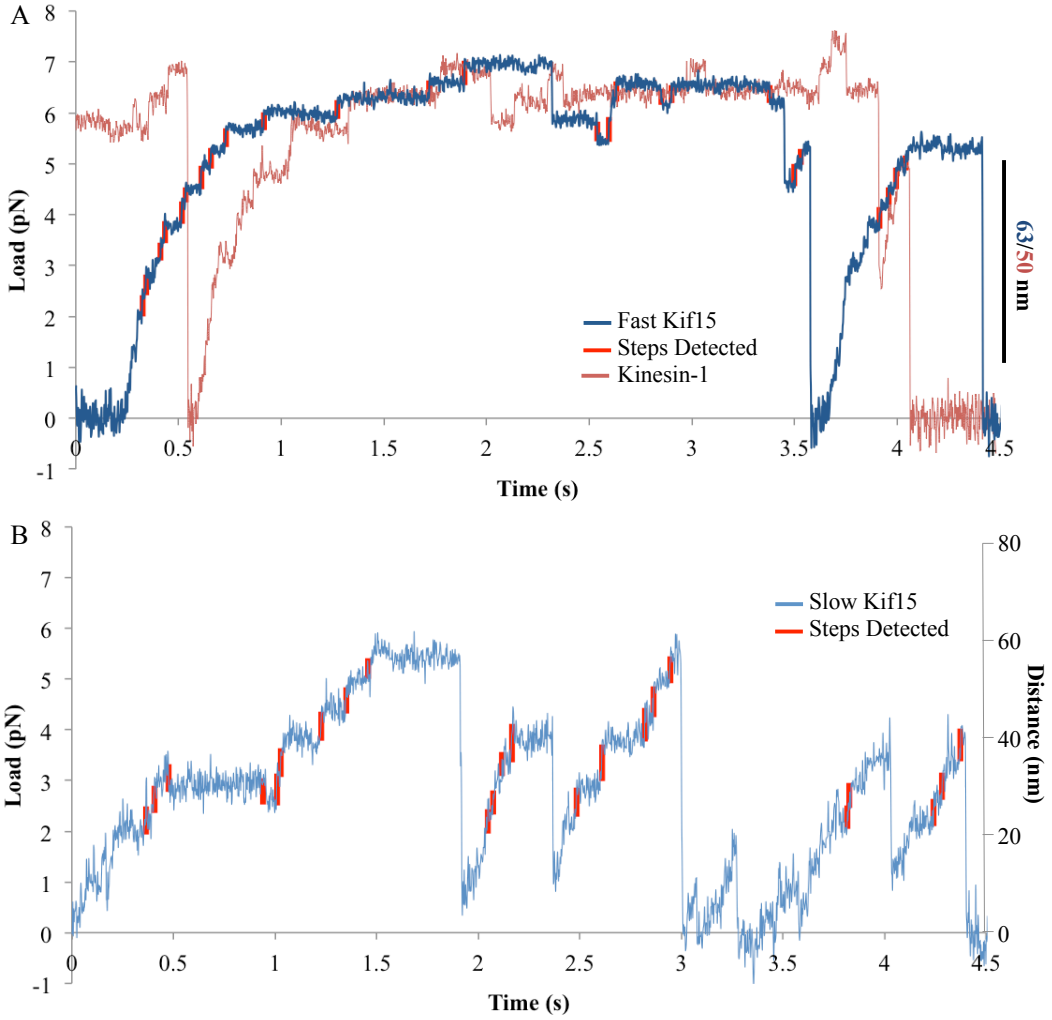

Figure 3.3: Example A) Fast and B) Slow Kif15 traces. A) Fast moving Kif15 motors show similar load dependent behaviour to Kinesin-1. In these example traces both the Kif15 and Kinesin-1 motors slow to a stall at around 6pN, both show clear 8nm steps in both the forwards and backwards directions. Trap stiffnesses are 0.063 pN/nm and 0.081 pN/nm for Fast Kif15 and Kinesin-1 respectively. B) Slow Kif15 traces show obviously different behaviour to Kinesin-1, they reach lower loads and step more slowly. Trap stiffness for this trace is 0.095 pN/nm. Traces were collected at 22kHz and have been filtered using a 50 point moving average and then sample down to 450Hz. Marked in red are the steps detected using a t-test based algorithm.

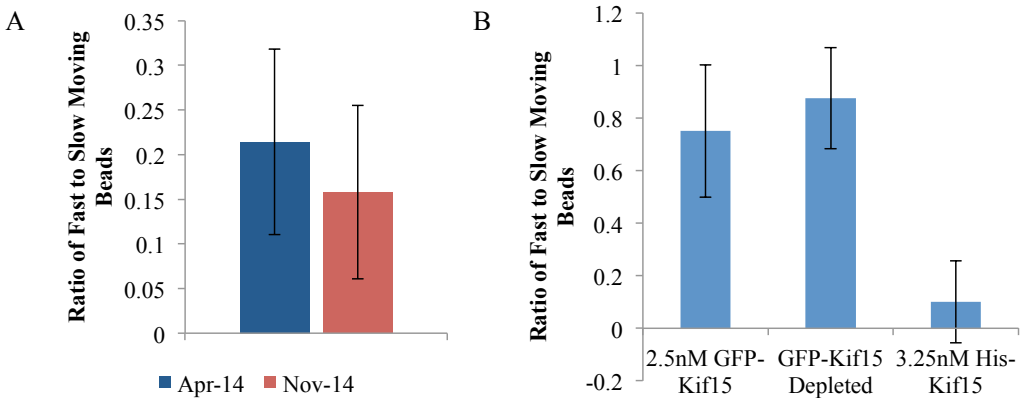

Figure 3.4: A) Proportion of moving motors with velocities greater than 400nm/s for beads from two different protein preparations, one in August 2014 and one in November 2014, no significant difference can be seen. Error bars show 95% confidence intervals. B) Proportion of moving motors with velocities greater than 400nm/s for beads incubated with GFP-Kif15, a GFP-Kif15 depleted solution and His-Kif15. The proportion of fast moving motors on the His-Kif15 beads is significantly less than for the other two solutions. Error bars show 95% confidence intervals.

3.4 Kif15 Step Size

In order to quantitatively investigate the load dependence of Kif15 and Kinesin-1, traces displaying 8 nm steps, such as those in Figure 3.3, were collected. Using the step detection software described in Chapter 2, steps were found in Kif15 and Kinesin-1 traces. Figure 3.5 shows the step size distributions for both the fast and slow Kif15 populations and Kinesin-1. The mean step sizes are summarised in Table 3.2. All mean step sizes are less than 8 nm which is expected for optical trapping data where a fixed trap is used and no compliance correction is applied to the data. This is due to increasing load with each step causing an extension of the linkages between the bead and the surface, meaning that the bead movement will always report back a smaller distance than the motor has moved. Both the Kif15 populations produce steps of amplitude similar to Kinesin-1, which are known to be 8 nm in size [100].

	Step Size Forward (nm)	$n_{forward}$	Step Size Backward (nm)	$n_{backward}$
Kif15 Fast	5.48 ± 0.02	4851	5.4 ± 0.1	887
Kif15 Slow	6.2 ± 0.1	314	6.8 ± 0.3	55
Kinesin-1	5.75 ± 0.03	1864	5.4 ± 0.1	583

Table 3.2: Mean step sizes with S.E and number of steps detected for forward and backward steps of Kif15 and Kinesin-1.

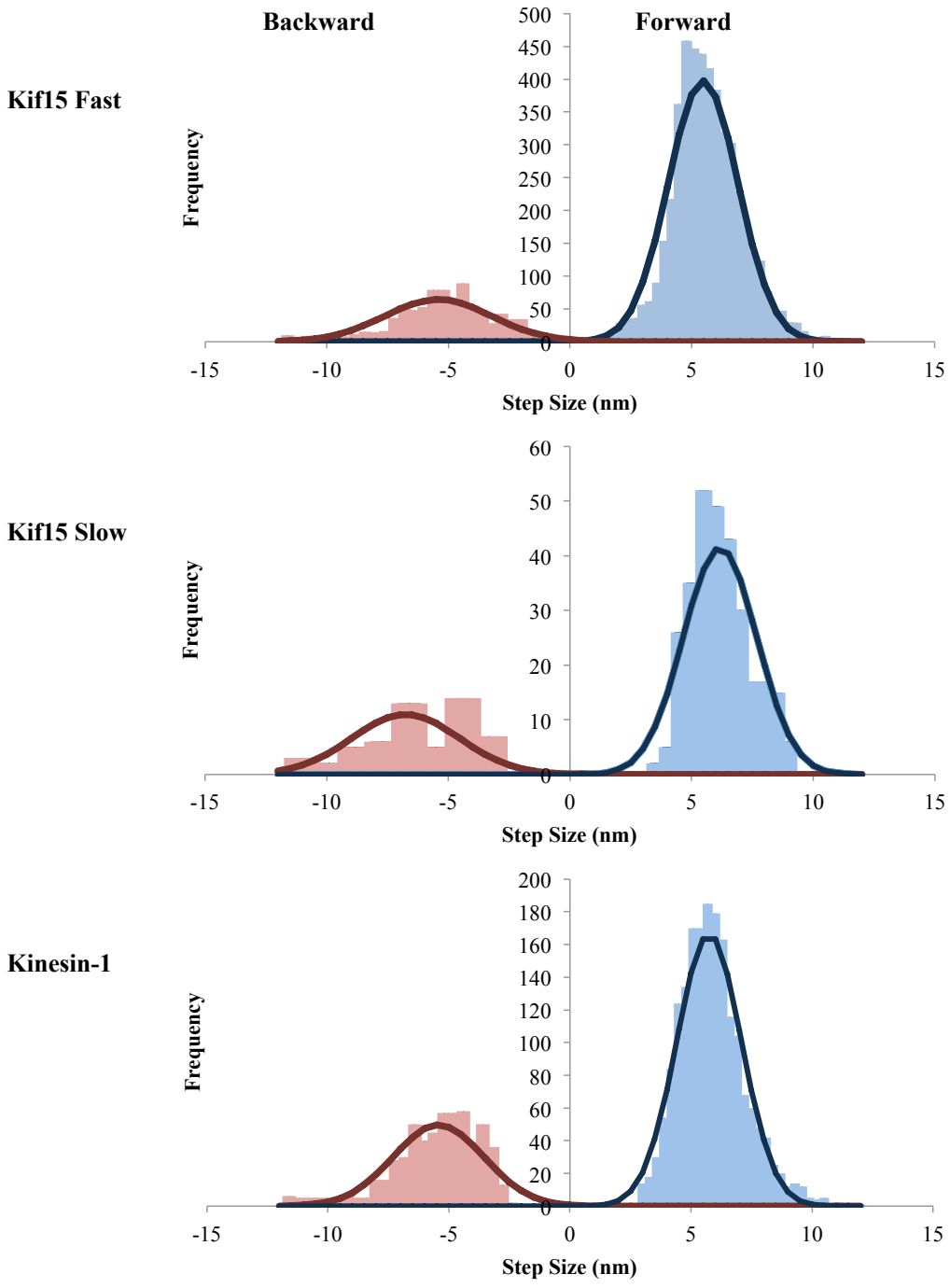

Figure 3.5: Step Size distributions for Kif15 and Kinesin-1, normal distribution curves have been fit to the forward (plus end directed) and backward (minus end directed) step distributions. The number of steps detected and the parameters for these curves are given in Table 3.2

3.5 Kif15 Load Dependence

Having detected steps in the data and confirmed that Kif15 makes steps of similar size to Kinesin-1, we then examined the effect of load on the rate of stepping for each motor. The times between consecutive steps are called dwell times, this is the time that the motor spends bound to the MT between steps. A low dwell time therefore corresponds to a high stepping rate and, in regions where steps are predominantly forward steps, a high velocity. Dwell time plots include data for both forwards and backwards steps. Below 1.5 pN the system stiffness is lower and the traces have high Brownian noise, so It is very difficult to detect steps at these low loads and no data from loads below 1.5 pN is included in the analysis.

At 2pN the mean dwell time for slow Kif15 motors is ∼100ms whereas for Kinesin-1 it is ∼25ms. As backwards load on the motors increases the dwell times also increase, Figure 3.6B. At loads above 7pN the dwell times for Kinesin-1 remain fairly constant at ∼160ms. Fast Kif15 has very similar dwell times to Kinesin-1 in the range of 2 to 7 pN. Above 7 pN the dwell times of Fast Kif15 and Kinesin-1 diverge, in this range data is gathered by the use of backpulls as described in Section 2.6.

The stall forces of the fast Kif15 motors and Kinesin-1 are also very similar, the stall force of Kinesin-1 is 6.8 ± 0.8 pN and for fast Kif15 it is 7.0 ± 0.7 pN, Figure 3.6B . From the similarity of their load bearing behaviour it seems very likely that the fast Kif15 and Kinesin-1 motors are in fact both Kinesin-1 motors. Any discrepancies in their high load dwell time data or stall force could be due to the comparatively small amount of data at these loads. Alternately the different sequences of the *Drosphila* Kinesin-1 and the *Spodoptera frugiperda* Kinesin-1 from the Sf9 cells used for the the Kif15 purification could cause small differences in motor mechanics. Additionally differences could arise from different post translational modifications or the presence of kinesin light chains. From here on references to Kif15 concern the slow moving motors only.

For slow Kif15 there is little data collected above 5pN and levelling out of dwell times cannot be seen. It has been hard to collect traces displaying steps for slow Kif15 motors as they

are less consistent in their movement than Kinesin-1. Motors frequently cease to walk on MTs and there are a large proportion of non-motile motors present. In order to study single molecule mechanics only 30% of beads should bind the MTs and as seen in Figure 2B this means that for Kif15 only 10% of beads will show movement.

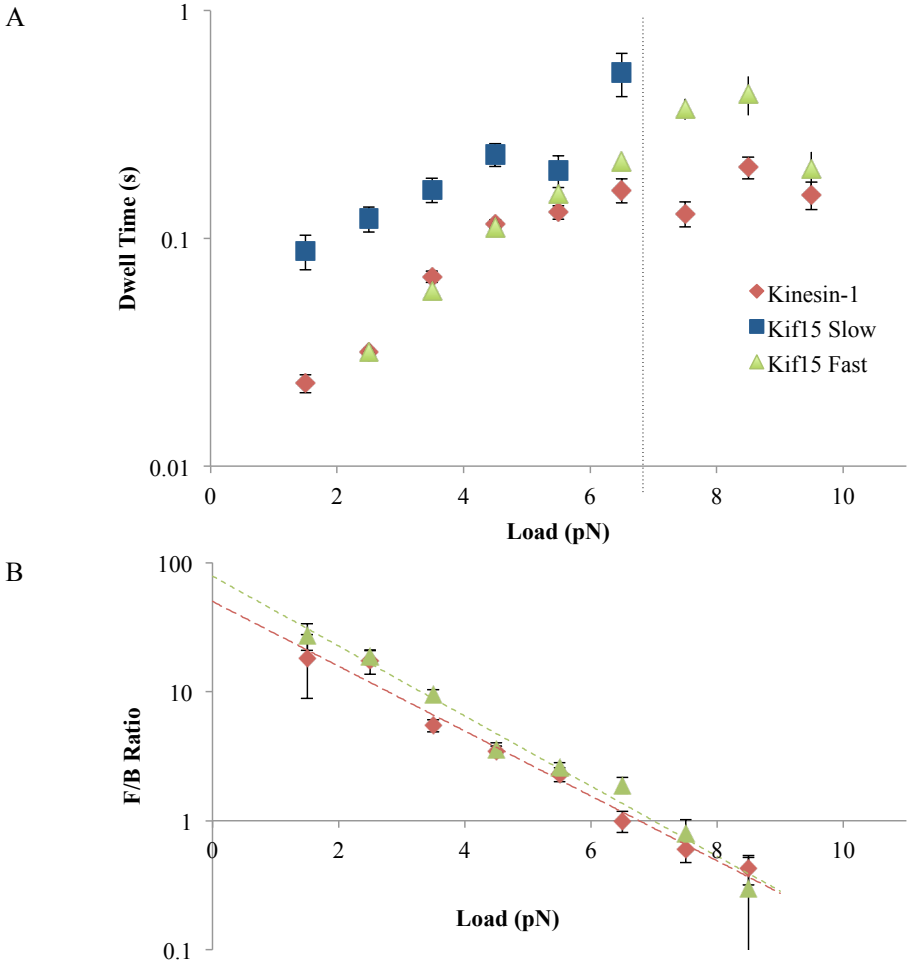

Figure 3.6: A) Dwell time distributions for Fast and Slow Kif15 and for Kinesin-1. Shown are the mean and S.E values for 1pN bins of dwell time values. A dwell is the time that the motor waits between steps. All three motors show an increase in dwell time at higher loads. Above Stall (dotted line), Kinesin-1 dwell times are constant. No flattening off is seen for Slow Kif15, although there is little high load data. B) Ratio of forward to backward steps for Kinesin-1 (red) and Fast Kif15 (green), loads from 1.5 pN to 8.5 pN. Dotted lines are least squares fitted exponentials.

3.6 Kif15 Processivity

A further complication for trapping with Kif15 is its low processivity, unlike Kinesin-1, Kif15 has a short run length when under load. This means that at low trap stiffnesses Kif15 will often detach before it reaches stall force. For example the two traces in Figure 3.7 show the movement of the same Kif15 motor walking in different trap stiffnesses. At low trap stiffness, 0.045 pN/nm, the motor rarely reaches loads of above 1.5 pN whereas at a trap stiffness of 0.113 pN/nm, the motor can walk forwards under loads of up to 4 pN. Figure 3.7C shows the average detachment loads for a Kif15 motor when different trap stiffnesses are used. As the trap stiffness increases the mean detachment load also increases. This behaviour continues within the range of trap stiffnesses used. This indicates that within this range it is the run length of Kif15 and not its ability to step under load that that is limiting its progress.

Long run lengths of 1900nm are recorded for Kif15 using single molecule fluorescence [34], and the motor can often move unloaded beads over distances greater than 1 bead diameter (560nm) in the trap. However even under low backwards loads it is rare that the motor moves the bead more than 80nm from the trap centre. Using our optical trap, it is not possible to measure the run lengths of the motors directly. Increasing load on the motors as they step away from the trap centre leads to a rotation of the bead in the trap and stretching of the bead tether. The movement of the bead in a fixed trap cannot therefore report the movement of the motor from the moment of MT attachment to detachment and accurately estimate the distance moved by the motor in this time. Only if a constant load were to be applied to the bead, as in an optical trap using force feedback, would it be possible directly measure the effect of load on run length.

The average uncorrected size for steps in the Kif15 data is 6.4nm, even large Kif15 bead displacements of 80nm therefore only correspond to a motor movement of approximately 12.5 steps or 100nm. This is clearly different from the unloaded run lengths of Kif15 and shows that under load Kif15 is less processive. This dramatic change in Kif15 processivity could be due to a second diffusive binding region as suggested in Sturgill et al. [33]. When unloaded this could, help unbound Kif15 motor domains to rapidly rebind the MT allowing

continuous motion of the unloaded motor. This is also consistent with the diffusive motion seen for full length Kif15 in TIRF [34].

The presence of a second diffusive binding region might be expected to affect fly back times when the motors detach from the MT and return to the trap centre. For Kif15 both fast and slow returns to trap centre are seen as shown in Figure 3.7D, where as for Kinesin-1 slow returns to trap centre are not seen. Slow returns to trap centre suggest that the motor is still in contact with the MT and is creating drag slowing the movement of the bead back to zero load. This behaviour is never seen in Kinesin-1 data.

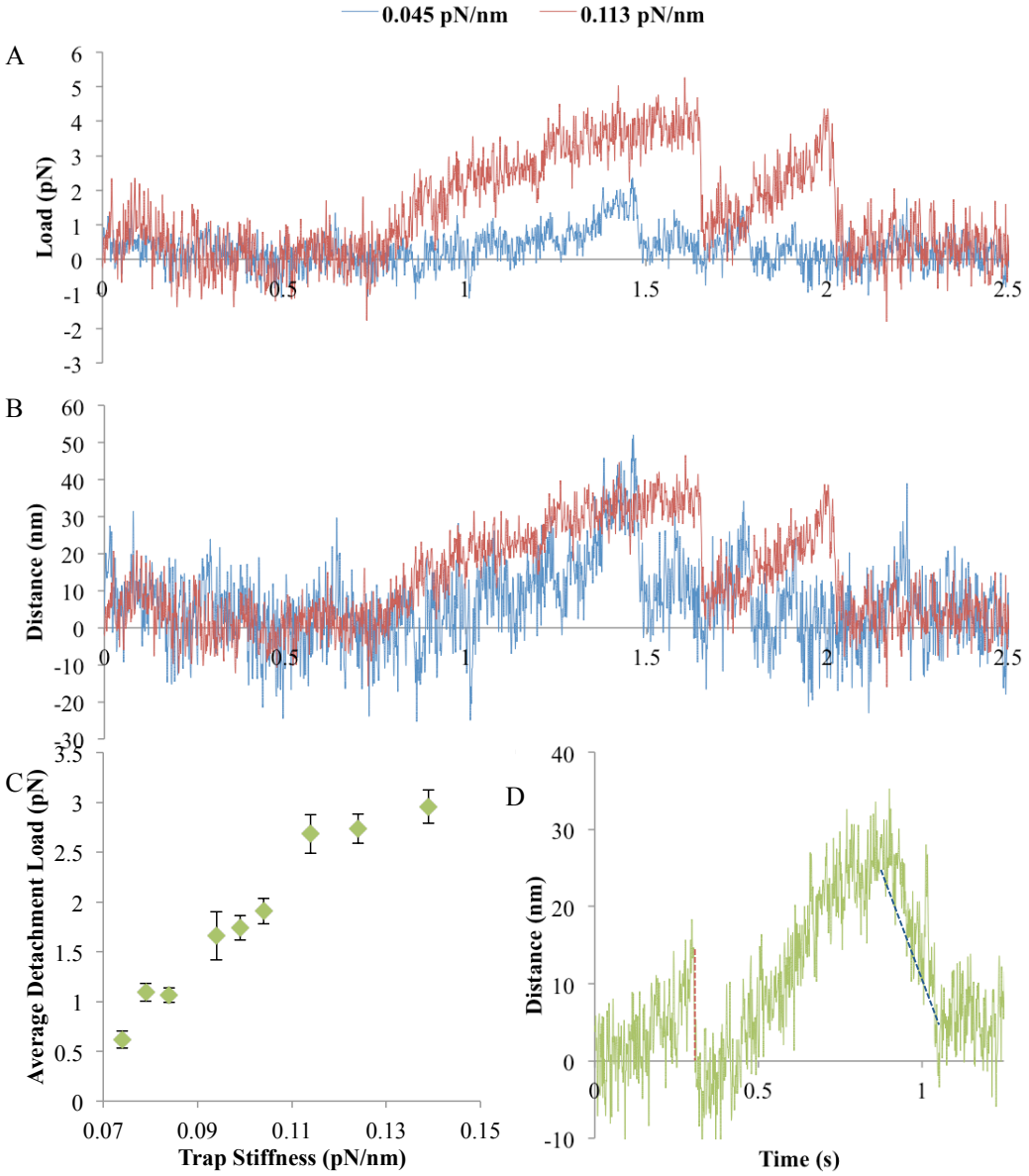

Figure 3.7: A & B) Example Kif15 traces for the same bead taken at trap stiffnesses of 0.045pN/nm (blue) and 0.113pN/nm (red). The traces are share the same load axis (A) and distance axis (B). Traces were collected at 22kHz and have been filtered using a 50 point moving average before sampling down to 450Hz. C) The average detachment loads for a series of traces from the same motor produced at varying trap stiffnesses are shown. The average detachment load increases with increasing trap stiffness. D) Example trace showing a fast (red) and slow (blue) return to trap centre. The trace was collected at 35.5kHz and has been filtered using a 50 point moving average and sampled down to 700Hz.

3.7 Comparision with Full Length Human Eg5

As described in Chapter 1 the single molecule behaviour of both the full length *Xenopus* Eg5 and a dimeric human Eg5 have been investigated [46, 93]. Eg5 is known to be less processive and to be less sensitive to load than Kinesin-1. There is some disagreement as to the effect of load on the run length of Eg5, with dimers still making several steps at loads up to 7 pN whilst the *Xenopus* tetramer detaches at loads of about 3 pN. We attempted to characterise the tetrameric human Eg5.

The short run length of Eg5 makes it difficult to use in the trap as most of the steps taken by the motor will act to rotate the bead in the trap rather than cause displacement. Several Eg5 traces were gathered and are shown in Figure 3.8A. These traces agree with the known data. They have short run lengths of less than 50 nm and they detach at low loads. Since the velocity does not change significantly under load a rough estimation of the velocity of the motors can be made by examining the gradient of the trace, Figure 3.8. This gives a minimum estimate of the velocity of approximately 50 nm/s. This is in keeping with reports on the velocity of human Eg5 dimers at 70 nm/s under 1pN backwards load [46]. The run lengths seen for Eg5 coated beads under load and the lack of processivity of unloaded Eg5 coated beads suggest that although Kif15 is not as processive under load as Kinesin-1 it is probably more processive than Eg5.

3.8 Addressing Kif15 Conformation

The conformation of Kif15 when bound to the beads is unknown as motors bind to the polystyrene beads non-specifically. It is not clear whether Kif15 tetramers are able to bind the MT with one or two pairs of motor heads. Two approaches have been used to address this issue, firstly the use of antibodies to bind the Kif15 to the beads, thus setting the orientation of Kif15 so that is is bound by its His-tagged motor domains, this was unsuccessful. A second approach was to increase the ionic strength of the bead incubation solution forcing the Kif15 tetramers to dissociate and bind the beads as dimers.

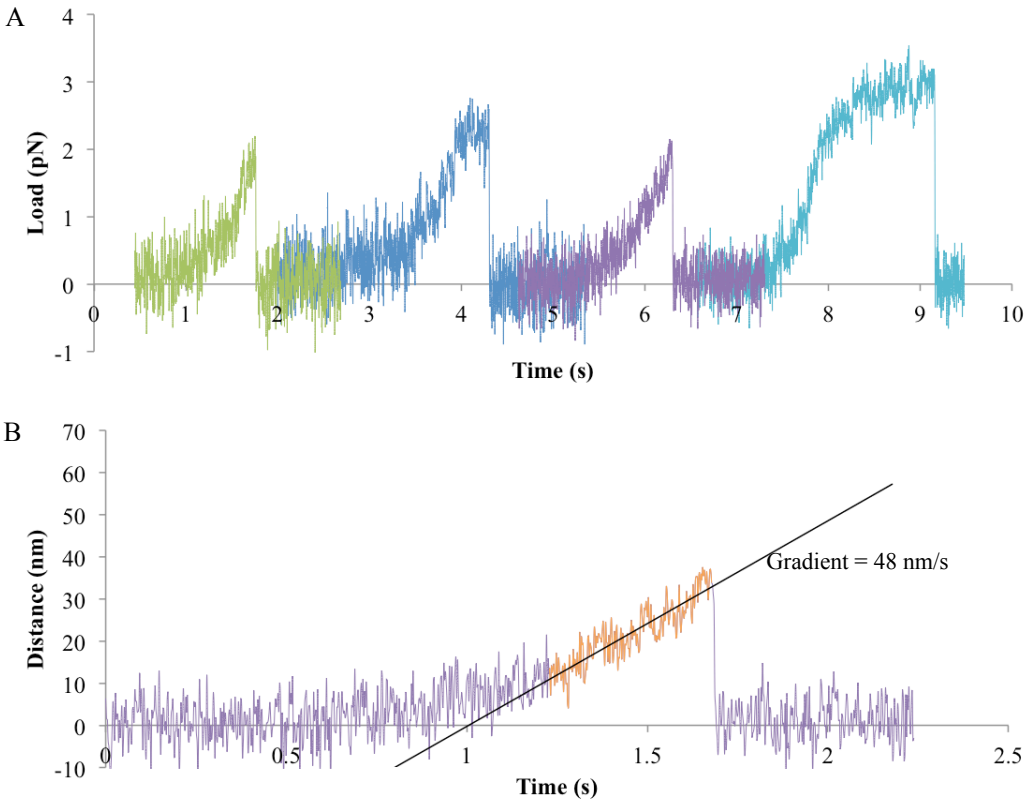

Figure 3.8: A)A Selection of Full Length Human Eg5 traces. Traces were collected at 22kHz and have been filtered using a 50 point moving average. Trap Stiffness was approximately 0.065 pN/nm. B) Eg5 trace (purple trace from top) with a linear least squares fit to orange section, the gradient of the fit is 48 nm/s.

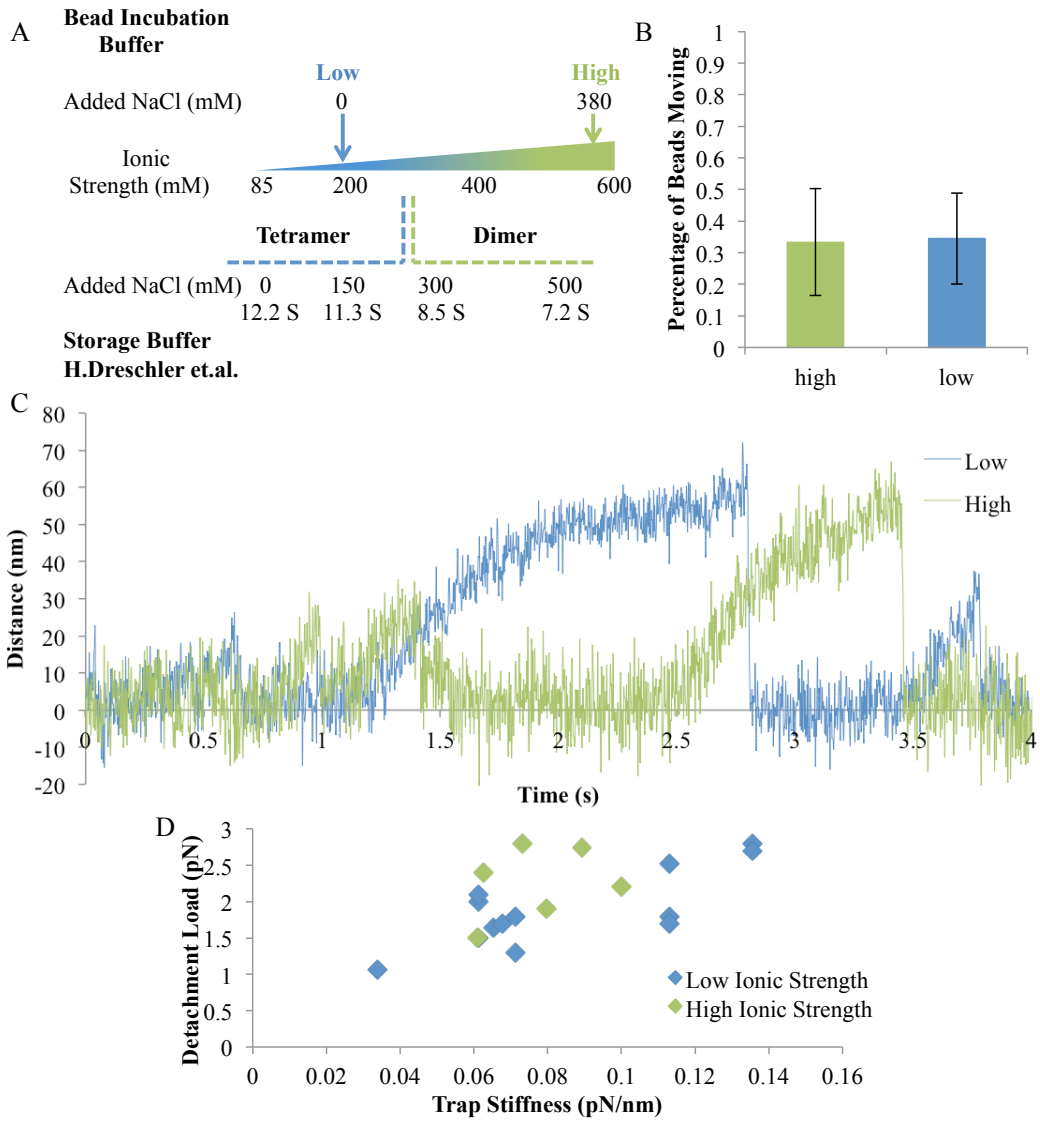

Figure 3.9: A) Schematic comparing the ionic strengths used in bead incubations with those used by Drechsler et al. [34]. Drechsler et al. show that Kif15 changes from a mostly tetrameric state at low ionic strength to a mostly dimeric state at high ionic strengths. The bead incubation buffer consists of 80mM K.PIPES (pH 7.0), 2mM $MgSO_4$, 1mM DTT and 3mg/ml D-Glucose. The storage buffer used by Drechsler et al. contains, 35mM Sodium Phosphate (pH 7.0), 1mM $MgCl_2$, 1mM EGTA, 0.1mM ATP. The sedimentation coefficients (S) determined for each ionic strength by Drechsler et al. [34] are shown. B) Percentages of binding beads which move along the MT for low salt (80mM PIPES) and then high salt (80mM PIPES + 380mM NaCl) incubations. C) Example traces for high (green) and low (blue) salt bead incubations. Traces were collected at 22kHz and have been filtered using a 20 point moving average before down sampling to 450Hz. Trap Stiffnesses of 0.07 and 0.09 pN/nm were used for high and low ionic strengths respectively. D) Mean detachment loads for high (green) and low (blue) salt bead incubations under varying trap stiffnesses.

3.8.1 High Ionic Strength Incubations

It has been shown that the ratio of tetramers to dimers in Kif15 solutions decreases at higher ionic strength [34], Figure 3.9A. By incubating Kif15 at high ionic strength before introduction to the beads, the chance that a motor binds a bead in the dimeric state is increased. A concern was that this high ionic strength might begin to denature the protein or decrease its affinity for binding the bead. As shown in Figure 3.9B, incubation with 380mM NaCl and 80mM PIPES, equivalent in ionic strength to the high salt conditions used by Drechsler et al. [34] showed no change in the proportion of moving beads compared to incubation with 80mM PIPES. Experiments for both high and low ionic strength incubations were performed in the same buffer (see Section 2.3).

Qualitatively, the traces gained from high ionic strength incubations (likely dimers) were the same as those from lower ionic strength incubations, Figure 3.9C. Beads incubated with motors at each ionic strength show the same unloaded velocities with means of 191±30 nm/s and 202±30 nm/s for high and low salt concentrations respectively. Both conditions appear to show very similar load behaviour with motors capable of walking forwards to loads of around 4/5pN before stalling.

If the low ionic strength traces were due to the combined efforts of two pairs of motor domains we might expect to see 4nm steps due to the two motors sharing the load. This is not seen, although Kif15 traces are in general noisy and detecting 4nm steps would be difficult in most cases. The average load at detachment for motors incubated at high and low ionic strength are also very similar, Figure 3.9D. This suggests that the same number of motor heads are binding the MT in both cases. If a second pair of motor heads were binding to the MT it might be expected that this would allow them to pull beads to higher loads, as is seen for beads with multiple Kinesin-1 motors bound.

3.9 Conclusions

The concentration of Kif15 necessary to see single molecule mechanical interactions has been determined and Kif15 has been shown to have a much lower affinity for polystyrene beads

than Kinesin-1. This has meant that very low levels of Kinesin-1 contamination in the Kif15 protein preparations could appear as a significant proportion of motile beads. Although we have been unable to prove that these fast moving beads are indeed Kinesin-1 by comparison with Kif15 single molecule fluorescence data and Kinesin-1 optical trapping data it seems highly likely.

Having investigated the single molecule mechanics of the slower population of Kif15 coated beads using the optical trap we have shown that Kif15 is slower and less processive than Kinesin-1. However Kif15 is still faster and more processive than Eg5. Kif15 has a variety of different MT binding states. It is capable of processive movement, diffusion and pausing as shown by both the optical trap and TIRF experiments. There is not enough evidence to state a clear stall force for Kif15, but it is capable of producing net forwards movement at loads up to at least 5pN.

The run length of Kif15 under load is significantly shorter than its unloaded run length. This suggests that Kif15 has a second, diffusive MT binding site in addition to its motor domains which is able to extend its unloaded run length. The conformation of Kif15 motors on the beads has been investigated and it appears that the movement seen in these experiments is produced by a single pair of Kif15 heads and not both ends of the tetramer, this is backed up by our ability to distinguish 8nm steps in the Kif15 data.

Chapter 4

Results: Kif15 Regulation

Through the use of tail-binding anti-bodies and by examining a truncated version of Kif15 we found that the C-terminal tail region of Kif15 is responsible for auto-inhibition of the motor. This tail region also contains the binding site for the MAP, Tpx2. Tpx2 is a microtubule associated protein which is responsible for the localisation of Kif15 to the mitotic spindle. We studied the effect of Tpx2 on single Kif15 and Kinesin-1 molecules, it was found to cause FL-Kif15 to stop stepping on the MT and instead bind tightly. Kinesin-1 is unaffected by Tpx2.

Removal of the auto-inhibition of Kif15 by using a tail-less construct, Kif15-1293, has enabled trapping to be performed more easily and a more quantitative description of the load dependent behaviour of Kif15 has been found. This construct, lacking the Tpx2 binding region, is unaffected by Tpx2.

4.1 Tail-Binding Antibodies

As described in Section 1.3 there were concerns about the origin of the fast moving motor fraction observed in the Kif15 experiments. One approach to address this that has not been discussed involves the use of anti-Kif15 antibodies. These are affinity purified rabbit polyclonal antibodies specific for Kif15. In these experiments beads were prepared as normal,

however 1mg/ml of anti-Kif15 antibody was introduced to the flow cell along with the running buffer. It was expected that the antibodies would bind to the Kif15 motors and impede their motion, whereas Kinesin-1 motors would be unaffected. In this way we could determine whether the fast motors were Kif15, in a different regulation state to that seen using single molecule fluorescence, or were an insect Kinesin-1 contaminant.

The presence of the antibodies did affect the motility of the Kif15 motors. Most significantly it increased the proportion of motors that would move slowly along the MT, as seen in Figure 4.1A. In the presence of anti-Kif15 antibodies 80% of motors that bound the MT now showed motility. The velocities of these motors are spread over a wide range from 32nm/s to 327nm/s, as shown in Figure 4.1B. No fast motors were seen in the presence of antibody however at the motor concentration used no fast motors were observed without antibodies present.

Motors are already bound to beads before the introduction of antibodies so this increased activity is not due to a change in the way that the motors are binding the beads. The increase in motility can be explained by a removal of some Kif15 inhibition due to binding of the antibody. The antibody was raised on the tail region of Kif15 shown in Figure 4.1C and so its binding region is likely to be in this area. If the tail region of Kif15 inhibits motor activity, as is the case for other Kinesin motor proteins such as Kinesin-1 [101] and Cenp-E [31], then binding of an antibody to this region might hinder the tail from binding to the motor domains and prevent the tail-region from interfering with stepping.

4.2 Kif15-1293 Truncation

Following the discovery that a tail-binding antibody increased the motility of Kif15 motors, a truncated Kif15 motor was used in the trap. This motor, Kif15-1293, lacks the 95 terminal amino acids from the tail region as shown in Figure 4.1C. This short truncation dramatically changes the amount of motility seen for the motors, Figure 4.1A. The truncated motor shows a high proportion of moving motors relative to static bound beads when compared to the full length motor, 80% instead of 30%. This result lends support to the concept of the tail region being necessary for the auto-inhibition of Kif15 as it shows that independently of

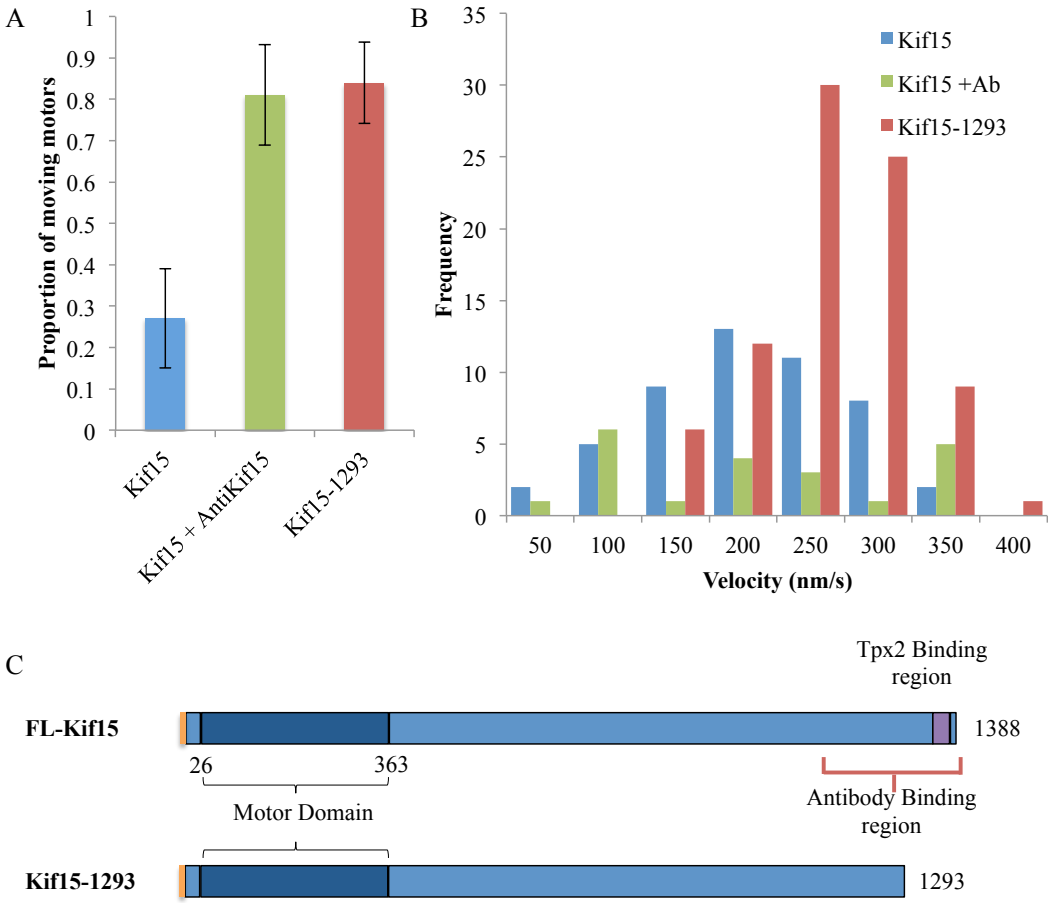

Figure 4.1: A) Proportion of moving beads from those that bind the MT for Kif15, Kif15 in the presence of 1mg/ml Anti-Kif15 antibody and for Kif15-1293. Error bars show region of 95% certainty. B) Unloaded velocities of Kif15, Kif15 with anti-Kif15 antibodies and Kif15-1293. C) Schematic of FL-Kif15 showing anti-Kif15 antibody binding region and the truncated Kif15-1293.

antibody binding it is possible to increase the proportion of Kif15 motors showing processive movement.

The unloaded velocities of the truncated motor are slightly faster than those of the full length Kif15 (FL-Kif15), Figure 4.1B. The mean velocity of FL-Kif15 in these experiments is 206±10 nm/s whereas for Kif15-1293 the mean velocity is 238±6 nm/s. The lower unloaded speed of FL-Kif15 could be caused by brief pauses on the MT during processive motion due to temporary inhibition by the tail region, these pauses would not be apparent when

tracking the unloaded bead in the trap.

4.3 The Effect of Tpx2 on Single Molecules of FL-Kif15

The microtubule associated protein Tpx2 is known to be necessary for the localisation of Kif15 to spindle microtubules *in vivo*. *In vitro* it is not possible to find motile beads in flow cells where a small amount of Tpx2 has been added to the buffer. In order to investigate this further, experiments were performed in which a motile bead was found under normal conditions. A new buffer containing 18nM Tpx2 was then washed into the flow cell replacing the original buffer, taking care not to lose or replace the trapped bead. The motility of the same molecule was then checked under the new solution conditions, this was done for both FL-Kif15 and Kinesin-1.

For Kif15 it was found that in the presence of Tpx2 a motor that was previously able to walk processively out of the trap would now statically bind to the microtubule, Figure 4.2. This was the case in 4 out of 5 experiments. The motor motility was then restored upon washout of the Tpx2, (2 of 2) this data is not shown as it was not possible to collect a trace at the final time point due to increased compliance in the MT surface attachment, but can be seen in Video 1. For Kinesin-1 the motor motility was unaffected by the presence of Tpx2, 5 of 5 experiments. The load bearing ability of MT bound Kif15 in the presence of Tpx2 appeared to be qualitatively stronger than in the absence of Tpx2.

4.4 Effect of Tpx2 on Kif15-1293

The truncated motor, Kif15-1293 lacks the C-terminal tail region that includes the Tpx2 binding site between 1359 and 1380 a.a. The stepping of Kif15-1293 should therefore not be affected by the presence of Tpx2, if this is the only means by which Tpx2 interacts with the motor. Figure 4.3 shows the effect of Tpx2 on beads with both FL-Kif15 and Kif15-1293 motors. As described in Section 4.3 in the presence of Tpx2 no movement is seen for FL-Kif15 motors. For the truncated Kif15-1293 motor, movement along the MT is still seen although there is an increase in beads that bind without movement. However

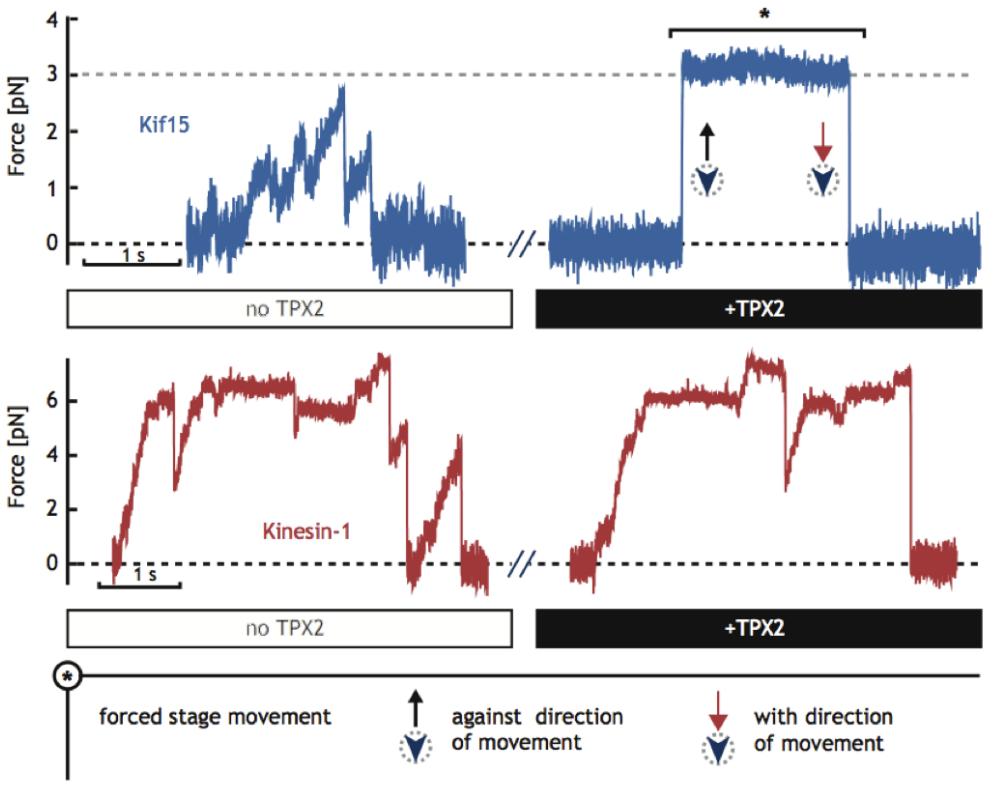

Figure 4.2: Addition of Tpx2 causes the motility of full-length Kif15 to stop. Kinesin-1 is unaffected by the presence of Tpx2. A bead with Kif15 (blue) is shown to be motile (top left) a solution of 36 nM Tpx2 is flowed into the cell and motility ceases (top right). A movement of the stage, indicated by the black and red arrows, shows the motor is binding the microtubule. The bottom right shows Kinesin-1 (red) with and without Tpx2, there is no change in motility.

Tpx2 in solution even in nano-molar concentrations is capable of binding beads to MTs without any motor present and this could account for the increase in binding in the case of Kif15-1293.

The moving Kif15-1293 motors show no significant change in velocity upon addition of Tpx2, Figure 4.3B. This shows that Kif15 motors moving along MTs are unaffected by lattice bound Tpx2 unless through an interaction with the C-terminal tail.

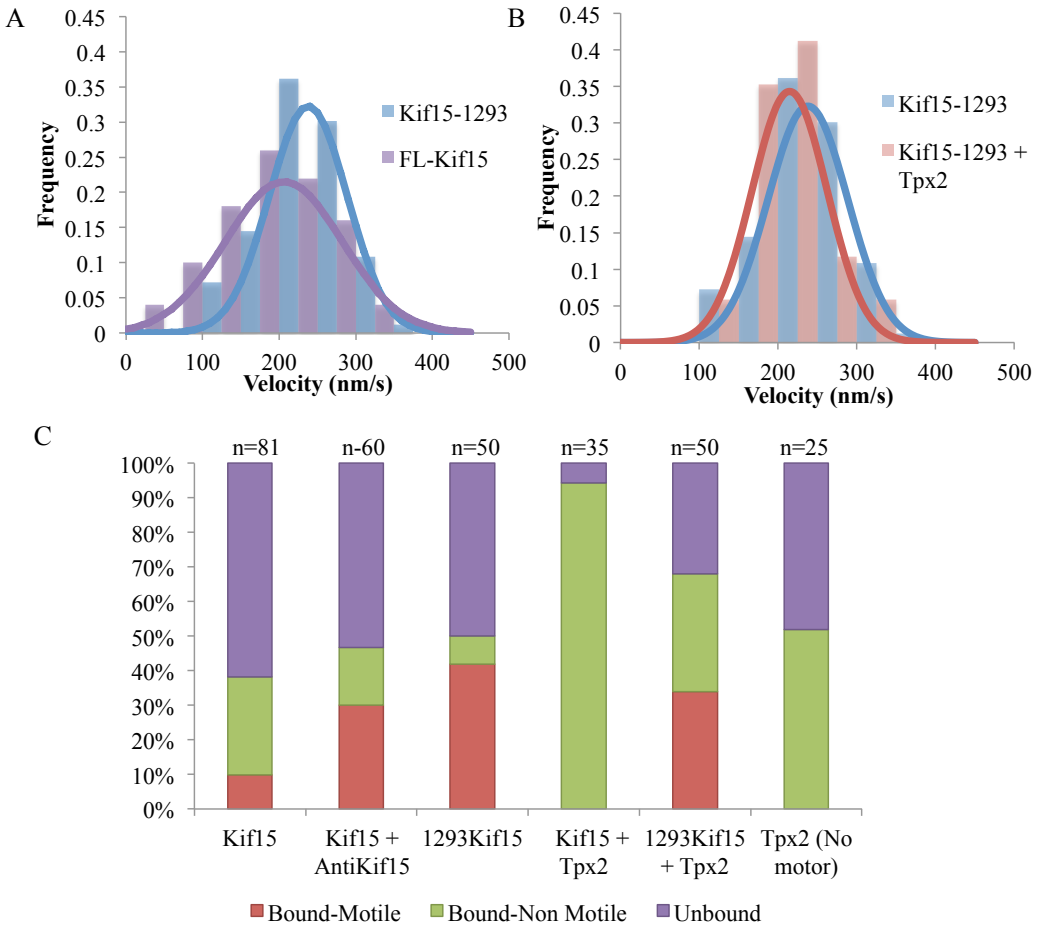

Figure 4.3: A) Unloaded velocities of Kif15-1293 motors (blue) and FL-Kif15 motors (purple). The velocity of Kif15-1293 is 238±6nm/s, and of FL-Kif15 is 206±10nm/s mean and SE. B) Unloaded velocities of Kif15-1293 motors in the presence of 18nM Tpx2 (red) and in the absence of Tpx2 (blue). There is only a very small difference in the velocities. The velocity with Tpx2 is 215±12nm/s without Tpx2, 238±6nm/s, mean and SE. C) Outcomes of Kif15, Kif15-1293 or uncoated beads introduced to the MT (introduced to >= 2 MTs for at least 30s) in the presence and absence of 18nM Tpx2.

4.5 Single Molecule Mechanics of Kif15-1293

Qualitatively Kif15-1293 traces look the same as those for FL-Kif15 (Figure 4.4A). In the trap the motor reaches similar loads (Figure 4.4B), suggesting that the load bearing ability of the motor is unchanged by the truncation. The average sizes of detachments for the

truncation and the full-length motor are also the same suggesting that the truncation and the motor both have a similar tendency to rebind the MT before the bead has reached trap centre (Figure 4.4C). This happens regularly for Kif15 and is probably a result of its diffusive region keeping the motor domains close to the MT during detachments. The traces in Figure 4.4A shows both fast and slow fly-backs for both motors suggesting that Kif15-1293 also can diffuse along MTs.

Since Kif15-1293 does not pause on the MT as FL-Kif15 does, its motility is more consistent and a higher proportion of beads are motile. Trapping with Kif15-1293 is easier than with FL-Kif15 as it is easier to find motile beads in the low MT binding single molecule conditions. It has been possible to collect more stepping data on this motor. Step size distributions for Kif15-1293 are similar to those for FL-Kif15, with a mean uncorrected step size of 7.14±0.01 nm for forwards steps and 7.24±0.29 nm for backwards steps, Figure 4.4D. More favourable experimental conditions have allowed a more complete picture of the effect of load on Kif15-1293 to be gained than was possible for FL-Kif15.

4.5.1 Dwell Time

Using the step finding algorithm described in Chapter 2 steps were detected in Kif15-1293 traces. The mean times between steps, dwell times, as a function of load, are shown in Figure 4.5A. This figure shows the dwell times for both forwards and backwards steps combined. At low loads around 1-2 pN Kif15-1293 has shorter dwell times than FL-Kif15 in agreement with the faster velocities seen for unloaded beads. At higher loads above 3pN the two motors have very similar dwell times indicating that under higher loads the presence of the C-terminal tail in FL-Kif15 has little effect on the stepping of the motor.

This could be due to the geometry of the FL-Kif15 binding to the bead, at higher loads the motor-bead tether is likely to be more extended perhaps stopping the tail domains from binding to the heads, Figure 4.6. However application of loads of up to 10pN were not sufficient to cause paused FL-Kif15 motors to resume stepping or unbind the MT. Either these motors are initially bound to beads in an orientation that encourages inhibition or the application of load is insufficient to 'undock' a the tail from an inhibited motor. Often

paused motors will begin stepping after the removal of an applied load perhaps suggesting that the load has changed their bead binding orientation to one less favourable for tail binding but inhibition was not released until the external load was removed.

At loads above 6 pN Kinesin-1 shows a flattening off of dwell times and Kif15-1293 may do the same, at these forces the majority of steps are backwards steps (Figure 4.5B). Constant dwell times at these loads show that the backwards stepping rate is not increasing when higher loads are applied.

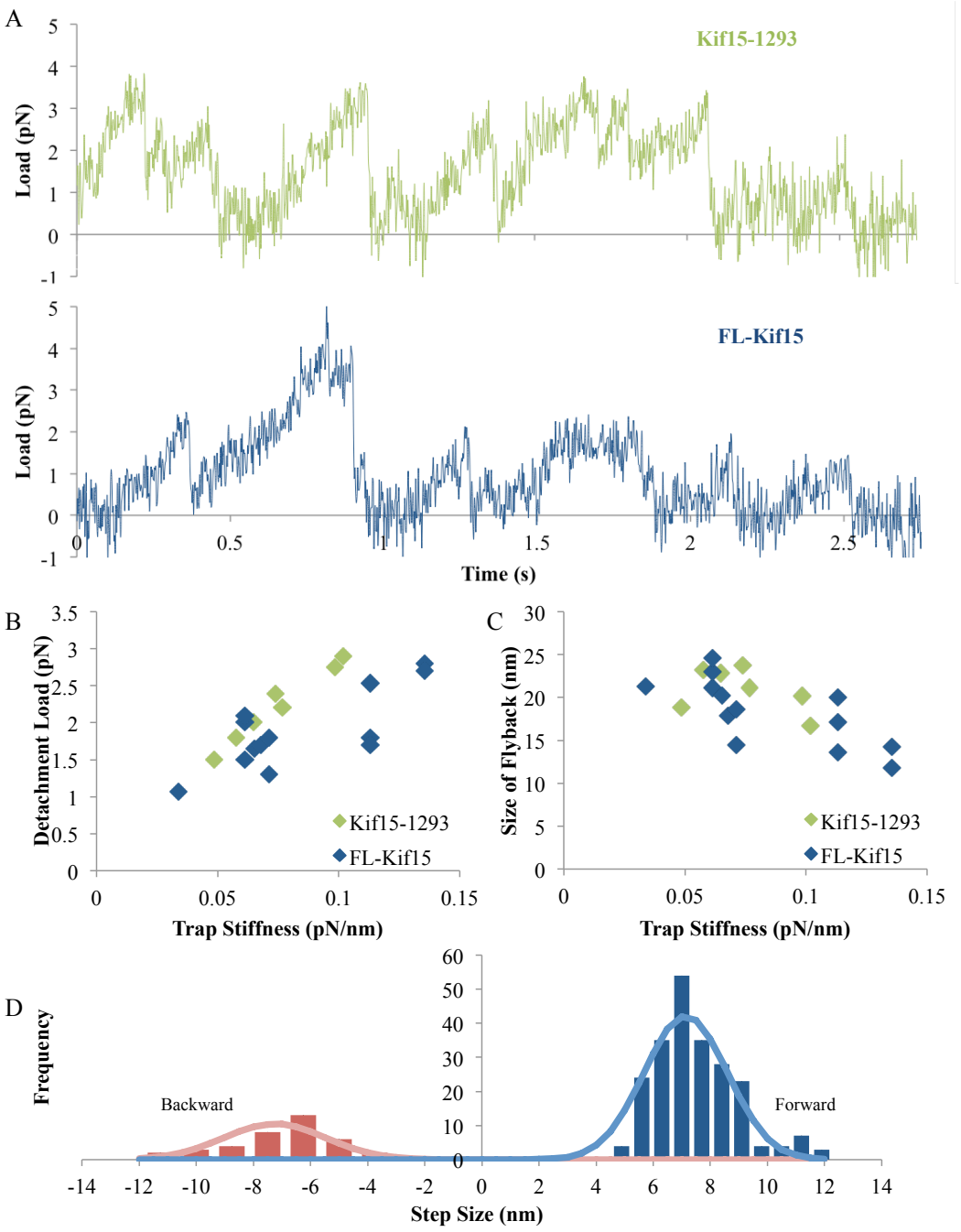

Figure 4.4: A) Example Traces for Kif15-1293 and FL-Kif15. Data was gathered at 22kHz smoothed with a 50 point moving average filter and then sampled down to 220Hz. Trap Stiffness was 0.062 pN/nm for both traces. B) Average detachment loads for FL-Kif15 (blue) and Kif15-1293 (green) traces at varying trap stiffnesses. C) Average size of detachments for FL-Kif15 (blue) and Kif15-1293 (green) traces at varying trap stiffnesses. D) Step size distributions for Kif15-1293 in the forwards and backwards directions, n_f=259 and n_b=38. Peaks are at 7.14±0.01 nm and 7.24±0.29 nm for forwards and backwards steps respectively. Mean and S.E.

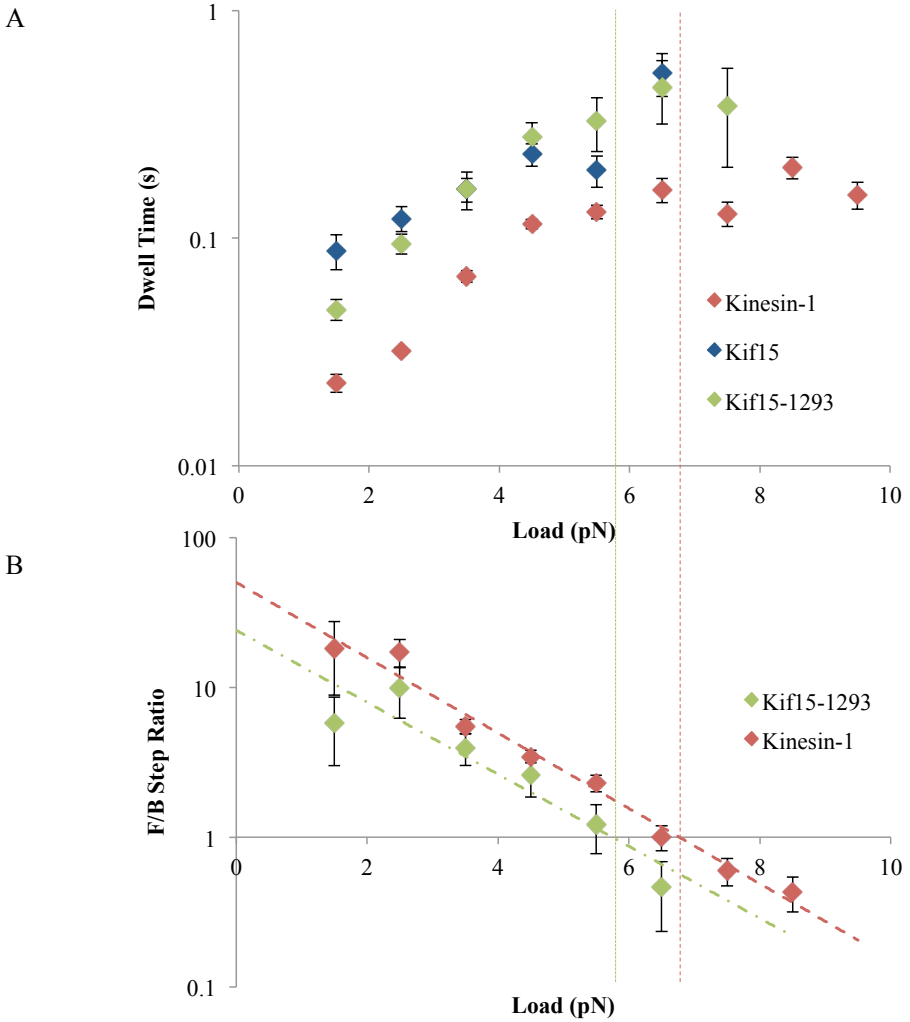

Figure 4.5: A) Dwell time distributions for Kinesin-1, FL-Kif15 and Ki15-1293. A dwell is the time that the motor waits between steps. All three motors show an increase in dwell time at higher loads. Above 6.5pN, Kinesin-1 dwell times plateau and Kif15-1293 may do the same. B) Forwards/Backwards stepping ratios for 1pN binned data for Kif15-1293 and Kinesin-1. Fitted lines are exponentials fit using least squares. The stall forces of the motors (when the number of forwards and backwards steps are equal) are 5.6±0.76 pN for Kif15-1293 and 6.76±0.76 pN for Kinesin-1. Errors in stall force are calculated from the standard error in the slope and intercepts of the least squares line fits.

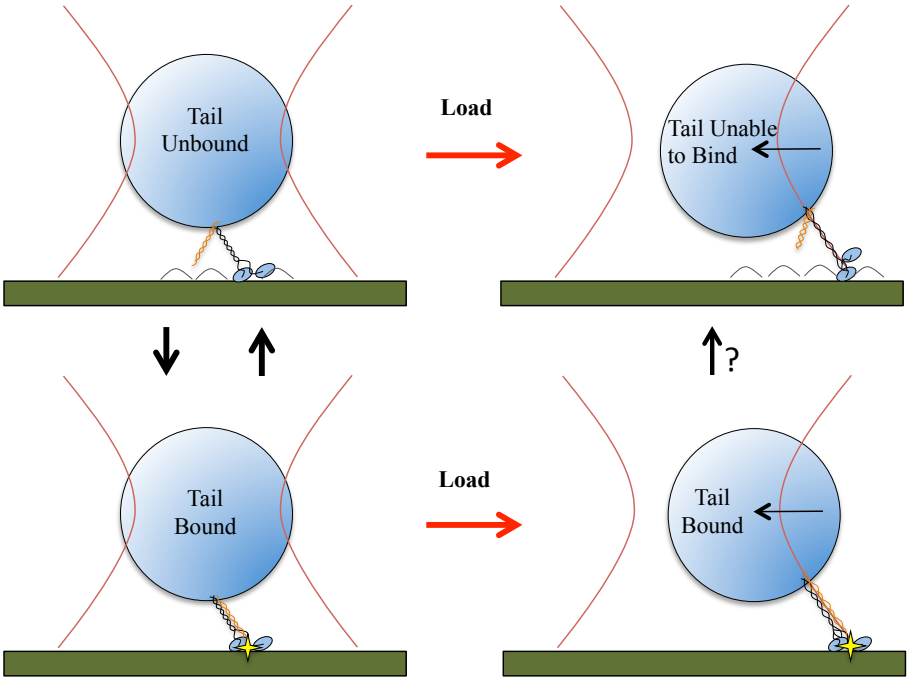

Figure 4.6: Cartoon depicting possible mechanism of FL-Kif15 tail inhibition under load in trapping experiments. Under low or no load the tail region is free to bind or unbind the motor regions. The motor can alternate between inhibited and uninhibited states. When load (above 3pN) is applied to an uninhibited motor the tether stretches increasing the distance between the motor heads and the bead, the tail can no longer bind to the heads. When load is applied to the motor in its tail docked, inhibited, state the tail and motor tethers are stretched simultaneously. Application of load does not appear to encourage the release of tail inhibition and may act to maintain the tail binding.

4.5.2 Stall Force

By examining the ratios of forwards to backward steps as the load on the motor is increased it is possible to define a stall force. The stall force is the load at which the motor is unable to make net forward movement, or the load where the forward stepping rate is equal to the backward stepping rate. Figure 4.5B shows the forward to backward stepping ratios (F/B ratios) for Kif15-1293 and Kinesin-1. From this graph we can see that the stall force of Kinesin-1 is 6.76±0.73 pN. This is slightly higher than the stall force for Kif15-1293 which is 5.6±0.73 pN.

4.5.3 Effect of Load on Velocity

Combining the dwell time data and F/B stepping ratio it is possible to calculate the average velocity of motors under load. The velocity for each 1 pN bin of Figure 4.7A (except at zero load), was calculated as in Equation 4.1 where n_f and n_b are the numbers of forward and backward steps counted and $\bar{\tau}$ is the average dwell time at that load. 8.1 nm is given as the assumed step size for the motor.

$$v = \frac{8.1(n_f - n_b)}{\bar{\tau}(n_f + n_b)} \tag{4.1}$$

Both Kif15-1293 and Kinesin-1 show a similar behaviour under load, their velocities are well fit by exponential curves. The load at which the velocities are half those of the unloaded motors are 1.37 pN and 1.57 pN for Kinesin-1 and Kif15-1293 respectively.

4.6 ATP Dependent Behaviour of Kif15-1293

Kinesin motor proteins use the hydrolysis of the nucleotide ATP to gain energy to make processive and directional steps [59]. When the concentration of ATP decreases the stepping rate and therefore the velocity of the motors also decrease. For Kinesin motors, the velocity of the unloaded motor is directly related to the reaction rate of hydrolysis. The motor acts as an enzyme for the conversion of ATP to ADP and the reaction rate (motor velocity) obeys Michaelis-Menten Kinetics. By varying the ATP concentration and measuring the unloaded velocities of the beads, Michaelis-Menten curves can be fit to the data, Figure 4.7B;

$$v = \frac{V_{max}[ATP]}{K_m + [ATP]} \tag{4.2}$$

The V_{max} for Kinesin-1 is 730±150 nm/s and the K_m is 70±29 μM roughly in agreement with previous steady state data [102]. For Kif15-1293 the K_m is 27±3 μM which is similar to the steady state $K_{M,ATP}$ for Kif15 monomers [42] (33 μM for Kif15$_{19-375}$), V_{max} is 247±22 nm/s .

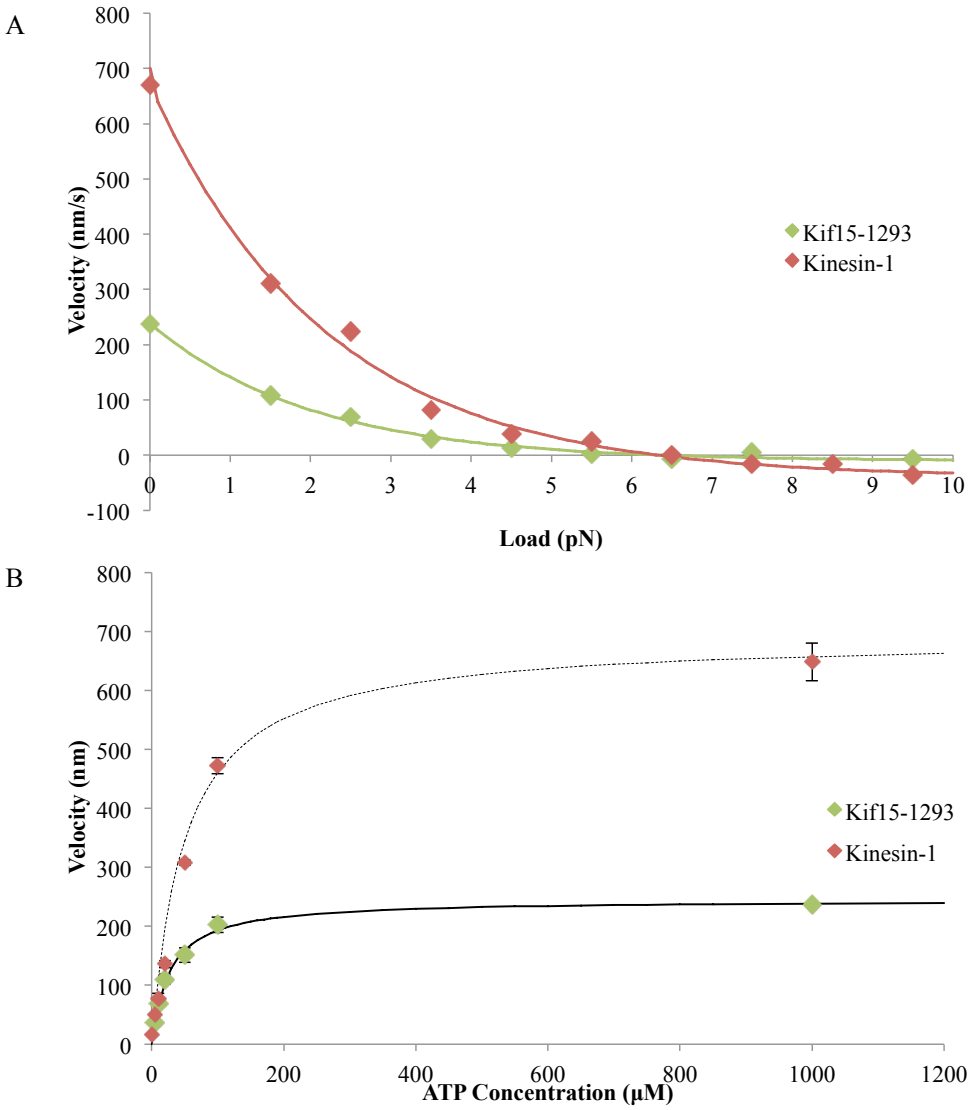

Figure 4.7: A) Dependence of velocity on load for Kif15-1293 (green) and Kinesin-1 (red). Both distributions are fit with exponential curves. B) ATP dependence of Kif15-1293 velocity. Unloaded bead velocities of Kif15 and Kinesin-1 at varying ATP concentrations, mean and S.E. Michaelis-Menten curves are fit by least squares.

4.7 Behaviour of Two Kif15-1293 Motors

For FL-Kif15 movement of beads dependent upon more than one motor were very rare as the majority of motors are in the inhibited state. This means that the likelihood of finding a bead with two uninhibited FL-Kif15 motors is very small. Since in Kif15-1293 this inhibition

is relieved it is possible to see the movement of beads under the influence of more than one motor. Figure 4.8A shows a trace from Kif15-1293 showing the behaviour of a bead with two motors bound. In this case although the majority of movement is due to a single motor, as in the first 3 seconds of the trace shown, occasionally a second motor will bind. The two Kif15 motors then cooperate pulling the bead to loads of up to 9 pN.

The distribution of detachment loads for a trace with two motors compared to a single motor case are shown in Figure 4.8B. Both sets of data were gained from experiments performed at the same trap stiffness of 0.053 pN/nm. The single motor detaches at 1.6 pN on average with only a few high load outliers. The multi-motor bead has a larger spread of detachment values with more high load detachments.

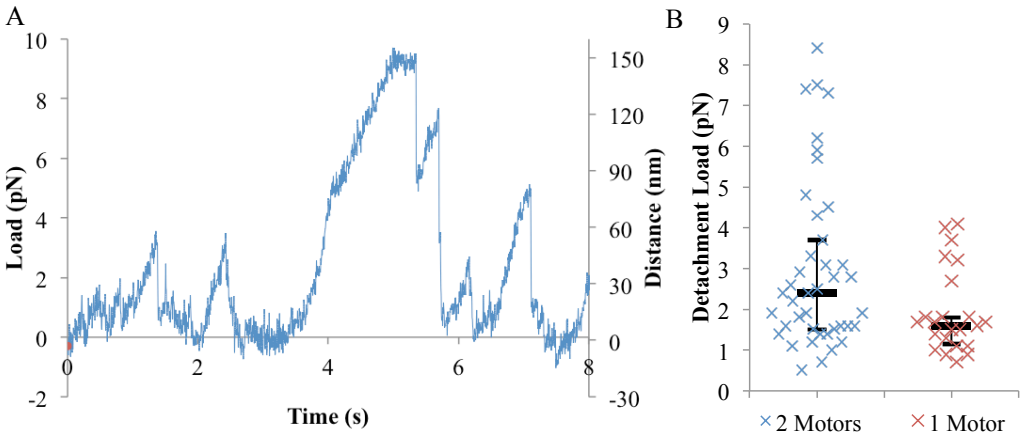

Figure 4.8: A) Example trace from a bead with two Kif15-1293 motors bound. Single motor behaviour is seen for the first 4 seconds, at which point the movement to higher loads due to the second motor can be seen. Data collected at 22kHz before smoothing with a 50 point moving average filter then sampling down to 110Hz. B) Detachment loads measured for beads with one (red) or two (blue) motors bound, shown in black are the median and upper and lower quartiles for the distributions.

4.8 Conclusions

The Kif15 tail region is responsible for inhibiting its movement on MTs, this can be relieved either sterically, through the binding of antibodies to the tail, or by deleting the final 100a.a. Since the tail region is not capable of binding MTs independently [42], this implies that the

tail region is able to interfere with the Kif15 stepping mechanism in some way. Upon binding of Tpx2 Kif15 motors but not Kinesin-1 pause on MTs, this effect is significantly reduced in the truncation mutant in which the Tpx2 binding region has been removed.

Further investigating the load dependence of the truncation, Kif15-1293, has revealed that its unloaded stepping rate is slightly faster than FL-Kif15. The lack of inhibition of Kif15-1293 makes it easier to collect traces and so more high load data has been gathered. This extra data allows us to determine a stall force of 5.6 pN and show that the motors velocity under load decreases in a similar manner to Kinesin-1. The velocity of unloaded Kif15-1293 decreases with the ATP concentration according to Michaelis-Menten Kinetics. Overall the mechanical properties of the Kif15 motor appear to be affected by load in a similar manner to Kinesin-1. Kif15 differs from Kinesin-1 in its slower velocity and substantially shorter run length under load.

4.8.1 Summary of "Biophysical Values"

	FL-Kif15	Kif15-1293	Kinesin-1
Velocity (Unloaded)	206±10 nm/s	238±6 nm	670±22 nm/s
Stall Force	UnKnown	5.6±0.73 pN	6.8±0.76 pN
Load at $V_{1/2}$	Unknown	1.37 pN	1.57 pN
K_m	Unknown	27±3μM	70±22μM
Tpx2 Inhibition	Yes	No	No

Table 4.1: Biophysical Values for FL-Kif15, Kif15-1293 and Kinesin-1.

Chapter 5

Results: Unbinding Loads for Kinesin-1

In previous experiments with Kif15 it was found that it was not possible to collect stepping data under assisting loads. This was because the run length under assisting load appeared to be very short. In order to investigate this further a new approach was used. This technique was first used by Uemura et al. [61] who discovered an asymmetry in the unbinding rate of Kinesin-1 under assisting and hindering loads. Uemura et al. [61] found that the motor could support 45% more load under minus end directed loads when in either the AMP-PNP bound or nucleotide free states.

In the experiments performed in this chapter we first attempt to replicate the experiments performed by Uemura et al. [61] with *Drosophila* Kinesin-1 in ADP and AMP-PNP conditions. Comparison of our AMP-PNP and ADP data with that of Uemura et al. [61] shows little or no difference. After confirming that our experimental conditions were able to reproduce previously published results we investigated the effect of motor stepping on unbinding load asymmetry. Experiments were performed in 5 μM ATP and 1 μM ATP. Under these conditions unloaded motors step at 50 nm/s and 10 nm/s, respectively.

5.1 The Unbinding Experiment

In the unbinding experiments described below, motors were allowed to bind to a MT moving past the trap centre at a constant rate. This meant that once a motor is bound to the MT it begins to move relative to the trap centre. This creates increasing loads upon the motor towards the trap centre. Eventually the motor will detach from the MT. The detachment loads have been measured with the load on the bead in an assisting, plus end directed manner and also in a hindering, minus end direction, Figure 5.1A.

Example data from these experiments can be seen in Figure 5.1B, the step like movements in the data are caused by the stage movement that occurs in 12.2 nm steps in the x and y directions. In order to confirm that these movements do not affect the unbinding loads seen in these experiments we compare our 1mM ADP and 1mM AMP-PNP results with those of Uemura et al. [61]. For experiments performed in either ADP or AMP-PNP and MT polarity was determined after data collection, by a wash through of a solution containing ATP. This caused motors to step on the MTs towards the plus ends, allowing polarity to be determined.

5.2 Models of Kinesin Unbinding Under Load

In order to interpret our unbinding load results we consider a model of motor-MT binding under load. A MT bound motor detaching from a MT is a poisson process; it has no 'memory' of how long it has been bound and the probability of unbinding at any point in time is constant. This means that after a time t the probability that a motor that bound the MT at $t = 0$ is still bound is given by;

$$P(t) = e^{-t/\tau} \tag{5.1}$$

Where the average binding time for the motor to the MT is τ. A model of the dependence of τ on load F that is used in previously [61, 69] is;

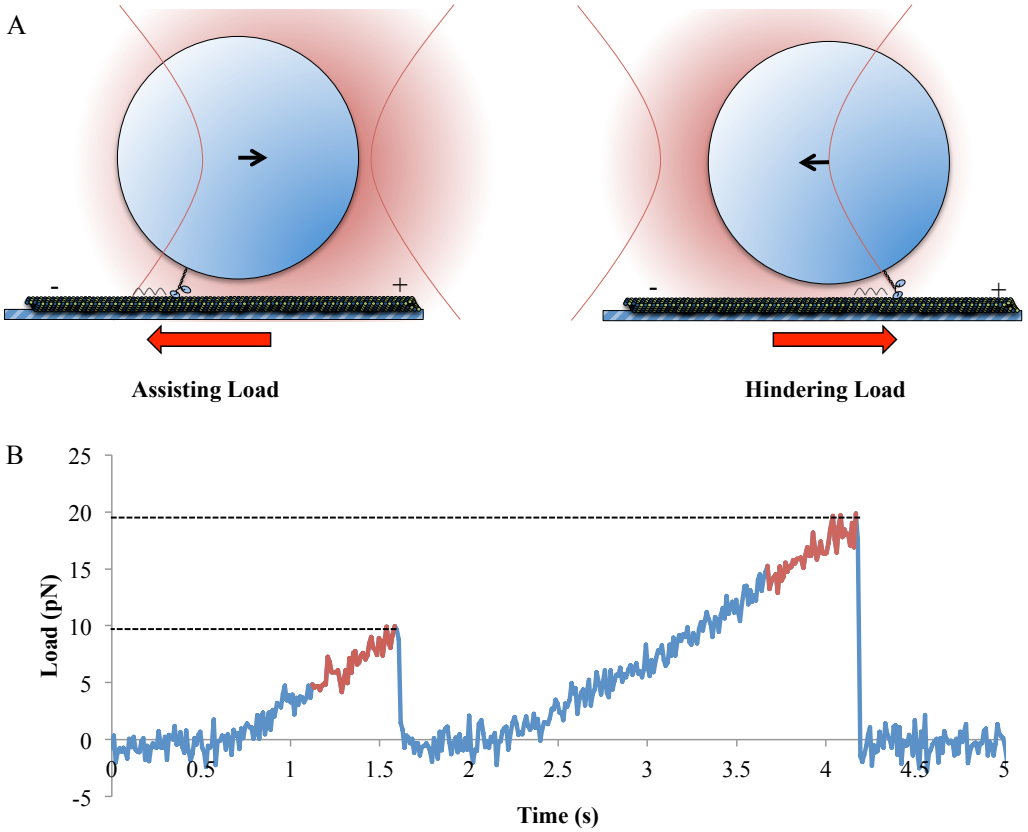

Figure 5.1: Experimental set up applying assisting and hindering loads. The directions of stage movement are shown by the red arrows. Directions of load on the bead are shown by the black arrows. B) Example trace from Kinesin-1 under hindering loads in 1mM AMP-PNP. Detachment loads (dotted lines) and region used to calculate loading rate (red) are shown. Data was collected and analysed at 22kHz, shown here sampled down to 44Hz, trap stiffness was 0.183 pN/nm, stage was moved at 100nm/s.

$$\tau(F) = \tau(0)e^{-Fd/k_bT} \tag{5.2}$$

Where $\tau(0)$ is the average time to unbinding at zero load, k_b is the Boltzmann constant, T is the absolute temperature and d is the characteristic distance. In our experiments the load is increased linearly over time, therefore $F{=}\alpha t$, where α is the loading rate. Previous experiments have used this equation to calculate the number of motors detaching per unit time and fitted these curves to data from single and double headed Kinesin-1. In our experiments this is not attempted as much of our data is collected in low ATP conditions

where the processive steps of the dimer along the MT complicates the model. Instead peaks in the data are found using MATLABs 'fitgmdist' function which uses Gaussian Mixture Modelling (GMM) to fit double or single gaussians.

5.3 Unbinding of Kinesin-1 in Single Nucleotide Conditions

Previously Uemura et al. [61] found that the unbinding of the ADP bound state occurs at around 3.5 pN and is invariant to the loading direction. The AMP-PNP bound state for Kinesin-1 gives two peaks in each direction, indicating that the motor is in equilibrium between two states with different unbinding loads. By comparison with the unbinding loads of single headed Kinesin-1 in the same nucleotide state they conclude that these two peaks represent single and a double head bound conformations (Figure 5.3). The unbinding loads found for the two headed Kinesin-1 under minus end directed (hindering) loads are 10pN and 17pN. The unbinding loads under plus end directed (assisting) forces are 6 pN and 12 pN, showing an asymmetry favouring unbinding under positive loads.

5.3.1 Unbinding of Kinesin-1 in the Presence of 1mM ADP

For Kinesin-1 the unbinding load in 1mM ADP under both assisting and hindering loads is similar at around 3.5 pN, Table 5.1. This is in close agreement with Uemura et al. [61]. Considering the distribution of data in these conditions a simple gaussian is possibly not the best fit, especially to the data under assisting loads, however there are only 25 data points in this data set and at low loads detection of binding is difficult in both directions as at these loads there is a lot of noise, Figure 5.2A.

Unbinding loads for Kinesin-1 in 1mM ADP increase with loading rate, Figure 5.2B. This is as expected, the time to detachment decreases with loading rate, although this effect is only very mild. Over all loading rates the average detachment time is 1.03s. This time is in agreement with the detachment rates of unloaded 2-headed Kinesin-1 from MTs seen in Hancock and Howard [103] of 1/s.

This unbinding in ADP conditions can be interpreted two ways. Firstly we might consider that in the presence of 1mM ADP a motor initially binds the MT upon ADP release in a no nucleotide state. It then releases the MT when it rebinds ADP, (Figure 5.3 (red arrows)). The unbinding load therefore has more to do with the rate of ADP binding than the binding strength of an ADP bound motor to the MT. Alternately we are looking at an ADP bound motor interacting with the MT, with no nucleotide exchange (Figure 5.3 (orange background)), and the slight reduction in average binding times under load is due to the same mechanism as AMP-PNP and no nucleotide conditions.

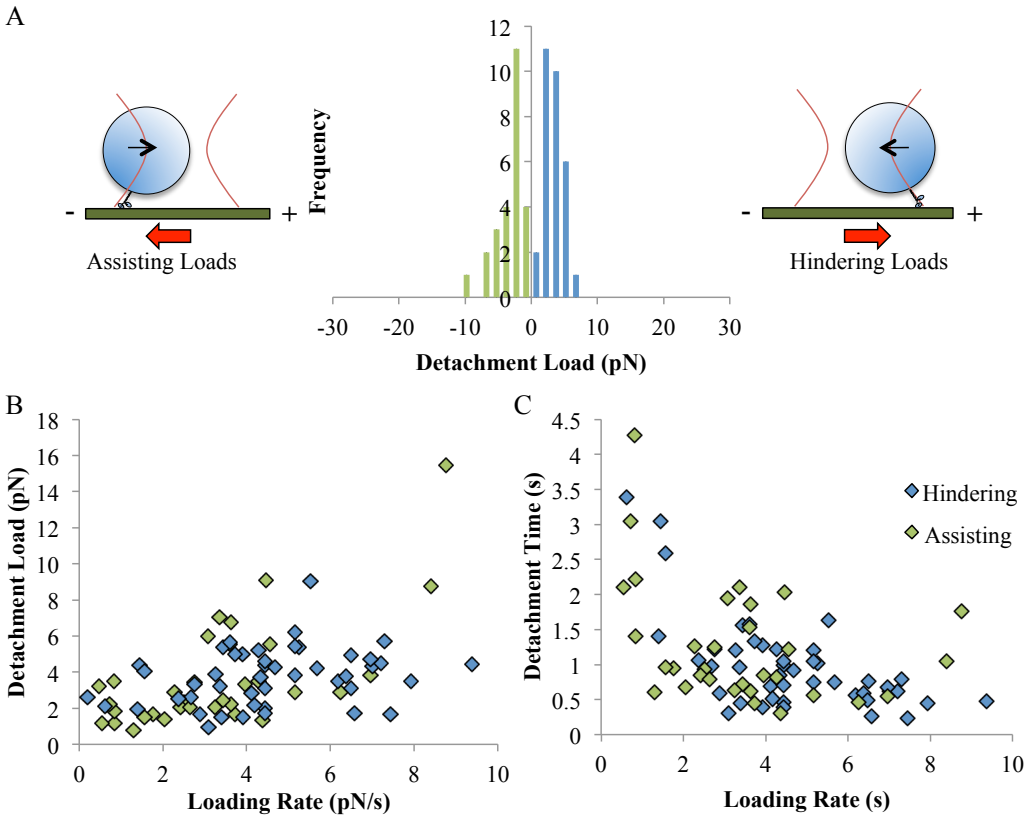

Figure 5.2: A) Detachment loads for assisting (green) and hindering (blue) loading of Kinesin-1 in the presence of 1mM ADP at 3.4pN/s loading rate, 1.5 pN bins, n = 53. B) Detachment loads and C)Detachment times against loading rate for assisting and hindering load combined.

Nucleotide	**n**	**Loading Rate (pN/s)**	**Assisting Load (pN)**	**Hindering Load (pN)**
1mM ADP	53	3.5±2.0	3.4±2.0	3.4±1.5
1mM AMP-PNP	91	6.5±1.6	6.4±1.8 (0.32) 12.7±2.5 (0.68)	9.0±3.0 (0.48) 18.9±2.5 (0.52)
5μM ATP	127	6.5±1.9	6.7±2.3 (0.7) 12.1±3.6 (0.3)	13.4±2.2 (0.68)* 20.6±1.8 (0.32)*
1μM ATP	76	6.5±3.0	8.8±2.3 (0.59) 15.1±1.7 (0.41)	9.3±3.1 (0.55) 18.5±2.7 (0.45)

Table 5.1: Mean loading rates and gaussian peak positions and standard deviations in unbinding load distributions for Kinesin-1 in varying nucleotide conditions. Two peaks have been assumed for the distributions in all conditions except 1mM ADP. The percentage of each peak in a double gaussian is shown in brackets. *Fitted to a histogram with 2pN bins and not underlying data in order to resolve peaks.

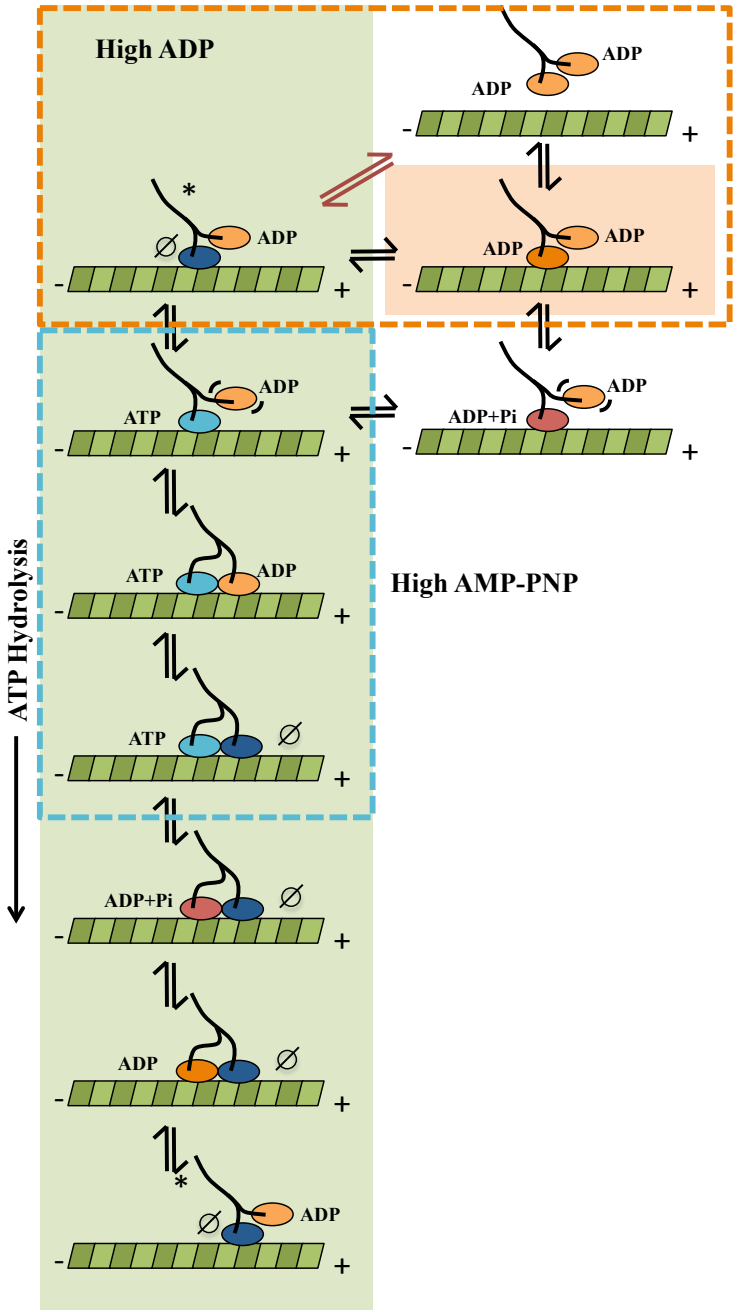

Figure 5.3: Overview of binding states. The possible MT binding states of Kinesin are shown. In green are MT binding states that are part of the stepping pathway. In high ADP (orange box) MT binding could occur via a strong-binding one head nucleotide free state or a weaker binding ADP state. Detachments are either load dependent from an ADP state or due to ADP binding the nucleotide free state. In high AMP-PNP (blue box) the motor could be in a single head MT-bound AMP-PNP state or a stronger binding two heads bound state. *These are the same single head bound waiting states.

5.3.2 Unbinding of Kinesin-1 in the Presence of 1mM AMP-PNP

When fitted with double gaussians, our data provides values for unbinding loads in the presence of 1mM AMP-PNP that are comparable with Uemura et al. [61]. In the presence of 1mM AMP-PNP Kinesin-1 shows an asymmetry in unbinding load, with the unbinding load under minus end directed (hindering) loads around 36% more than under plus end directed (assisting) loads, Figure 5.4A. This is slightly less of an asymmetry than the 45% seen in previously published data. Hindering loads give two peaks found to be at 9±3.0 pN and 18.9±2.5 pN. The error on these values is large however they are very similar to the 10.2 pN and 17 pN seen by Uemura et al. [61]. The model predicts that around 50% of the data is in the lower peak indicating that the motors are being detached from a two head bound state and a one head bound state with equal likelihood. The peaks in unbinding load for Kinesin-1 in 1mM AMP-PNP under assisting loads are at 6.4±1.8 pN and 12.7±2.5 pN, again in close agreement with Uemura et al. [61]. Under assisting loads approximately 70% of the data collected is from the high load peak.

Uemura et al. [61] use a loading rate of 5.0±1.7 pN/s, our data was collected at 3.7±1.3 pN/s and 6.1±2.0 pN/s for ADP and AMP-PNP respectively. The loading rates used in our experiments only differ slightly from those used by Uemura et al. [61], however subtle differences in the loading rate, from 5 to 7 pN increase the average load at which the motors detach by approximately 2pN under hindering loads, Figure 5.4B.

By calculating the average time to unbinding in AMP-PNP conditions we can get additional information. As can be seen in Figure 5.4B the unbinding loads under plus and minus end directed forces become less similar at high loading rates. In Figure 5.4C the average time to unbinding is plotted. Since for Kinesin-1 we know the average unbinding time of double headed kinesin from the AMP-PNP bound state is approximately 100 s [103] it is possible to fit Equation 5.2 to the data. Setting $\tau(t) = \bar{\tau}$ the average time at detachment and $F = \alpha\bar{\tau}$ gives the equation;

$$\alpha = \frac{-k_b T}{d\bar{\tau}} ln\left(\frac{\bar{\tau}}{\tau(0)}\right) \tag{5.3}$$

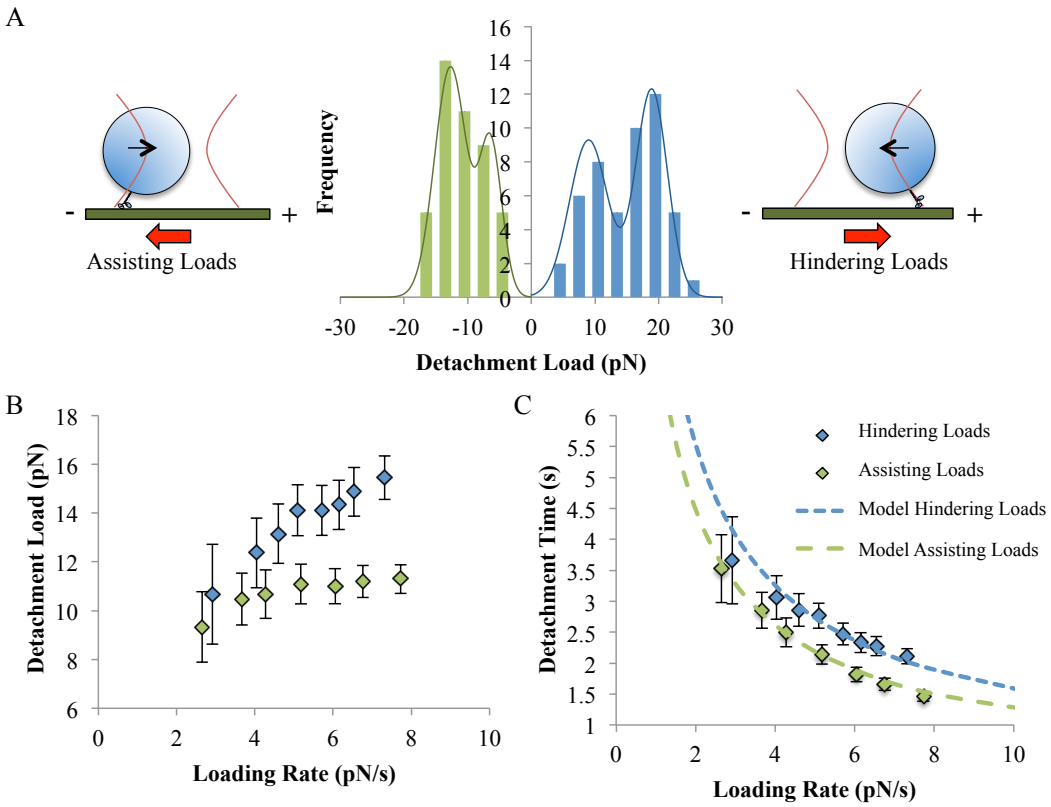

Figure 5.4: A) Detachment Loads for assisting (green) and hindering (blue) loading of Kinesin-1 in the presence of 1mM AMP-PNP at 6.5 pN/s loading rate, 3.0 pN bins, n = 91. Fitted curves show double gaussians fits to the data using MATLABs 'fitgmdist' function. Mean and standard deviations of the peaks are given in Table 5.1. Mean and SE for B) Detachment Loads and C) Average Detachment Times against loading rate for assisting and hindering load combined. Dotted lines show least squares model fits to Equation 5.3, $\tau(0)$ is assumed to be 100 s, fitted values of d_p=1.5 nm and d_m=1.1nm, for plus end directed (assisting) and minus end directed (hindering) loads.

Where α is the loading rate, $\tau(0)$ is average time to unbinding for unloaded motors, k_b is the Boltzmann constant, T is the temperature and d is a characteristic distance. This line has been fit to the data in Figure 5.4C, the values of d are 1.5 and 1.1 for plus and minus end directed loading giving a ratio of plus to minus of 1.36 similar to the ratio of 1.33 seen for one headed kinesins by Uemura et al. [61].

Given the small amount of data and slight differences in the experimental design, the similarity in the peak values found and the dependence on loading rate can give confidence

in our experimental set up. It appears that the discrete stepping of our stage, as opposed to the smooth movement by which load was applied in previous experiments, makes little difference to unbinding loads.

5.4 Unbinding of Kinesin-1 in the Presence of ATP

Having confirmed that our experiments were capable of reproducing previously published data, we proceeded to attempt the same experiments in the presence of low levels of ATP. At the concentrations used, 5μM and 1μM, Kinesin-1 steps slowly at rate of 50 and 10 nm/s respectively. Figure 5.6 shows the distributions of data collected under ATP and AMP-PNP conditions.

5.4.1 Unbinding of Kinesin-1 in the presence of 1μM ATP

At 1μM ATP, Kinesin-1 steps at a rate of 10nm/s or 1.25 steps per second. In these conditions the unbinding load distributions were expected to be very similar to those from the no nucleotide state, with the majority of data in a single peak at around 6pN under assisting and 10pN under hindering loads. It was surprising therefore to find that the distributions of unbinding loads in 1μM ATP and 1mM AMP-PNP were very similar (Figure 5.6).

Under hindering loads the distribution of detachment loads does shift towards the lower peak when compared with 1mM AMP-PNP data, however this is not to a large extent (Figure 5.6). As the stepping rate of Kinesin-1 decreases exponentially with load it is not expected that the motor stepping will make much difference to the distribution of data under hindering loads. Therefore most of the detachments in this region are expected to occur from a nucleotide free waiting state (Figure 5.5).

Under plus end directed, assisting loads the distributions of data between the peaks in the 1μM ATP and 1mM AMP-PNP distributions are almost identical (Figure 5.6). According to the Uemura et al. [61] interpretation of binding states the motor spends a significant proportion of its time in a two head bound state even in very low levels of ATP. The peak values under assisting loads in 1μM ATP are shifted to slightly higher loads than in the

1mM AMP-PNP, at 8.8 and 15.1 pN as opposed to 6.4 and 12.5pN. These shifts are only minor and there is error in the fitting of these peaks.

Under assisting loads little difference is seen in the stepping rate of Kinesin-1 [55] such that the motor is still stepping at ∼1.25 steps per second. At the loading rate of 6.5pN/s used to collect the data shown in Figure 5.6 this means that the majority of motors have made at least one step before detaching. One explanation for the continued presence of high load detachments under both assisting and hindering loads is that these are alternate nucleotide free states (Figure 5.5).

The movement of peak positions to higher loads under assisting but not hindering forces could suggest that the no-nucleotide binding state is slightly less asymmetric in its detachment properties compared to the AMP-PNP state. This suggestion contradicts the data presented by Uemura et al. [61] who find that detachments from the AMP-PNP state take longer to occur. However, others have found the average unbinding times of both the nucleotide free and AMP-PNP states of the Kinesin-1 dimer to be very similar [103].

5.4.2 Unbinding of Kinesin-1 in the Presence of 5μM ATP

In the presence of 5μM ATP Kinesin-1 is capable of making around 6 steps per second when unloaded. As can be seen in Figure 5.6, under hindering loads this increases the average detachment load. Under assisting loads the increase in ATP and therefore the stepping rate leads to an average detachment load significantly below that seen for the 1mM AMP-PNP and 1μM ATP conditions.

In Figure 5.8 A and C the average detachment loads of Kinesin-1 in 1μM and 5μM ATP under varying loading rates are compared with those of the 1mM AMP-PNP conditions. Under nearly all assisting loading rates the Kinesin-1 in 5μM ATP detaches at a lower load than both 1mM AMP-PNP and 1μM ATP. The run length of Kinesin-1 has been shown to be very sensitive to assisting loads. Under assisting loads of 4pN then the run length of Kinesin-1 is 7/8 steps [62] down from about 100 steps when unloaded. This suggests that assisting loads interfere with the gating mechanisms of Kinesin-1 allowing it to enter the double head ADP-bound state more often. In our experiments in 5μM ATP at loading rates

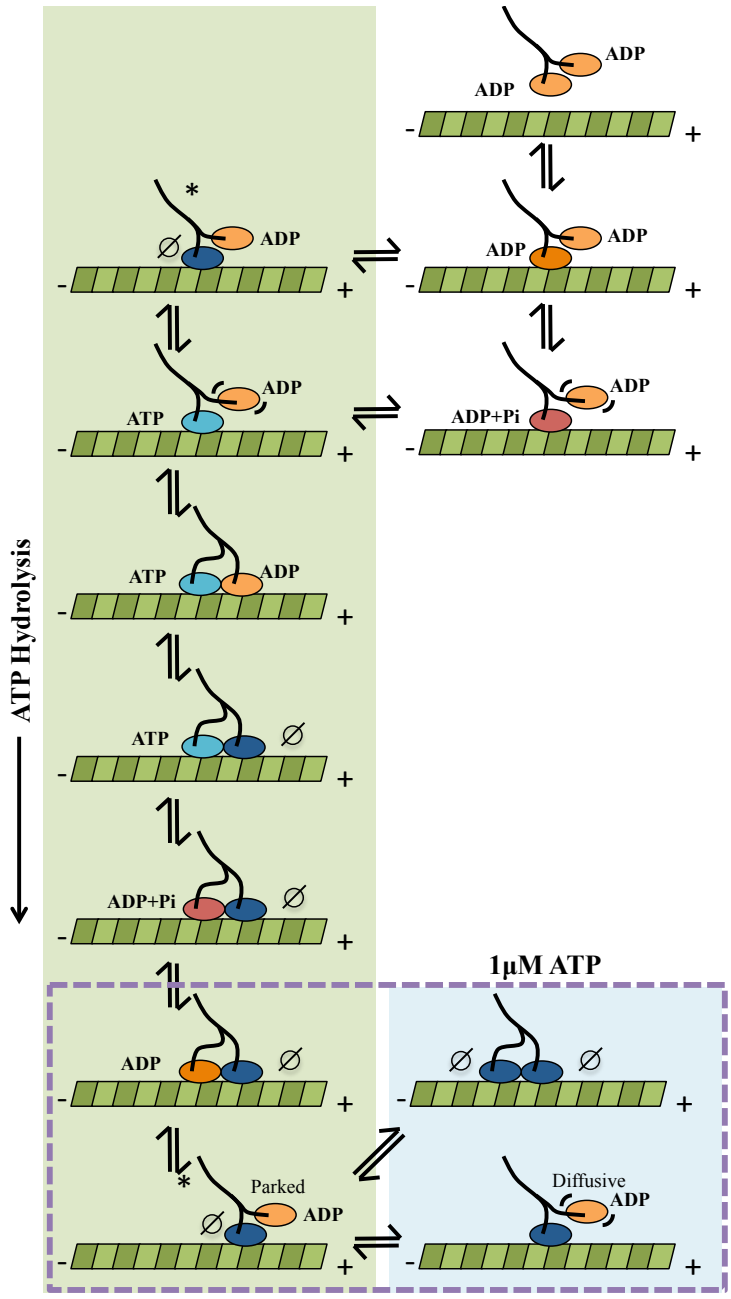

Figure 5.5: Overview of binding states in 1μM ATP. In 1μM ATP the motor unbinds predominantly from a nucleotide free state (purple box). The continued presence of peaks in the data suggests that in these conditions, like the AMP-PNP conditions, motors can exists in more than one MT binding state. We have suggested two possible states that could effect MT-binding strength (blue background).

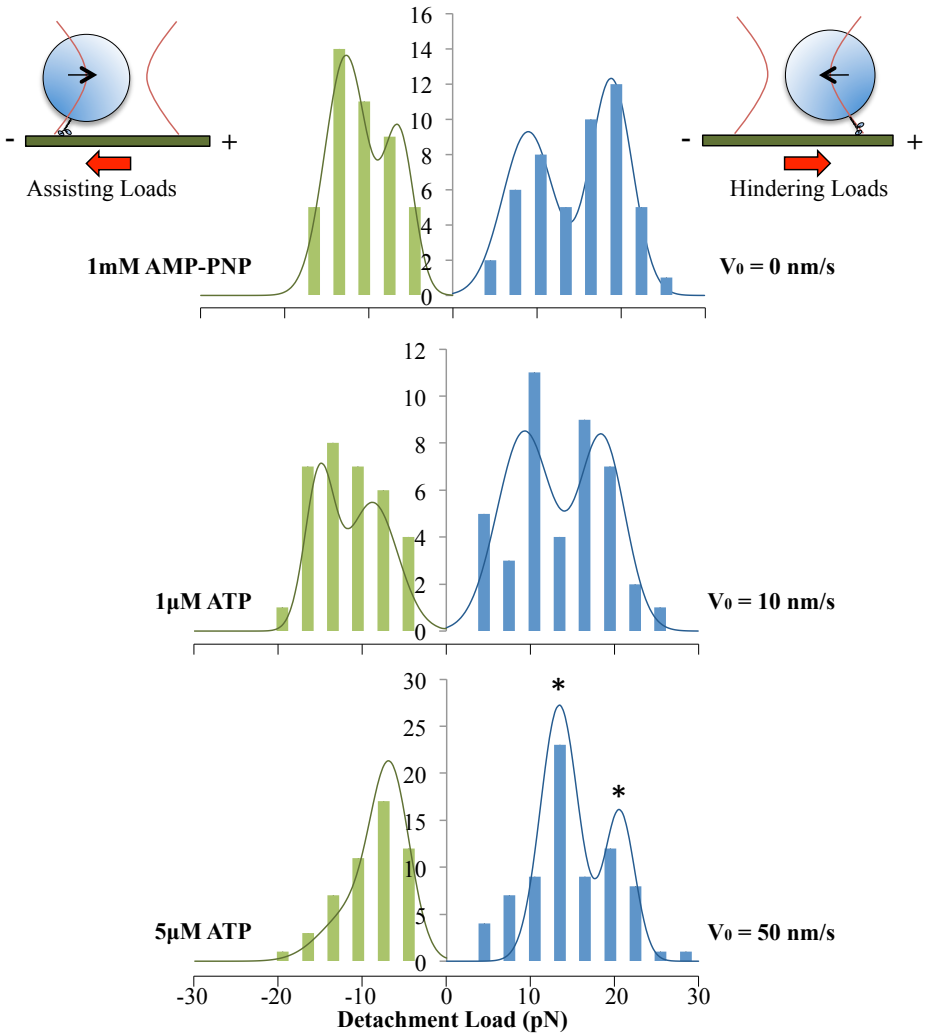

Figure 5.6: A) Detachment Loads for assisting (green) and hindering (blue) loading of Kinesin-1 in the presence of 1mM AMP-PNP (top), 1μM ATP (middle) and 5μM ATP (bottom) at 6.5 pN/s loading rate, 3.0 pN bins. Fitted curves are double gaussians fits to the data using MATLABs 'fitgmdist' function, mean and standard deviations of the peaks are given in Table 5.1. *The double gaussian for hindering load and 5μM ATP conditions were fit using a double gaussian to histogram data with 2pN bin widths in order to resolve the peaks. In the presence of ATP motors are able to step, the unloaded stepping rate, V_0, for each condition is shown.

of 4pN/s, motors detach at about 7pN and will have made on average 11 steps at this point. It is therefore likely that in 5μM ATP conditions, motors under slowly applied assisting loads detach from an ADP-bound state, as shown in Figure 5.7 (red box).

Under fast assisting loads (around 11pN/s) Kinesin-1 takes approximately 1s to detach. In this time the motor in 5μM ATP will have made around 6 steps and reached assisting loads of around 11pN. In 1μM ATP the motor will have made only one step in this time, however it will still detach at a similar average assisting load. It is likely that in these conditions the majority of detachments in both 5 and 1 μM ATP occur from a no-nucleotide state, (Figure 5.7 (purple box)).

In the presence of 5μM ATP the motor will step slowly under low hindering loads and as the load increases the stepping rate will decrease up to ~7pN where the rates of forwards and backwards steps are the same. Above this load the stepping rate remains constant but the majority of steps will be backwards steps. From data collected by Carter and Cross [55] in 10μM ATP we can put an upper bound on the stepping rate at stall of 1 step per second, although stepping in 5μM ATP is likely to be considerably slower. At higher loading rates the chance that a motor makes a step before detaching is slim, however if load is applied slowly then it is possible that the motor may make several steps before detaching.

The unbinding loads of Kinesin-1 in 5μM ATP conditions under hindering loads as in 1μM ATP are expected to occur from a nucleotide free state (Figure 5.7). The unbinding loads in 5μM ATP are slightly higher than those in 1mM AMP-PNP and 1μM ATP. The largest difference between the conditions is seen at low loading rates. At low loading rates the 5μM ATP unbinding loads are up to 4pN higher than those in 1mM AMP-PNP, it therefore takes longer for the motor to detach. The shift in detachment loads in 5μM ATP to higher loads affects both peaks in the distribution, with the lower peak increasing from 9 to 13.5 pN and the higher peak increasing from 18.9 to 20.5 pN. The reason for this shift is not clear at this stage and will be discussed later.

5.4.3 Kinesin-1 Asymmetry in Low ATP Conditions

Figure 5.8 B and D show the unbinding load asymmetry from Kinesin-1 in 1mM AMP-PNP, 1μM ATP and 5μM ATP conditions. In all conditions the detachment load under hindering loads is greater than under assisting loads. This is most striking in the 5 μM ATP conditions, where at low loading rates the average hindering unbinding load was twice that of assisting

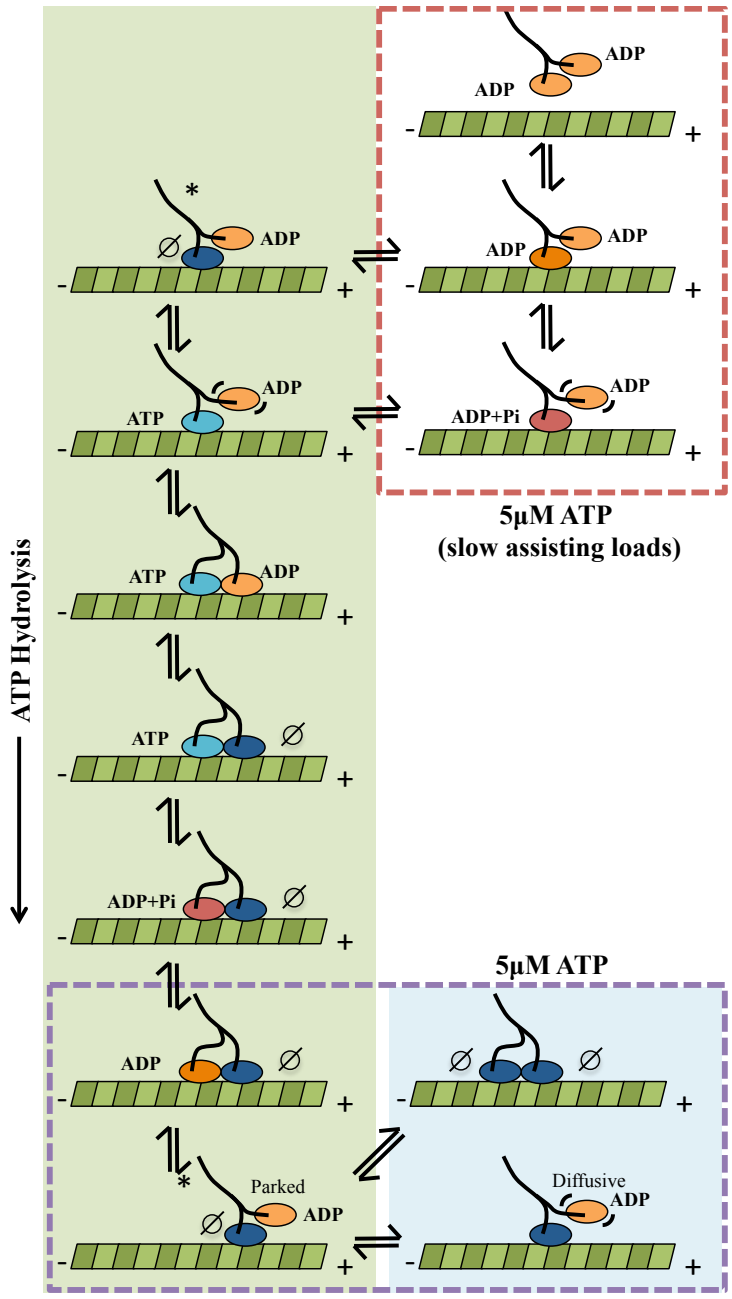

Figure 5.7: Overview of binding states in 5μM ATP. In 5μM ATP the motor unbinds predominantly from a nucleotide free state under hindering loads when stepping is slow (purple box). Under assisting loads the motor steps faster and detaches from a double head ADP bound state accessed by loss of head-head co-ordination (red box).

unbinding loads. In 1mM AMP-PNP conditions the unbinding asymmetry increases with increasing loading rate. This is expected but the gradient of this curve is significantly

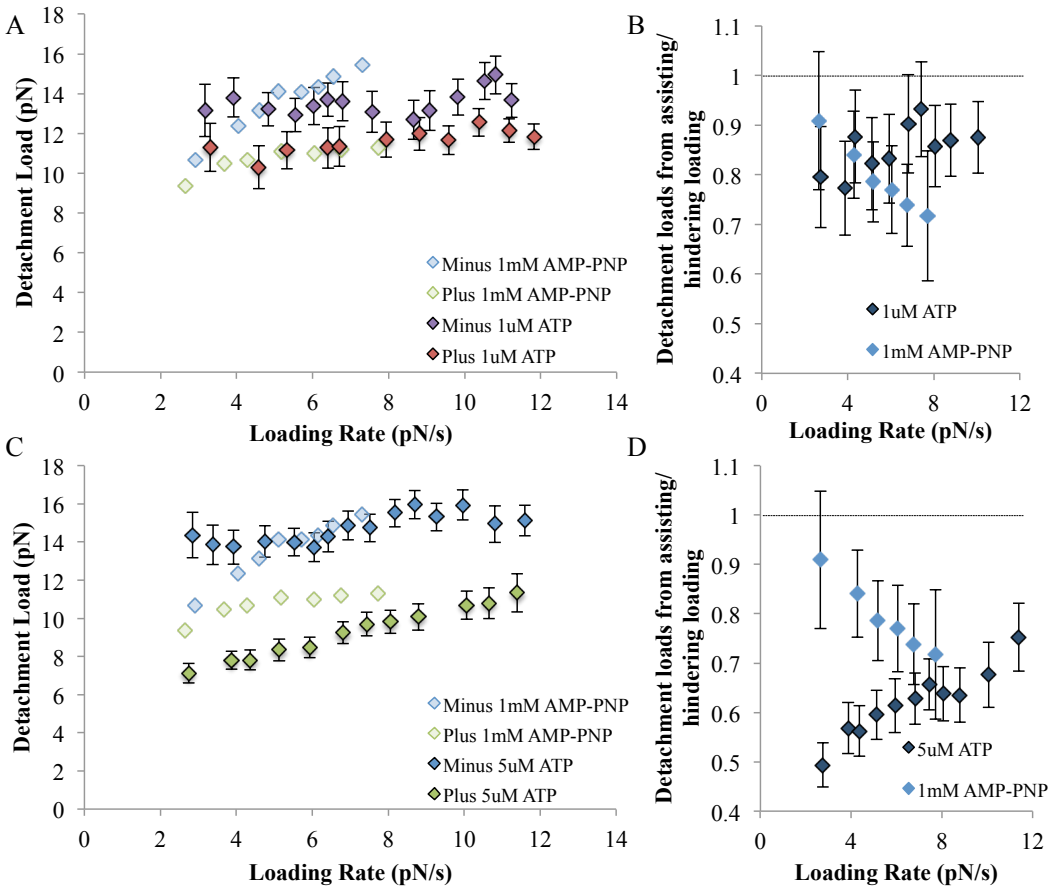

Figure 5.8: Detachment Load with loading rate and assisting/hindering load asymmetries for Kinesin-1 in the presence of ATP. A) Detachment Loads for assisting (red) and hindering (purple) loading of Kinesin-1 in the presence of 1μM ATP over a range of loading rates (mean and SE) B) Ratio of average detachment load from assisting/hindering loads as it varies with loading rate for 1mM AMP-PNP conditions (blue) and 1μM ATP conditions (purple). C) Detachment Loads for assisting (green) and hindering (blue) loading of Kinesin-1 in the presence of 5μM ATP (black edges) and 1mM AMP-PNP over a range of loading rates (mean and SE) D) Ratio of average detachment load from assisting/hindering loads as it varies with loading rate for 1mM AMP-PNP conditions (blue) and 5μM ATP conditions (purple).

steeper than predicted from simple considerations of average detachment time calculated from Equation 5.3. The predicted asymmetry changes from 0.8 at 2pN/s loading rate to 0.78 at 9pN/s, differing significantly from the change from 0.9-0.7 seen experimentally. This is probably due changes in the sizes of peak populations depending on loading rate [69]. The simple model fitted here ignores this peak structure.

Interestingly, the asymmetry seen for Kinesin-1 in the presence of ATP shows an opposite trend, being asymmetric at slow loading rates. This is most striking for the 5μM ATP conditions, Figure 5.8D, where ratios go from 0.5 at 3pN/s to 0.75 at 12pN/s. This asymmetry change is due to differences in the unbinding loads under assisting forces, which increase with loading rate whilst those under hindering loads remain constant. The trend towards less asymmetry suggests that for loading rates of 23pN/s the detachment load under both conditions would be the same. Since the low unbinding loads of Kinesin-1 in 5μM ATP are due to a weakly bound state incurred whilst stepping, we would suggest that this asymmetry would be more pronounced in faster stepping motors.

5.5 Conclusions

Initial findings for Kinesin-1 unbinding loads in single nucleotide conditions are in agreement with the work of Uemura et al. [61]. In 1mM ADP motors detach at low loads of around 3.5 pN and show no direction dependent asymmetry. Uemura et al. [61] find that there are two peaks in the value of unbinding loads in the presence of 1mM AMP-PNP. If double gaussians are fitted to our data the positions of the two peaks are similar to those of Uemura et al. [61]. The 1mM AMP-PNP conditions give a directional asymmetry of 35% higher loads under minus end directed loading.

In the presence of 5 or 1μM ATP unloaded Kinesin-1 motors step at 50 and 10 nm/s respectively. Unbinding loads in the plus end direction for 1μM ATP are slightly higher than in 1mM AMP-PNP. In 5μM ATP the detachment loads at low assisting loading rates are much lower than in 1mM AMP-PNP and 1μM ATP conditions. It is suggested that this is due the greater number of steps leading to a higher probability of entry into a weak binding state whilst stepping.

Unbinding loads under hindering loads for both 1μM ATP and 1mM AMP-PNP conditions show peaks at around 18.5 pN corresponding to a two heads bound state and at 9pN a one head bound state. In the 5μM ATP condition the peak structure is less clear but higher average unbinding loads are seen especially at low loading rates. The presence of double peaks in the data for 1μM and 5μM ATP data is surprising as it is expected that the motor

will mostly be in a no nucleotide waiting state. This throws in to question whether these peaks are a result of a one or two head bound state, or whether these two binding states might have a different interpretation (Figure 5.5).

Chapter 6

Results: Unbinding Loads for Kif15

In the previous chapter unbinding experiments were tested on Kinesin-1 and found to give results which were comparable with previous observations [61]. It was found that the stepping of Kinesin-1 lead to a greater asymmetry in unbinding under assisting and hindering loads. In this chapter we use the same approach to investigate the asymmetry of Kif15 binding under externally applied loads. Since Kif15 is thought to work in the spindle overlap or K-fibre bundles this is of particular interest as a differing response to loads towards plus and minus ends of the MTs could affect the sliding of MTs within bundles.

We look first at Kif15-1293 and FL-Kif15 in the presence of ADP. Next the unbinding loads of Kif15-1293 in AMP-PNP are examined, before comparison of both motors in the presence of 5μM ATP. Finally the effect of Tpx2 on the unbinding load of FL-Kif15 is investigated.

6.1 Unbinding of Kif15-1293 and FL-Kif15 in the Presence of 1mM ADP

FL-Kif15 and Kif15-1293 differ only in the lack of the C-terminal region responsible for motor inhibition and Tpx2 binding. Comparing the unbinding loads of the two motors in 1mM ADP shows a surprising difference. Kif15-1293 has a similar unbinding load distribution to Kinesin-1 in 1mM ADP detaching at loads of around 3.5 pN, Figure 6.1A. Interestingly FL-Kif15 appears to have secondary peaks at 11.8 and 8.5 pNs under minus and plus end directed loads respectively, Figure 6.1B. In these conditions insufficient data was gathered to use GMM fitting, instead gaussians were fitted to the histograms of unbinding loads and not the underlying data, Table 6.1.

More data would be need to be collected to confirm the presence of these peaks, however they do suggest that the presence of the inhibitory C-terminal tail of Kif15 encourages the motor to bind the MT in a strong binding state even in the presence of high ADP. From data on FL-Kif15 dwell times it appears that the tail of Kif15 is able to interfere with the stepping of the motor at loads below 3pN (Figure 4.5A). Above these loads the tail can no longer begin to interfere with motor stepping, however motors that are already in an inhibited state remain so. The peaks seen in the unbinding loads of FL-Kif15 in the presence of 1mM ADP suggest that in a small proportion of motors (around 20%) the tail region may interfere and encourage a more tightly bound state, this is likely to be a nucleotide free state (Figure 6.2).

Motor	**n**	**Loading Rate (pN/s)**	**Assisting Load (pN)**	**Hindering Load (pN)**
Kinesin-1	52	3.5±1.3	3.6±2.0	3.5±1.4
Kif15-1293	45	3.6±1.4	3.2±1.1	3.9±1.6
FL-Kif15	66	3.6±1.6	2.1±1.8 (0.73) 8.4±2.9 (0.27)	4.3±1.9 (0.84) 11.2±0.9 (0.16)

Table 6.1: Loading rates and Unbinding load peaks for Kinesin-1, Kif15-1293 and FL-Kif15 in 1mM ADP, peak proportions are shown in brackets.

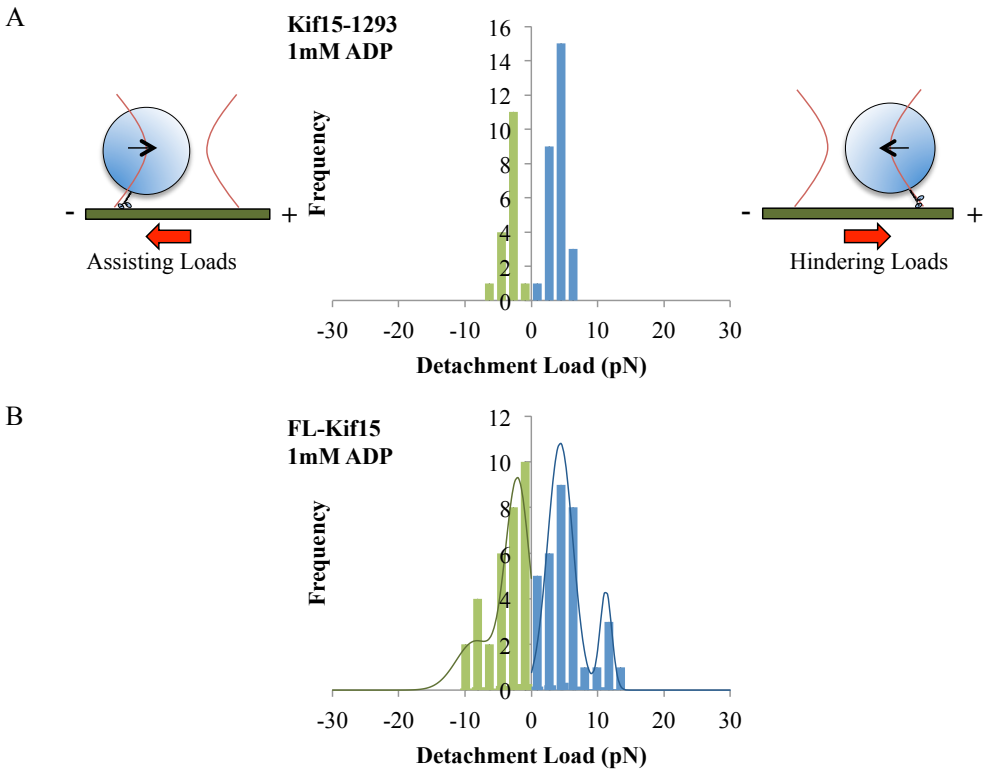

Figure 6.1: Unbinding Load distributions for Kif15-1293 and FL-Kif15 in the presence of 1mM ADP. Negative loads (green) are detachments under assisting loads. Positive loads (blue) are detachments under hindering loads. Bin widths are 1.8 pN. B) Dark green and blue fitted lines are double gaussians fitted to the assisting and hindering load histograms. Details of peak positions and number of data points are shown in Table 6.1

6.2 Unbinding of Kif15-1293 in the Presence of 1mM AMP-PNP

In the presence of 1mM AMP-PNP Kif15-1293 unbinding under hindering loads can be fit with two peaks, each of these is of a lower load than the corresponding peak in Kinesin-1 data (Figure 6.3A). This suggests that Kif15-1293 in the AMP-PNP bound state is either slightly less tightly bound than Kinesin-1 or is more load sensitive. The average unbinding loads of Kif15-1293 in 1mM AMP-PNP under varying hindering loading rates suggests the former. The detachment load variation with loading rate is very similar to Kinesin-1 but with an average unbinding load around 5 pN lower at all loading rates, Figure 6.3B. The

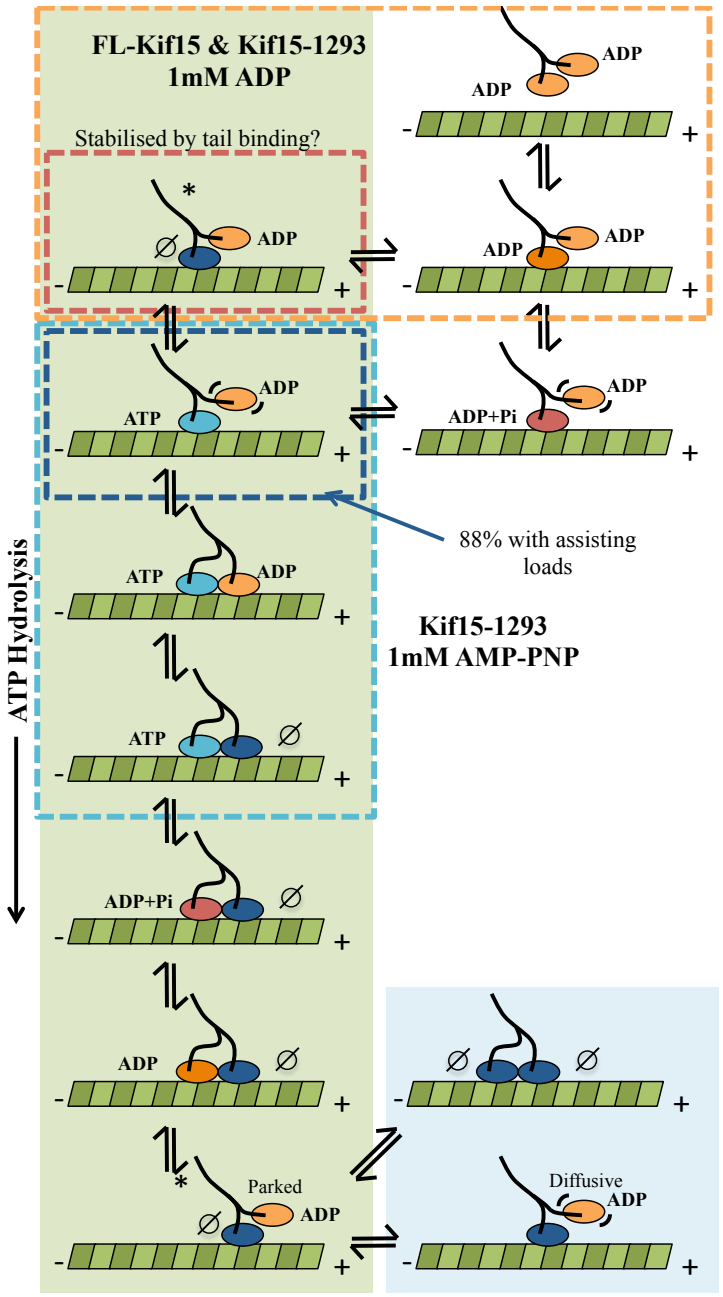

Figure 6.2: Overview of binding states for FL-Kif15 and Kif15-1293. In 1mM ADP the majority of motors unbind similarly to Kinesin-1 (orange box). FL-Kif15 however also displays a small subset of motors that unbind from a stronger binding state possibly a stabilised nucleotide free state (red box). In 1mM ANP-PNP Kif15-1293 detaches from a single or double head bound state (blue box), however under assisting loads the majority of motors unbind from a single head bound state (dark blue box).

proportion of motors that detach at the higher peak for Kif15-1293 under hindering loads is approximately 40% at 4.6pN/s loading rate. This is only slightly less than Kinesin-1, where the detachment peaks are evenly populated.

Plotting this data in terms of average time to detachment against loading rate shows that at low loading rates the time to unbinding for Kif15-1293 is about half that for Kinesin-1, suggesting that its unloaded average binding time is significantly shorter. This has been shown to be the case for FL-Kif15 with an average unbinding time of 12.2s in 1mM AMP-PNP [33]. The unloaded average binding time for Kinesin-1 with AMP-PNP is 100 s [103]. It appears that for Kif15-1293 the unbinding time is less sensitive to load as the average unbinding time is fairly constant.

Motor	**n**	**Loading Rate (pN/s)**	**Assisting Load (pN)**	**Hindering Load (pN)**
Kinesin-1	104	6.0±1.8	6.4±1.8 (0.32) 12.7±2.5 (0.68)	9.0±3.0 (0.48) 18.9±2.5 (0.52)
Kif15-1293	107	4.6±1.3	4.4±2.0 (0.88) 16.3±6.0 (0.12)	6.3±2.2 (0.59) 13.7±5.5 (0.41)

Table 6.2: Loading rates and unbinding load peaks for Kif15-1293 and Kinesin-1 in 1mM AMP-PNP.

Under assisting loads, Kif15-1293 in 1mM AMP-PNP shows a major peak at 4.4 pN and a second poorly defined peak at 16.6 pN. The low unbinding load under assisting loads for Kif15-1293 is very similar to that seen in 1mM ADP. The majority of the data, 88%, is in the lower peak for Kif15-1293, a distinct difference between Kinesin-1 and Kif15-1293. The average unbinding load under minus end directed forces for Kif15-1293 is 31% more than under plus end directed forces at 4.5pN/s loading rate. This is a greater asymmetry than the 18% seen for Kinesin-1 at a similar loading rate of 4.3pN/s. Under assisting forces the average unbinding times for Kif15-1293 seem less affected by loading rate than those for Kinesin-1. This means that as the loading rate increases the average unbinding load for Kif15 increases more rapidly than it does for Kinesin-1.

As demonstrated in the previous chapter, it is possible to fit a curve to the average unbinding

time data, fitted parameters are shown in Table 6.3. The average residency time of FL-Kif15 dimers in the presence of 1mM AMP-PNP has been found to be 12.2 s [33]. Using least squares fitting the characteristic distances for Kif15-1293 are 1.4 and 0.8 nm for plus and minus end directed loading respectively. This shows a larger asymmetry than Kinesin-1 which has characteristic distances of 1.5 and 1.1 nm.

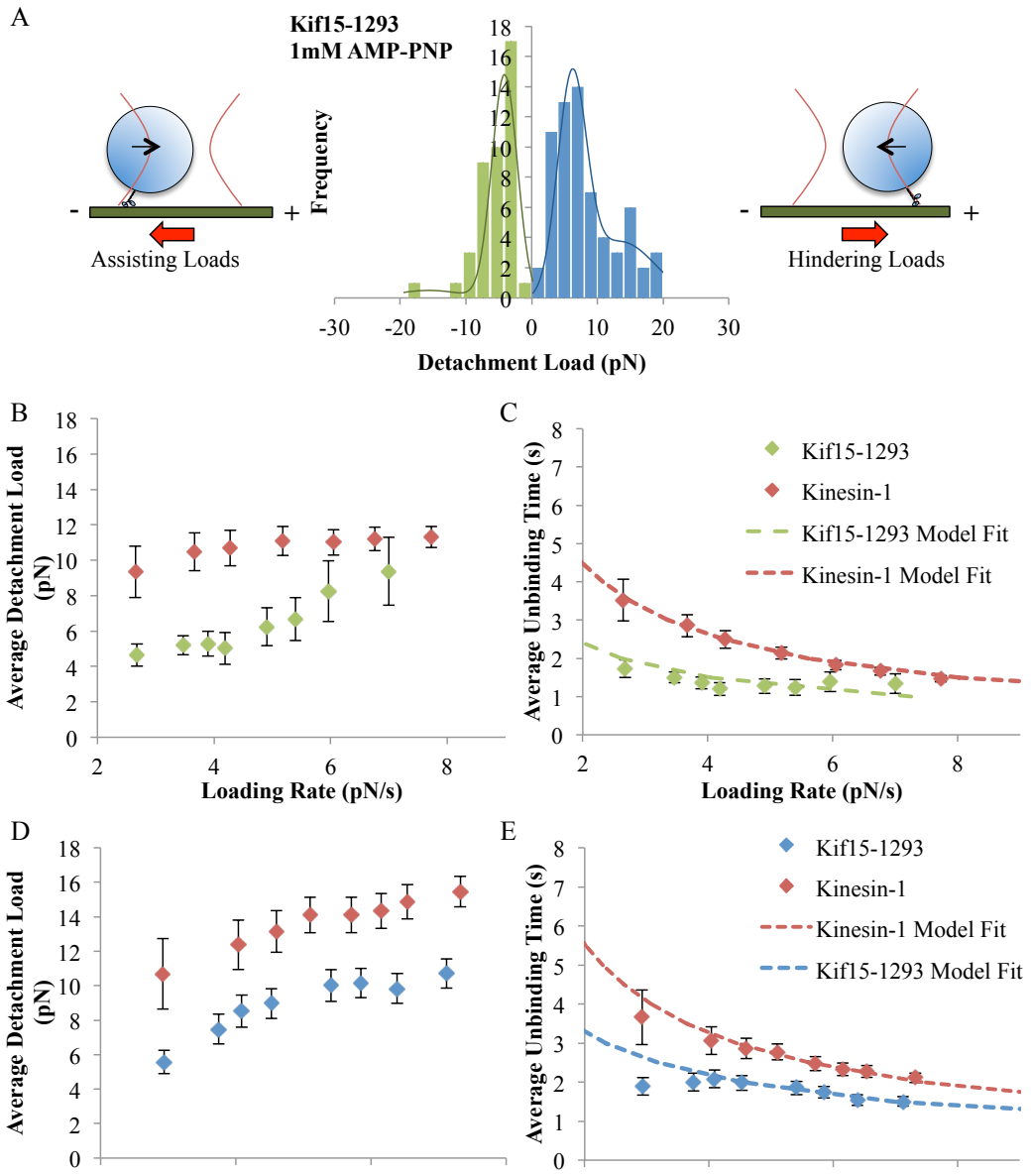

Figure 6.3: A) Unbinding Load distributions for Kif15-1293 in the presence of 1mM AMP-PNP. Loading Rate is 4.6pN/s, bin widths are 2 pN. Dark green and blue fitted lines are double gaussians fitted to the assisting and hindering load histograms. Details of peak positions and number of data points are shown in Table 6.4. B) Average load of detachment under assisting loads at varying loading rates for Kif15-1293 (green) and Kinesin-1 (red) , mean and SE. C) Average time until detachment at varying assisting loading rates for Kif15-1293 (green) and Kinesin-1 (red), mean and SE. Dotted lines show least squares model fits to Equation 5.8. For parameters see Table 6.3. D) Average load of detachment under hindering loads at varying loading rates for Kif15-1293 (blue) and Kinesin-1 (red) , mean and SE. E)Average time until detachment at varying hindering loading rates for Kif15-1293 (blue) and Kinesin-1 (red), mean and SE. Dotted lines show least squares model fits to Equation 5.8. For parameters see Table 6.3.

Motor	$\tau(0)$ (s)	d_a (nm)	d_h (nm)	d_a/d_h
Kinesin-1	100	1.5	1.1	1.36
Kif15-1293	12.2	1.4	0.8	1.75

Table 6.3: Parameter values for Kif15-1293 and Kinesin-1 AMP-PNP model fits, $\tau(0)$ values are taken from literature [103, 33] whilst characteristic distances under assisting loads, d_a, and hindering loads, d_h, are found by least squares fits to data shown in Figure 6.3.

6.3 Unbinding of Kif15-1293 and FL-Kif15 in the Presence of 5 μM ATP

We next looked at Kif15-1293 and FL-Kif15 in the presence of 5 μM ATP. At this ATP concentration Kif15-1293 steps at 36 nm/s and FL-Kif15 at a slightly slower rate. The rate of unloaded stepping for FL-Kif15 is unknown, as the motor movement was not consistent enough to get a good reading from the DIC display. Best estimates are between 10 and 30 nm/s. This means that under plus end directed loads it is likely that Kif15-1293 makes at least 4 steps per second and FL-Kif15 between 1 and 4 steps per second. Unlike Kinesin-1 the velocity dependence of Kif15 under assisting loads is not known, it is possible that the stepping rate of Kif15 increases significantly under assisting loads.

Kif15-1293

Under plus end directed loading Kif15-1293 has a similar unbinding load profile in 5μM ATP as in 1mM AMP-PNP. It shows one major peak at low loads of 3.3 pN, this is also similar to its behaviour in 1mM ADP. The lack of a secondary peak shows that in these conditions the majority of motors unbind from a one head bound state under plus end directed loads. Likely unbinding states are shown in Figure 6.5 (red box). Since there is little data in these conditions it is possible that a second higher load peak might emerge but it is clear that this is a small minority.

In 5 μM ATP and under hindering loads Kif15-1293 shows an increase in the unbinding loads of both peaks in the distribution compare to AMP-PNP conditions, Figure 6.4A. The two

peaks are at approximately 10 and 20 pN as opposed to 11 and 16.5 pN in 1mM AMP-PNP. This increase in average unbinding load in the presence of 5 μM ATP is similar to that seen for Kinesin-1. The majority of unbinding events (75%) under hindering loads take place from the more weakly bound state.

There is a striking difference in the effect of loading rate upon the average load of detachment between Kif15-1293 in 1mM AMP-PNP and 5 μM ATP, Figure 6.4B. In the presence of ATP the load at which the motor detaches in both the plus and minus end directions appears unchanged when the loading rate is varied. Conversely, in the presence of 1mM AMP-PNP, unbinding loads increase with loading rate. Invariance to loading rate means that in 5 μM ATP the ratio of unbinding loads under plus and minus end directed loading remains constant whereas in 1M AMP-PNP the unbinding load asymmetry is greatest at around 4-5 pN and decreases at higher and lower loading rates.

In low ATP conditions a similar argument to that used for Kinesin-1 is possible. That is, the unbinding loads seen for this motor in these conditions are from the no-nucleotide state (Figure 6.5). For Kif15 it would appear that this state is significantly more tight binding than the AMP-PNP bound state. This state detaches at a fairly constant load and not a constant time as seen for the AMP-PNP bound state (Figure 6.4C). By extrapolating to unloaded motors this suggests that the no-nucleotide state has a much longer MT binding lifetime than the AMP-PNP bound motor.

Under assisting loads Kif15-1293 also detaches at more constant loads when in ATP than AMP-PNP conditions. In AMP-PNP faster loading rates cause the motor to detach at higher loads of around 8pN, however in 5μM ATP the motor always detaches below 5pN, Figure 6.4B. This could indicate that some part of its stepping cycle is very weakly bound and susceptible to assisting loads. Alternately it could be likely to lose head-head co-ordination and enter a double head ADP bound state (Figure 6.5). Since the detachment loads of both the ADP and AMP-PNP conditions are so similar under plus end directed loading, perhaps this leads to a loss of stepping co-ordination under assisting loads. In the time taken for the motor to detach Kif15-1293 is likely to have made at least 2 steps before detaching even at the fastest loading rates. If assisting forces speed up Kif15-1293 stepping this number could be higher.

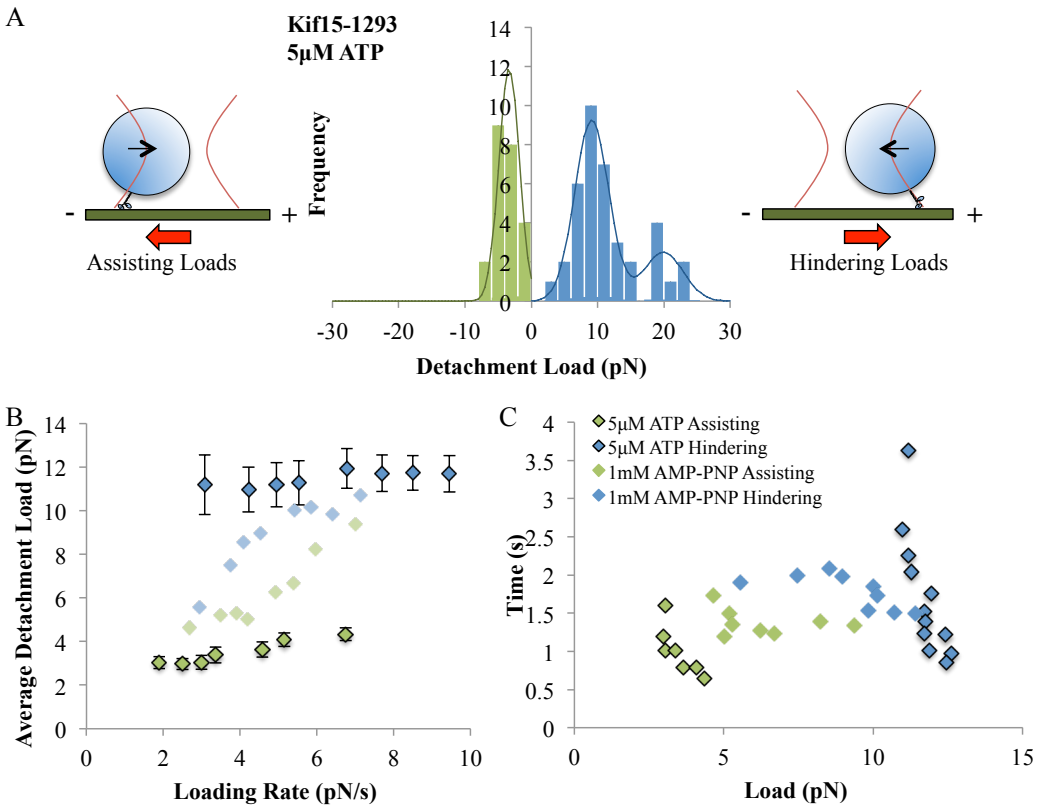

Figure 6.4: A)Unbinding Load distributions for Kif15-1293 in 5 μM ATP under plus (green) and minus (blue) end directed loads. Fitted lines represent peaks in the data found by fitting a double gaussian using MATLABs 'fitgmdist' function. Bin widths are 2 pN. B) Average load of detachment under varying plus (green) and minus (blue) end directed loading rates in the presence of 1mM AMP-PNP (light colours) and 5 μM ATP (dark colours), mean and SE. C) Time to detachment versus detachment load for plus (green) and minus (blue) end directed loading in the presence of 1mM AMP-PNP (light colours) and 5 μM ATP (dark colours)

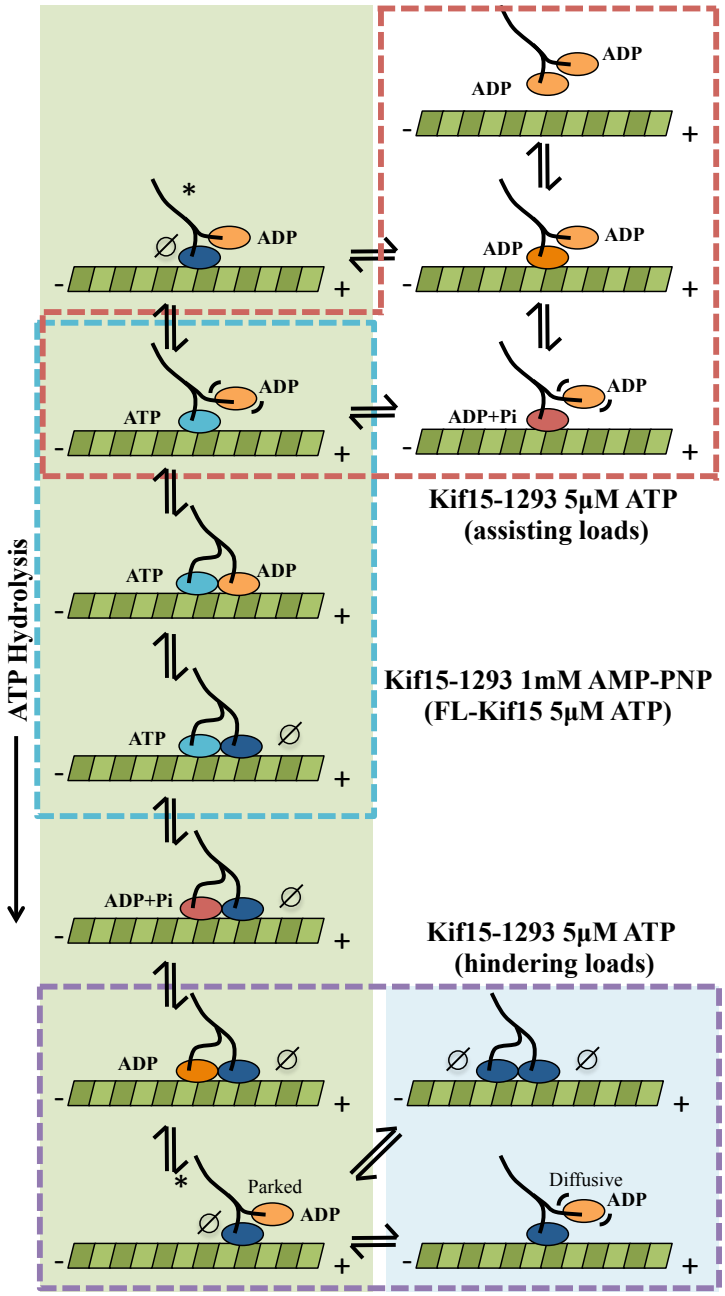

Figure 6.5: Overview of binding states for Kif15-1293 and FL-Kif15 in 5μM ATP. In 5μM ATP the Kif15-1293 unbinds predominantly from a nucleotide free state under hindering loads when stepping is slow (purple box). Under assisting loads the motor steps faster and detaches from a double head ADP bound state accessed by loss of head-head co-ordination or from a weakly MT-bound ATP state (red box). The detachment loads of FL-Kif15 are similar to those of Kif15-1293 in 1mM AMP-PNP (blue box).

Motor	n	Loading Rate (pN/s)	Assisting Load (pN)	Hindering Load (pN)
Kinesin-1	104	6.5±1.8	6.7±2.3 (0.7) 11.3±3.6 (0.3)	11.3±4.8 (0.67) 16.5±5.0 (0.33)
Kif15-1293	62	5.2±2.3	3.8±1.5	9.1±2.6 (0.76) 20.0±3.0 (0.24)
FL-Kif15	104	4.8±2.8	3.9±1.8 (0.65) 9.2±2.5 (0.35)	6.0±2.9 (0.69) 14.4±2.5 (0.31)

Table 6.4: Loading rates and unbinding load peaks for Kinesin-, Kif15-1293 and FL-Kif15 in 5 μM ATP.

FL-Kif15

FL-Kif15 in 5 μM ATP under both plus and minus end loading appears very similar to Kif15-1293 in the presence of 1mM AMP-PNP, Figure 6.6A. The unbinding loads under plus end directed loading show two peaks at 4.8 and 9.2 pN. The second peak for FL-Kif15 suggests that it spend more time in a strongly bound state that Kif15-1293 in the presence of either 1mM AMP-PNP or 5 μM ATP, although it still unbinds from a predominantly one head bound state.

Under minus end directed loading FL-Kif15 unbinds from two peaks at 6.3 and 14.4 pN, very similar to the 6.3 and 13.7 pN seen for Kif15-1293 in 1mM AMP-PNP. The distribution of loads between the two peaks is also very similar in these two cases. Variation of unbinding load with loading rate for FL-Kif15 in 5 μM ATP also bears a lot of similarity to the 1 mM AMP-PNP conditions for Kif15-1293 (Figure 6.6 B). This suggests that the FL-Kif15 motor is not stepping and spends much of its time in an AMP-PNP-like state (Figure 6.5).

This observation needs to be reconciled with the extra peaks in the 1mM ADP data from FL-Kif15. The appearance of extra peaks in this dataset suggests that the inhibited state can be accessed from either nucleotide free or ADP bound state. The high load peaks in the ADP data set occur around the same loads as in the ATP data set, suggesting that the tail has induced the same state in both situations. One simple explanation is that the tail

acts upon a nucleotide free state and serves to induce an AMP-PNP like conformation in the heads. More experiments will be needed to fully explain the mechanism behind Kif15 tail inhibition.

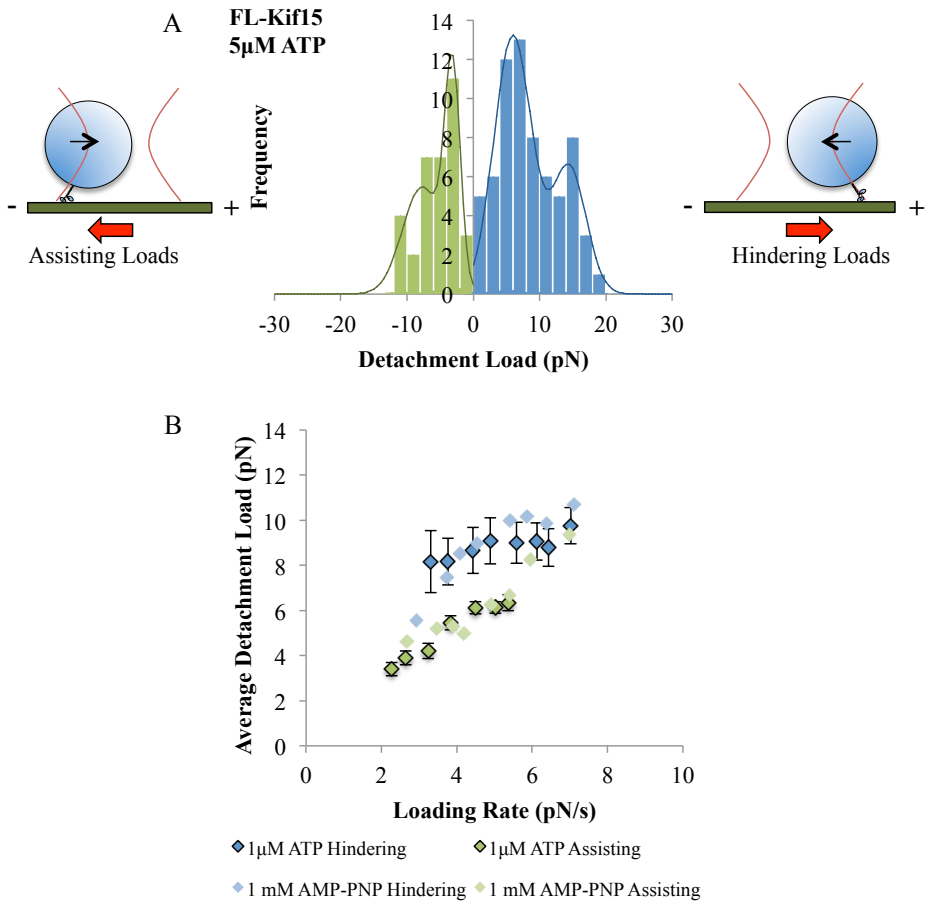

Figure 6.6: A)Unbinding Load distributions for FL-Kif15 in 5 μM ATP under plus (green) and minus (blue) end directed loads. Fitted lines represent peaks in the data found by fitting a double gaussian using MATLABs 'fitgmdist' function. Bin widths are 2 pN. B) Average load of detachment under varying plus (green) and minus (blue) end directed loading rates for Kif15-1293 in the presence of 1mM AMP-PNP (light colours) and FL-Kif15 in the presence of 5 μM ATP (dark colours), mean and SE.

6.4 Unbinding Asymmetries

Figure 6.7 and Table 6.5 show the ratio of unbinding loads due to hindering over assisting loads. Higher values represent states where the load needed to detach the motor by pulling

towards the minus end of the MT is more than the load needed to detach by pulling towards the plus end. Values of one represent a symmetrical state where the direction of loading makes no difference to the unbinding load.

The first thing to notice is that for both Kif15-1293 and Kinesin-1 the most asymmetric state is the 5 μM ATP condition. In this case the motors are able to step, especially under plus end directed loading. Under minus end directed loads we know that the stepping of both motors is slowed significantly, Section 4.5.3. In the presence of 1 mM AMP-PNP there appears little difference in the asymmetry of Kinesin-1 and Kif15-1293, however in 5 μM ATP Kif15-1293 shows far more asymmetry than Kinesin-1. This not the case for FL-Kif15.

This asymmetry under stepping conditions for both motors is thought to be caused by the high chance of failure for motors making steps under forwards load. For Kinesin-1 it is known that the run length under assisting load is short [62] and it seems likely given our data that the same is true for Kif15-1293. Under hindering loads the occasional steps made by the motor are fewer and less likely to fail than under assisting loads. The greater asymmetry of Kif15 when compared to Kinesin-1 is the result of both a greater weakness under assisting loads and a greater binding strength of the no-nucleotide state compared to the AMP-PNP bound state.

The behaviour of the motors in 1mM ADP also have large error bars making it hard to judge the extent of any asymmetry. For Kinesin-1 previous experiments have show no asymmetry, the results here show that there is asymmetry favouring detachment under minus end directed loads. Especially for the highest loading rate of 7 pN/s this is not a reliable value, there being only 17 data points in this data set. Again for Kif15-1293 and FL-Kif15 the asymmetry suggested is not convincing, more data would be needed to confirm or deny any asymmetry.

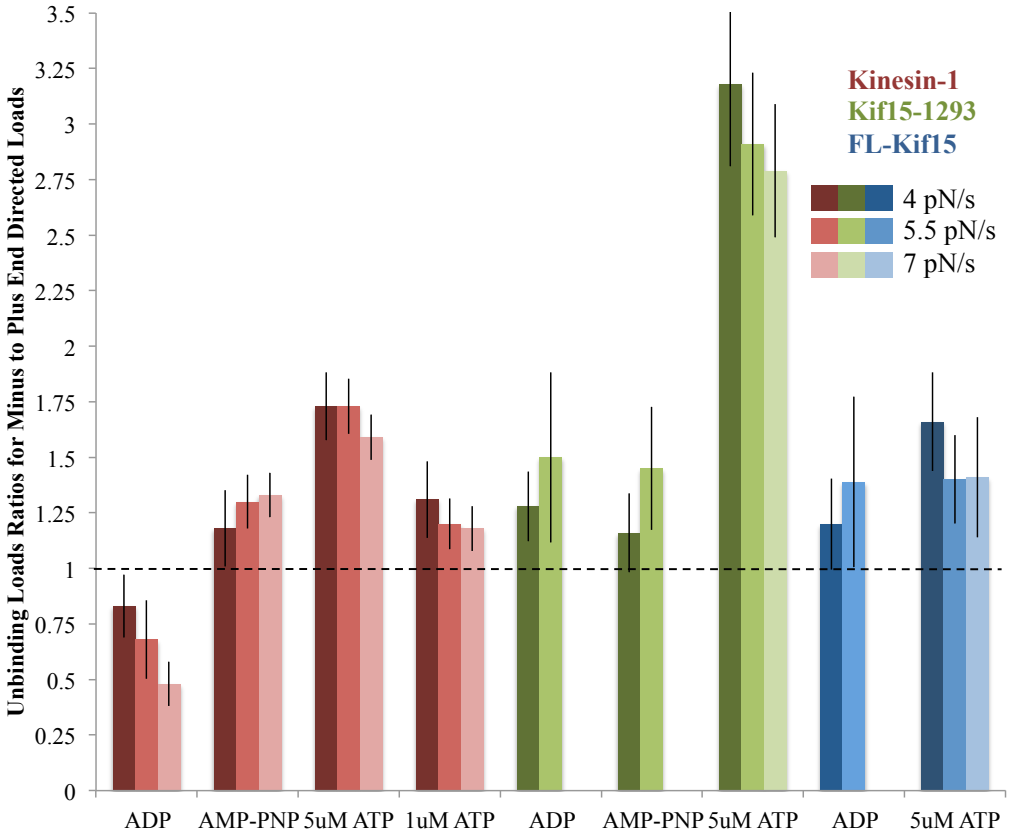

Figure 6.7: Ratio of unbinding loads due to minus end loading to those from plus end loading for Kinesin-1 (red), Kif15-1293 (green) and FL-Kif15 (blue) in varying nucleotide conditions. Mean and SE at three loading rates, 4 pN/s (dark colours), 5.5 pN/s (medium colours) and 7 pN/s (light colours). See Table 6.5 for values.

	Kinesin-1			Kif15-1293			FL-Kif15		
	Loading Rate: 4 pN/s								
Nucleotide	n_p	n_m	Ratio $\frac{L_m}{L_p}$	n_p	n_m	Ratio $\frac{L_m}{L_p}$	n_p	n_m	Ratio $\frac{L_m}{L_p}$
1mM ADP	24	39	0.8±0.1	14	33	1.3±0.2	20	31	1.2±0.2
1 mM AMP-PMP	22	20	1.2±0.2	31	63	1.2±0.2	-	-	-
5 μM ATP	51	37	1.7±0.2	38	26	3.2±0.4	44	46	1.7±0.2
1 μM ATP	15	29	1.3±0.2	-	-	-	-	-	-
	Loading Rate: 5.5 pN/s								
Nucleotide	n_p	n_m	Ratio $\frac{L_m}{L_p}$	n_p	n_m	Ratio $\frac{L_m}{L_p}$	n_p	n_m	Ratio $\frac{L_m}{L_p}$
1mM ADP	9	32	0.7±0.2	5	16	1.5±0.4	4	11	1.4±0.4
1 mM AMP-PMP	39	42	1.3±0.1	23	43	1.5±0.3	-	-	-
5 μM ATP	52	69	1.7±0.1	19	43	2.9±0.3	19	51	1.4±0.2
1 μM ATP	26	51	1.2±0.1	-	-	-	-	-	-
	Loading Rate: 7 pN/s								
Nucleotide	n_p	n_m	Ratio $\frac{L_m}{L_p}$	n_p	n_m	Ratio $\frac{L_m}{L_p}$	n_p	n_m	Ratio $\frac{L_m}{L_p}$
1mM ADP	4	13	0.5±0.1	-	-	-	-	-	-
1 mM AMP-PMP	33	37	1.3±0.1	-	-	-	-	-	-
5 μM ATP	72	89	1.6±0.1	10	28	2.8±0.3	7	10	1.4±0.3
1 μM ATP	35	45	1.2±0.1	-	-	-	-	-	-

Table 6.5: Sample sizes and ratios of unbinding loads from minus to plus end directed loads for Kinesin-1, Kif15-1293 and FL-Kif15.

6.5 MT Sliding Experiments with Tpx2

The final experiments performed examined the effect of Tpx2 on the load bearing ability of FL-Kif15. Since in previous experiments Tpx2 was shown to cause sticking of the polystyrene beads to the surface of the slide a first experiments was to perform the unbinding experiments on blank beads in order to see the effect of Tpx2 in solution. Blank beads were prepared in the same manner as those with motors attached, with prior incubation in 0.3mg/ml casein before introduction to the flow cell. Tpx2 was added in 18 nM concentration to the running buffer. Since the beads in these experiments contained no motors it was not possible to determine the polarity of the MTs and so both plus and minus end loading data is combined.

The results of the blank bead control are shown in Figure 6.8A. In the absence of motors Tpx2 in solution causes beads to occasionally bind to MTs or the surface. This loads at which these binding events detached are distributed in an exponential manner. Loads in the lowest, 0-2 pN, bin are lower most likely due to difficulty scoring events in this range.

6.5.1 Full Length Kif15 and Tpx2

In order to make the unbinding experiments in the presence of Tpx2 comparable with previous data 5 μM ATP was also included. As in previous chapters at a concentration of 18nM Tpx2 in solution no motility was seen. In order to ensure we were seeing the behaviour of an active FL-Kif15 motor the motility of a motor was first checked in the absence of Tpx2 and the MT polarity was marked. Flow throughs were performed with buffer containing 5μM ATP and 18nM Tpx2, data was then collected.

As can be seen in Figure 6.8B the unbinding of FL-Kif15 is similar to the 5 μM ATP results, albeit with some blurring due to Tpx2 sticking. However this is not because Tpx2 caused no binding load increase. In presence of Tpx2 FL-Kif15 often bound to MTs and were capable of withstanding loads of over 30 pN at the loading rates used. This was true for both assisting and hindering loads. In order to increase the trap stiffness bead of larger diameter were used allow us to access loads of up to 40 pN, this was still not enough to

unbind the motors from the MT. The unbinding loads shown in Figures 6.8 B and C are therefore the unbinding events of FL-Kif15 motors which have not encountered Tpx2 in their MT binding.

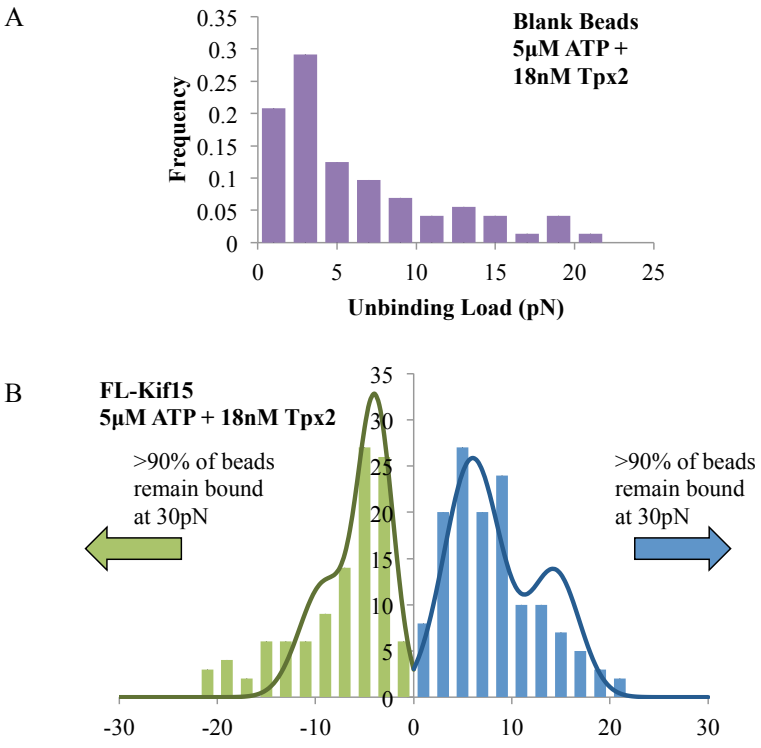

Figure 6.8: A)Unbinding load distributions for blank beads and B) FL-Kif15 in the presence of 5 μM ATP and 18nM Tpx2. Dark green and blue lines show the distribution fitted to FL-Kif15 in 5μM ATP in the absence of Tpx2. After several runs more than 90% of beads became irreversibly bound, such that loads of greater than 30pN were not sufficient to cause MT release.

6.6 Conclusions

It appears that Kif15-1293 in the presence of 1mM ADP has a low unbinding load similar to Kinesin-1. FL-Kif15 in 1mM ADP appears to show a secondary peak, suggesting the presence of a tighter binding mode encouraged by the inhibitory tail domains. In 1mM AMP-PNP Kif15-1293 has lower average unbinding loads than Kinesin-1 and is more likely

to detach from a one head bound state. The characteristic distances calculated from the variation of unbinding times with loading are more asymmetric for Kif15-1293 than for Kinesin-1 and the asymmetry of unbinding loads in 1mM AMP-PNP at comparable loading rates shows a small difference between the two motors.

In 5 μM ATP Kif15-1293 shows little change when compared to 1mM AMP-PNP under slow assisting loads however under hindering loads detachments happen at much higher loads than in 1mM AMP-PNP. Under minus end directed loads both peaks in the 5μM ATP data are shifted to about 50% higher loads than the corresponding peaks in 1mM AMP-PNP. Since the motor is likely to be in a predominantly no-nucleotide waiting state in these conditions, this suggests that the no-nucleotide state of Kif15 is considerably tighter binding than the AMP-PNP bound state, a prediction that need to be tested. The same is not true of FL-Kif15 which appears very similar to Kif15-1293 in 1mM AMP-PNP at all loading rates, again showing an effect due to its tail region inhibition.

Overall it appears that for both Kinesin-1 and Kif15-1293 the ability of the motor to step increases the motor asymmetry. For Kif15-1293 this effect is significantly more marked than for Kinesin-1. In the presence of 18nM Tpx2 FL-Kif15 binds very tightly to the MT. The loads needed to detach the motor in this state are beyond the scope of the optical trap and it is often more likely to detach the MT from the surface than the motor from the MT in the presence of Tpx2.

Chapter 7

Discussion

We investigated the mitotic motor protein Kif15 from a single molecule mechanical perspective. By comparing the mechanochemical characteristics of Kif15 with those of other motor proteins such as the cargo transporting protein, Kinesin-1, and the MT sliding protein, Eg5, we have distinguished possible mechanisms by which Kif15 might operate in its role of spindle maintenance. We can also hypothesise mechanisms through which Kif15 might be able to replace the *in vivo* roles of Eg5 in spindle morphogenesis and maintenance.

The results of my experiments show that Kif15 motors walk along MTs processively at 240 nm/s , slower than Kinesin-1 motors but faster than Eg5 motors. Likewise they have shorter run-lengths in a fixed trap ($\sim$50 nm at 0.08pN/nm stiffness) than Kinesin-1 ($\sim$100 nm) but walk further than Eg5 ($\sim$ 30 nm) . The velocity of Kif15 motors is more sensitive to load than Eg5 and the motor stepping rate decreases under load in a similar manner to Kinesin-1. These properties indicate that Kif15 is unlike either Kinesin-1 or Eg5 and is likely to perform its *in vivo* function via it own distinctive mechanism.

We found mechanical evidence of several regulatory mechanisms for Kif15. My data suggest that Kif15 has a second, diffusive MT binding region in addition to the motor domains. A second diffusive binding site would explain the enhanced run lengths of the unloaded motor when compared to those seen under load. I also found that the C-terminal tail region of Kif15 inhibits stepping and causes the motors to pause on the MT. The tail region of Kif15

contains a Tpx2 binding site, which is important for the targeting of Kif15 to spindle MTs *in vivo*. I have shown that the interaction of Tpx2 with this binding site causing FL-Kif15 motors to pause and bind stably to their MT track.

Finally I performed unbinding experiments to look into the load-dependence of Kif15 detachment under assisting or hindering loads. We found that the unbinding rate at a particular load depended very strongly on loading direction, and found also that the stepping of both Kif15 and Kinesin-1 motors whilst in 5μM ATP caused a significant increase in asymmetry compared to 1mM AMP-PNP conditions, with detachment occurring at higher hindering loads for both motors. For Kif15 this asymmetry was extreme, with mean unbinding loads under hindering forces as much as three times those under assisting forces. This asymmetry has implications for the behaviour of Kif15 in MT bundles and in MT sliding situations where external loads are in play. The unbinding experiments also enable us to make some suggestions as to how the tail of Kif15 acts to inhibit stepping and why Kif15 is so much less processive under load than Kinesin-1.

7.1 Kif15 Processive Stepping and Diffusion

Our results show that Kif15 is a slow-stepping and only mildly processive motor. Unloaded, it steps at velocities of 200-240 nm/s depending on whether or not it has a C-terminal truncation. These stepping rates of ~30 x 8nm steps/sec at zero load are significantly slower than the transport motor protein, Kinesin-1 and distinct also from other mitotic motors such as Eg5, at 70nm/s [104], and Cenp-E, at 400nm/s [105].

Besides its processive stepping mode, Kif15 displays several other important MT bound modes. It is capable of both one-dimensional diffusion along the MT lattice and of pausing for long periods of time. In the first of these modes it behaves similarly to Eg5 [106]. When unloaded, this diffusive mode helps Kif15 to maintain processive movement over distances up to 2 microns. By comparing the unloaded run lengths of Kif15 with those of Kif15 under load, we find that run lengths decrease dramatically under load, to a limit of around 40-80nm (5-10 steps) depending on the trap stiffness. This suggests that the unloaded run length of Kif15 is enhanced by its diffusive binding region, which keeps the motor domains

in close proximity to the MT lattice, allowing for rapid rebinding upon dissociation of the motor domains (Figure 7.1B). Sturgill et al. [33] propose that for Kif15 a secondary binding region is found in the coil one region of the motor (Figure 7.1A). Since the second binding domain is diffusive it does not stop the motor returning to the trap centre when the motor heads detach under load.

The diffusive mode of Eg5 also enhances it processivity. This method of extending MT dwell time and run length is a common feature of several kinesins, including Kif1A [107] and Kif18A [108]. For these other proteins, the diffusional domain has been found in the tail region, as in Eg5 tetramers and Kif18A dimers. Kif18A dimers use this tail region to accumulate at MT plus ends where they promote MT catastrophe [109]. By contrast Kinesin-1, which has no secondary MT binding domain, continues to walk straight off the ends of MTs without pausing. Kif15 pauses at plus ends of MTs. It seems possible that the diffusive binding region of Kif15 is responsible for this.

The diffusive MT binding site of Kif15 has several possible *in vivo* functions. Firstly, it may allow the motor to bind and move along one MT whilst also binding another, thereby enhancing the motors MT bundling capabilities (Figure 7.1C). This is true whether Kif15 is a dimer, as suggested by Sturgill et al. [33] or a tetramer as suggested by Drechsler et al. [34]. Secondly, the function of Kif15 under load might require short run lengths, for example if the motor works in teams to slide MTs. This has been proposed as a reason why Eg5 might benefit from a shortened run length under load [110]. In this case the diffusive region might be necessary to help the motor remain MT-bound whilst allowing it to localise towards MT plus ends and the spindle midzone. The diffusive binding region and short run lengths of the motor domains are likely to encourage MT switching as seen by Drechsler et al. [34] which could help the motor to negotiate bundled K-Fibre MTs.

If this region were to be responsible for binding to MT plus ends then this could enable Kif15 to affect MT dynamics, as has been shown for other plus tip dwelling kinesins such as the Kinesins-8 [108], which act to promote shrinkage, or CENP-E, which has been suggested to promote growth [111]. Alternately, binding of one end of a Kif15 tetramer to MT plus ends could enable the motor domains at the other end to bind to, and walk towards, the plus end of a second MT, providing a mechanism for creating parallel bundles (Figure 7.1D).

Both of these mechanisms could be of use if Kif15 plays a role in K-Fibre stabilization, as suggested by Sturgill and Ohi [82].

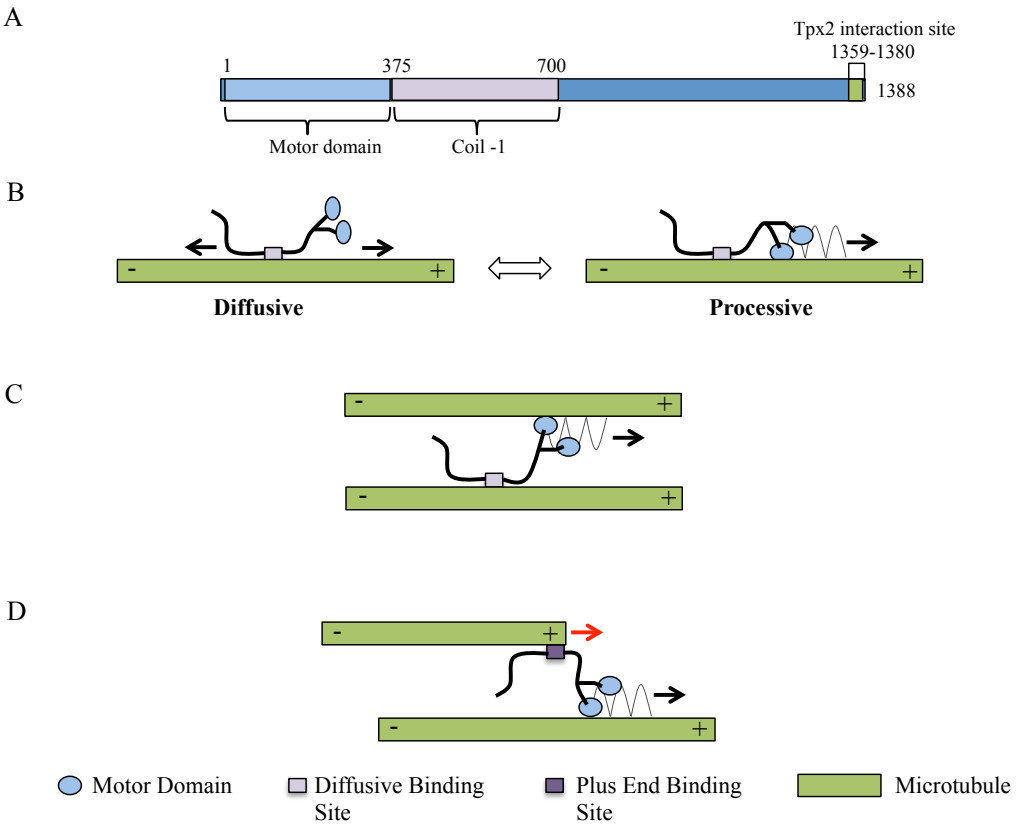

Figure 7.1: Cartoon showing possible roles of the diffusive binding site of Kif15, Kif15 is portrayed as a dimer in these images however these roles could equally apply in a tetramer. A) Schematic of Kif15 domain structure. B) Diffusive region allows Kif15 motor domains to rapidly rebind the MT and continue processive movement after unbinding. C) The diffusive region could allow cross-links to be formed in dimeric Kif15 or strengthen cross-links in Kif15 tetramers. D) Plus end binding by the diffusive region could increase plus tip dwell times enabling Kif15 to tow MTs by their plus ends (red arrow).

7.2 Kif15 Under Load

Under load, Kif15 velocity slows and at loads above 5.6pN, the motor steps backwards. The load-dependence and stall force are similar to both CENP-E [112] and Kinesin-1. Under hindering loads Kinesin-1 slows to stall at around 7pN, at this point the motor no longer

makes net forward movement and instead steps backward and forward at equal rates. The stall force of Kif15, at 5.6pN, is slightly less than Kinesin-1 and considerably less than Eg5, which continues to make net forwards progress at loads of over 8pN [46]. Under hindering loads the velocity of stepping for both Kif15 and Kinesin-1 decays exponentially with load.

A marked difference between Kif15 and Eg5 is found in the response of their stepping action to backwards loads. Eg5, unlike Kif15 and Kinesin-1 has very little load dependence. This means that under both hindering (minus end directed) and assisting (plus end directed) loads Eg5 velocity and run length change very little [46]. For Kif15 and Kinesin-1 the velocity of the motor is halved by the application of low loads around 1.5pN. The half maximum velocity of Eg5 occurs at around 4pN of backwards load [46]. For both Eg5 and Kinesin-1 the velocity is not significantly increased by assisting loads. For Kif15, the the motor detaches so easily under plus end directed (assisting) loads that it was not possible to measure a stepping rate under assisting load (see below).

The run length of Eg5 is very short, and similar under assisting and hindering loads [92]. For Kinesin-1, run length has been shown to decay to half of the maximum under 2pN of hindering load and under assisting loads the average run length drops dramatically from more than 100 steps at zero load to only 7-8 steps at 4pN [62]. The run lengths of Kif15 have not been determined but they appear to be qualitatively more similar to those of Eg5 than Kinesin-1. The lack of success in gaining stepping data from Kif15 under assisting loads suggests that Kif15 may be even more asymmetric than Kinesin-1 respecting its response of run length to loading direction.

The differences between the mechanics of Eg5 and Kif15 are likely to impact on MT cross-linking and sliding, Figure 7.2. Eg5 is thought to work in large teams. In this situation, consistency of motion over a range of loads, along with a short run length is likely to lead to overall efficiency of sliding. This would be especially important where many motors are cross-linking several anti-parallel MTs that all require sliding at the same rate. The slip-clutch mechanism suggested for Eg5 tetramers by Korneev et al. [93] whereby Eg5 releases at loads above 3pN would support a consistent sliding velocity in situations involving large groups of Eg5 motors. In these situations motors such as Kif15 and Kinesin-1 would be

predicted to slow in some areas and speed ahead in others, creating irregular forces and possibly less efficient sliding.

It has been suggested that insensitivity to forwards loads might cause kinesin-5 proteins in *C.elegans* to act as brakes during anaphase [113], effectively causing friction between MTs that are sliding apart by continuing to walk at the same rate despite the assisting forces that are acting (Figure 7.2C). The force profile of Kif15 suggests that it operates in a similar manner to Kinesin-1, implying that this braking mode would not be possible with either Kinesin-1 or Kif15. This will be discussed later.

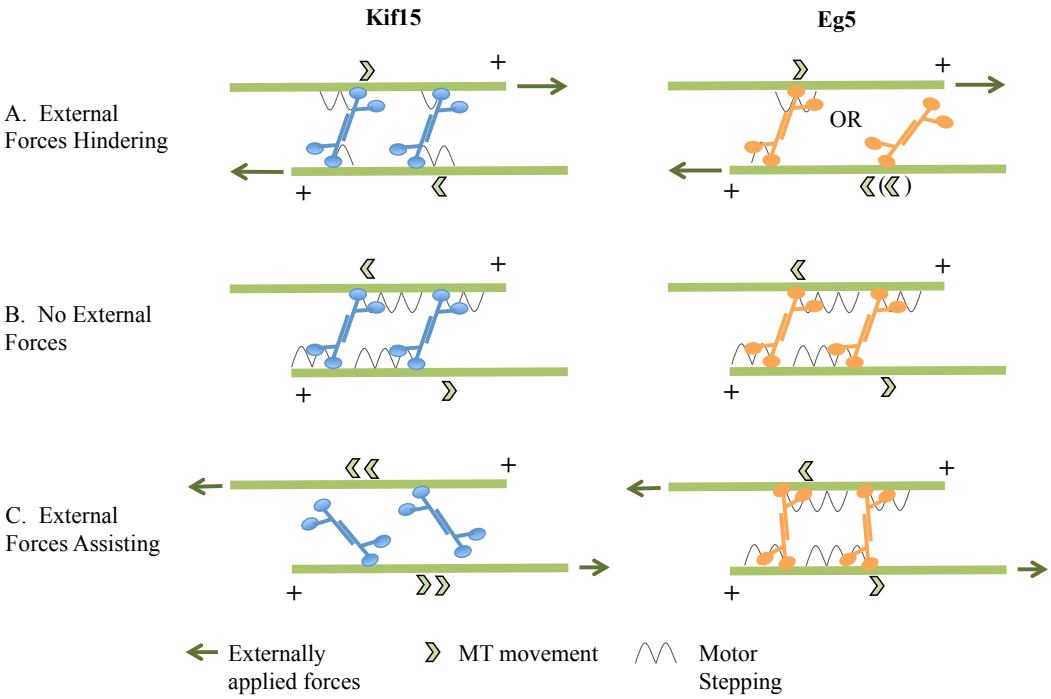

Figure 7.2: Cartoon of antiparallel MT sliding with Kif15 and Eg5. A) With external forces countering motor mediated sliding both Kif15 and Eg5 slow MT sliding whilst stepping both forwards and backwards. (Brackets) If the load is too high Eg5 may release the MT without slowing [93]. B) With no external forces both Kif15 and Eg5 step towards MT plus ends and create separation forces, Kif15 walks faster than Eg5. C) With external forces assisting MT separation Eg5 continues to step to plus ends slowing MT separation, Kif15 detaches from the MT allowing MTs to slide apart more quickly.

7.3 Auto-inhibition of Kif15

In Chapter 4, evidence for an auto-inhibitory mechanism in Kif15 was presented. It was found that the presence of the C-terminal tail region of Kif15 was responsible for the pausing behaviour often seen for beads with FL-Kif15 motors. This auto-inhibition reduced the velocity of unloaded motor movement from around 240 nm/s to around 210 nm/s. Some motors in FL-Kif15 assays do not move at all but instead bind statically to the MT. We propose that bead-binding might lock these motors into their inhibited conformational state.

For FL-Kif15 motors that do step, the presence of the C-terminal tail region only affects those that are walking at low loads. Above 3pN, the load versus dwell time relationships of the full length and truncated motors converge. An explanation for this is that load-induced extension of the coiled-coil between the motor and the bead at higher loads moves the tail region out of range of its inhibitory binding site. Conversely the decrease in velocity of the motor at low loads would be due to the tail region moving in and out of its binding region, alternately turning inhibition on and off, resulting in a slowing of the overall stepping rate of the motor domains.

It has been shown that the tail domains of Kif15 cannot bind MTs independently [42]. The inhibition must therefore require simultaneous binding of one of the MT-bound regions of the motor to the MT, either the motor heads or the diffusive binding domain. One possible method of inhibition would be for the interaction between the head domain(s) and the tail region to block nucleotide binding into the catalytic pocket of the MT bound motor head. This would have the effect of trapping the motor in a tightly MT bound single head no-nucleotide state where it is unable to step. Alternately the tail might interfere in the process of phosphate release after hydrolysis, locking the motor to the MT in a two heads bound state. Further work will be required to explore these possibilities.

The auto-inhibition of Kif15 into a MT bound state is unusual. Many other kinesin motor proteins display auto-inhibition, often mediated via the tail regions. However, they typically act to decrease the affinity of the motor for the MT [70, 48, 31, 114]. This tail- mediated inhibition is relieved in various ways, for example by cargo binding in Kinesin-1[115] or by cell

cycle regulated phosphorylation as is the case for CENP-E [31]. This method of inhibition means that kinesin motors are not MT-bound and under-going hydrolysis, wasting fuel and creating unwanted forces when not performing their specific *in vivo* role.

One possible reason for Kif15 to auto-inhibit in a tight-binding state could be that the paused state of Kif15 is required for its *in vivo* function, perhaps allowing it to form stable static cross-links within bundles of MTs. The tail inhibition would then require tight spatial and temporal regulation within the spindle, to ensure that Kif15 is in the correct mode, stepping, diffusing or pausing.

7.4 Kif15 Regulation

Since Kif15 displays a variety of MT bound behaviours it is likely that at least some of these are promoted or inhibited at specific times and places by regulation factors. Kif15 is known to interact with several other proteins during mitosis. We have investigated one of these proteins, Tpx2. Tpx2 is a key player in the regulation of spindle assembly and maintenance. It has been shown to affect the behaviour of several other mitotic proteins such as Eg5 and Aurora A, and to aid in MT nucleation around the chromosomes and branching from MTs [26]. Kif15 has also been shown to interact with Ki67 on the chromosomes during mitosis [116] and with actin in neuronal cells [36].

The interaction of Kif15 with Tpx2 operates via the C-terminal tail region, which is also responsible for auto-inhibition. Tpx2 and Kif15 tails only form a complex when Tpx2 is MT bound [42]. The stepping of the motor domains of both Kinesin-1 and Kif15 are unaffected by MT bound Tpx2 in the absence of Kif15 tails. When full length Kif15 encounters Tpx2 on the MT lattice it stops moving processively and thereafter remains tightly bound to the MT. Experiments investigating the load bearing ability of this state revealed that it can withstand high loads of over 40pN without detaching, double the highest load that can be sustained by a Kif15 motors in the absence of Tpx2.

The mechanism by which Tpx2 and the Kif15 tail domain interact to inhibit the motor is not clear. Tpx2 might bind the tail of Kif15 to the MT and have no direct interaction with the motor domains (Figure 7.3A). Alternatively, Tpx2 could stabilise the auto-inhibited

conformation of Kif15 (Figure 7.3B). If Tpx2 only acts to deactivate the motor, creating static cross-links and preventing futile hydrolysis then the second theory seems more likely. However, it is possible that *in vivo* Tpx2 can coordinate Kif15 to remain anchored to one MT whilst walking along another (Figure 7.3A.). For tetrameric proteins with two sets of tail domains, this scenario seems less plausible because the tail domains of one dimer are likely to be very near to the head domains of the other dimer, as shown in Figure 7.3B.

Tpx2 also inhibits Eg5 motility via interaction with its tail domains [72]. This could turn stepping motors into static cross-links, which might strengthen bonds between antiparallel MTs. For Kif15 this probably helps in the bundling of parallel MTs due to its localisation to K-fibres. The interaction of Kif15 with either Ki67 or actin has not been explored. It is possible that Kif15 binding to either actin or Ki67 might release tail inhibition and promote either stepping or diffusive behaviour.

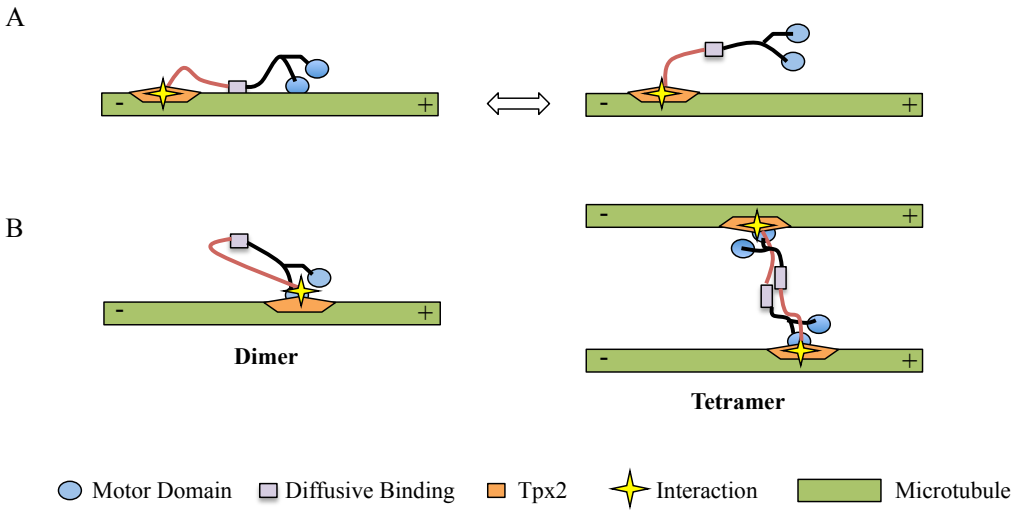

Figure 7.3: Cartoon showing possible methods of Tpx2 inhibition A) Tails bind Tpx2 leaving motors in an uninhibited state free to bind a second MT. B) Tpx2 inhibits motor stepping for dimers or tetramers of Kif15. Kif15 tails are shown in red.

7.5 Asymmetric Unbinding

The unbinding experiments described in Chapters 5 and 6 revealed several interesting behaviours of Kif15 and Kinesin-1. The shift in detachment loads in a variety of different

nucleotide types and concentrations, the implications of Kif15 unbinding asymmetries *in vivo* and the effects of the inhibitory Kif15 tail on the binding stability of the motor in different nucleotide conditions are discussed below.

7.5.1 Unbinding Load-Dependence of Kif15 is More Asymmetric than that of Kinesin-1

Whilst stepping at low ATP concentrations, the load-dependence of Kif15 unbinding from the MT is much more asymmetric than Kinesin-1. Given the similarity of its stepping behaviour under assisting and hindering loads, it is very likely that the load-dependence of Eg5 unbinding would be more symmetric than either Kif15 or Kinesin-1. High asymmetry of the load-dependence of unbinding could have important implications for the cross-linking and sliding behaviour of Kif15. Kif15s asymmetric response means that under assisting loads, it will release rapidly from the MT, allowing it to contribute very little friction. By contrast, when hindering loads are applied to Kif15 the motor binds much more stably to the MT, such that its average detachment load is similar to that of Kinesin-1 under backwards load. Essentially, this mechanism means that the MT-Kif15 interaction has the properties of a mechanical ratchet and pawl, such that the motor can freewheel in one direction, but engage and hold force in the other.

In comparison, Eg5 shows very similar velocities and run lengths regardless of the direction of the applied load [46]. On anti-parallel MTs, this will allow Eg5 both to generate centrosome separation forces and to slow the speed of separation if pulling forces are too great. Kif15 by contrast will generate separation forces, but will not act as an overspeed-brake on pole separation (Figure 7.2C). This suggests that the role of Kif15 in stopping Eg5-dependent spindle pole separation overshoot [82] is performed either by the paused state of Kif15 (through auto-inhibition or Tpx2 binding) on the MT overlaps or an indirect effect via the regulation of K-fibre dynamics.

In parallel MT bundles, Kif15 tetramers walking on two MTs will walk at the pace of the fastest pair of motor heads, with the other pair being dragged behind. This will create no overall sliding forces on the MTs but instead will lead to accumulation of Kif15 motors at

MT plus ends (Figure 7.4). If one end of a tetramer encounters and binds statically to a MT plus tip, the other pair of motor heads could continue walking along their MT pulling the MT plus-ends into alignment. This could be a possible mechanism for Kif15 to regulate K-fibre organisation.

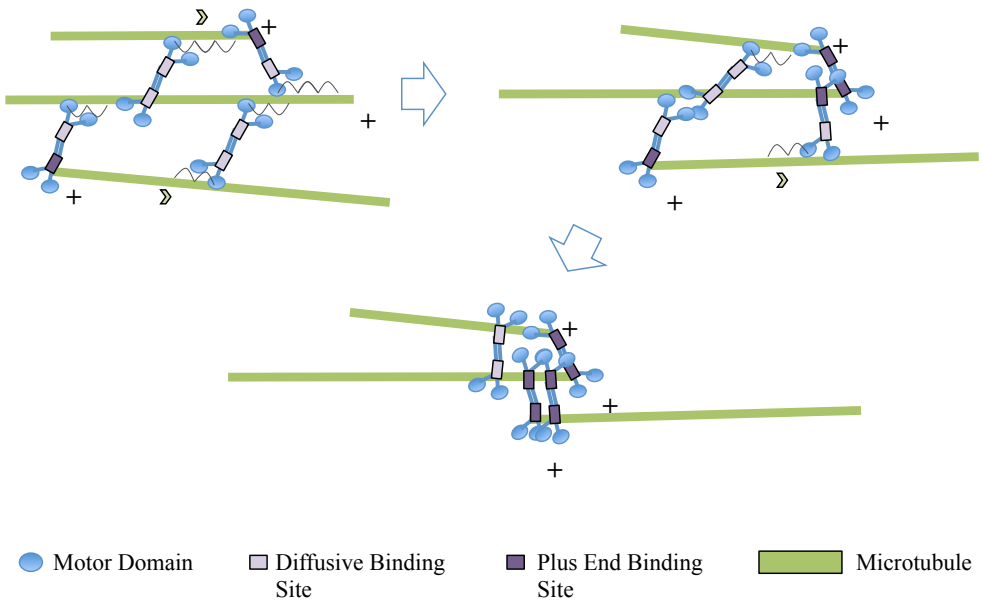

Figure 7.4: Cartoon showing MT sorting by Kif15, this mechanism shows how the combination of easy unbinding under forwards loads, for example if walking on two parallel MTs that are sliding relative to one another can allow rapid accumulation of Kif15 at MT plus tips. Binding at plus tips also allows for the sorting of MTs into bundles of parallel MTs and shows a mechanism for the 'tiling' effect of MTs in a gliding assay seen by Sturgill et al. [33] where MTs are aligned end to end.

7.5.2 Kif15 Spends Most of its Time in a Single Head Bound State

One possible reason for the asymmetrical load-dependence of Kif15 detachment and possibly also for its short run length, is the amount of time the motor spends in a single head bound state. Data from 1mM AMP-PNP conditions under hindering loads shows that 50% of Kinesin-1 unbinding events are from a double head bound state compared to only 20% of Kif15-1293 events. Under assisting loads the percentage of motors unbinding from a double head bound state for Kif15-1293 is even less. This suggests that the double head bound

state for Kif15 is rarely visited, or is less stable, even in AMPPNP.

Under assisting forces the differential in binding strength between the ADP and AMP-PNP bound states for Kif15 is far less than for Kinesin-1. This means that motors are able to unbind from the AMP-PNP state with a similar likelihood to the ADP state. This suggests that for Kif15, once ATP binds to the trail head and sanctions the unbound head to make a step, there is a risk that the rear head will release in its ATP state before the front head has released its ADP. For Kinesin-1, this risk is less. The fast unbinding of ATP bound Kif15 under forward loads will also make Kif15 stepping very susceptible to poor head co-ordination and early unbinding. Under hindering loads MT binding by ATP bound Kif15 is more stable and this loss of co-ordination is less likely. This is in agreement with our detachment load data in low ATP conditions, where Kif15 is stepping slowly.

Our data indicate a clear difference between Eg5 and Kif15. Eg5 is predicted to show limited head-head co-ordination due to its ability to bind both heads to the MT simultaneously, and the insensitivity of its detachment rate to loading direction. This allows the hydrolysis cycles of the motor domains to lose synchronisation, leading to early detachment and short run lengths [94]. Kif15 detaches rapidly under assisting loads and shows limited processivity under hindering loads. We propose that its limited processivity occurs because during a step, the rear head tends to detach prematurely in its ATP state.

7.5.3 Motor Unbinding Loads are More Asymmetric in the Presence of ATP

Our data from 5μM ATP conditions for both Kif15-1293 and Kinesin-1 motors show significantly more directional asymmetry of detachment under load than any of the nucleotide states described by Kawaguchi et al. [69]. In order to explain the distribution of detachments in our ATP data it is necessary to extend the model previously suggested by Kawaguchi et al. [69] (the Ishiwata model).

The Ishiwata model

In high AMP-PNP and ADP conditions our Kinesin-1 data are in close agreement with those of Uemura et al. [61]. The 1mM ADP data displays only one peak in detachment load. Under both assisting and hindering loads detachments occur at an average of 3.5 pN. Our 1mM AMP-PNP data display two peaks of load-dependent detachment, corresponding to the single and double head bound states of the motor. In AMP-PNP Kinesin-1 detaches at lower assisting loads than hindering loads. These features are in close agreement with Uemura et al., despite potential minor technical differences between the two sets of experiments. Furthermore we obtained qualitatively similar behaviour for the ADP and AMPPNP states of Kif15, despite the potential mechanistic differences between the two motors.

In work from the Ishiwata lab the assignment of single and double head binding to the two peaks of load-dependent detachment comes from work by Uemura et al. [61], which used single headed Kinesin-1 in 1mM AMP-PNP and no nucleotide (apyrase) conditions. Under both conditions, detachment loads were 9 and 6 pN for hindering and assisting loads respectively. For double-headed Kinesin-1 in no nucleotide conditions this behaviour was unchanged, suggesting a single head bound waiting state. In the presence of AMP-PNP the motor displays a second, higher load peak in both loading directions. This was taken to indicate MT-binding by the second head, sanctioned by the binding of AMP-PNP to the first head. The average detachment load of a dimeric motor in the AMP-PNP state is therefore higher than in the nucleotide free state, due to the binding of the second motor head to the MT.

Possible Mechanisms: Detachments in 5 and 1 μM ATP (assisting loads)

We have extended this picture by collecting data from Kinesin-1 and Kif15 motors stepping in low levels of ATP. The detachment load distributions in both 1μM and 5μM ATP are qualitatively similar to that of the 1mM AMP-PNP data.

In our data assisting loads applied to motors in 5μM ATP show the largest departure from the 1mM AMP-PNP detachment loads. In these conditions, the motor is able to make $\sim$7 steps a second. It is clear from its reduced run-lengths [62] that under assisting loads the

head-head coordination of Kinesin-1 becomes weaker. The motor is more likely to enter a 2-heads ADP-bound state whilst making a step, causing it to release from the MT. Because of the comparatively high ATP turnover in 5μM ATP conditions, compared to 1μM ATP and 1mM AMP-PNP, these motors will spend a higher proportion of their time in a weak MT-binding ADP-bound state, and as a consequence a significant percentage of the population detaches at low loads.

Problems with the Ishiwata Model

Despite their similarity to the AMP-PNP data, our data on kinesin-1 detachment loads in slow stepping conditions, either low ATP or hindering loads, does not fit with the Ishiwata model. Motors in these conditions will spend the majority of their time in the nucleotide free waiting state. According to the Ishiwata model these motors should therefore detach at lower loads than motors in 1mM AMP-PNP as they will be predominantly detaching from a single head bound nucleotide free state at an average of 6 or 9 pN depending on loading direction.

As can be seen in Figure 5.4 this is not the case. For motors under hindering loads in both the 1μM and 5μM ATP conditions, as well as those in 1μM ATP under assisting loads, a considerable proportion of detachments occur at loads above 10pN.

We can envisage two possible explanations: Firstly these high load detachments might be from an AMP-PNP-like state that is accessed during the stepping of these motors and accounts for a reasonably large proportion of their stepping cycle. Secondly, these detachments might occur from the nucleotide free waiting state.

This second suggestion seems more likely although it is not in keeping with the model proposed by Kawaguchi et al. [69] who find that the AMP-PNP binding state has higher average unbinding loads than the nucleotide free state. This contrasts with our experiments, which show that there is little difference between the average detachment loads for high AMP-PNP conditions and low ATP (mostly no nucleotide) conditions. Since Kawaguchi et al. use apyrase, which tends to denature kinesins [117], to deplete nucleotides in their experiments their results in nucleotide free conditions could be unreliable.

Other studies have compared the binding strengths of the AMP-PNP and no nucleotide states. Experiments by Hancock and Howard [103] show that when in the AMP-PNP bound state the unloaded detachment rate of a single-headed kinesin-1 is half that of the nucleotide free dimeric motor. These experiments use no apyrase so trace amounts of ADP (∼100nM) and ATP (∼1nM) are present in solution and will contribute to the MT-detachment rate of the motor. Hancock and Howard [103] also use a dimeric Kinesin-1 and find that the AMPPNP unbinding rate is unchanged whilst the nucleotide free unbinding rate has dropped to a similar level. This again suggests that the shorter unbinding times (lower detachment loads) of the dimeric Kinesin-1 found by Kawaguchi et al. [69] in no nucleotide conditions may not be accurate, lending support to the concept of our high load detachments occurring from a nucleotide free state.

For our Kinesin-1 data the detachment loads of motors in AMP-PNP and low ATP are not markedly different. If we accept that low ATP detachments occur from a mostly nucleotide-free state then this suggests that the binding strength of both the AMP-PNP and no nucleotide states to the MT are very similar. For Kif15-1293 the detachment loads in 1mM AMP-PNP and 5μM ATP are very different. The low ATP detachments for Kif15-1293 occur at much higher loads, with peaks at 10 and 20pN as opposed to 6 and 14pN in AMP-PNP. This suggests that the nucleotide free binding state of Kif15 binds the MT more tightly than the AMP-PNP state.

The increase in the asymmetry of detachment loads with increasing ATP concentration for Kinesin-1 can be explained by a decrease in unbinding loads under assisting forces, whilst no change occurs under hindering loads. The faster detachment under assisting loads reflects a shortened run length, with detachments tending to occur from a double head, ADP-bound state caused by loss of head co-ordination whilst stepping. Under hindering loads we find no difference between the AMP-PNP and nucleotide-free binding states in terms of average detachment load for Kinesin-1.

For Kif15-1293 under hindering loads, motor stepping occurs too slowly to have a sizeable impact on detachment loads. Detachment loads in no-nucleotide states are dramatically higher than in AMPPNP, and this causes an even greater increase in unbinding asymmetry.

7.5.4 No Nucleotide Peak Structures

For Kawaguchi et al. [69] the model for single and double headed binding states leading to two peaks in AMP-PNP data is quite convincing since it is widely accepted that AMP-PNP bound dimeric motors can bind the MT with both heads [60, 68]. The assignment of a double peak structure for the nucleotide free binding state (the ATP-waiting state) of dimeric Kinesin-1 is more problematic. The nucleotide free state of Kinesin-1 is known to bind to MTs with one head whilst retaining ADP in the other head [68]. It is not expected that in the waiting state, the motor will be moving between one and two heads bound states.

There is some uncertainty as to the conformation of the single head bound waiting state of Kinesin-1. Two models are suggested for the position of the second 'tethered head in the ATP-waiting state. One of these models states that the second head is positioned behind the MT-bound head, near to its previous binding site. The tethered head is able to diffuse freely about this position until ATP binds, at which point the MT-bound head docks its neck-linker and moves the tethered head on to its next binding site [60]. The other model predicts that the tethered head is docked just in front of the MT-bound head and a parking interaction with the MT-bound head inhibits its binding to the MT [68]. This means that the tethered head is unable to bind to the MT until ATP binding in the MT-bound head releases it allowing it to bind to the MT.

Given these competing models, we consider two mechanisms by which nucleotide free MT-binding states with two different characteristic detachment loads could occur.

Firstly, given that AMP-PNP states can access single and double headed binding it is possible the same occurs for the nucleotide-free state. Although there is little evidence that the unloaded nucleotide free waiting state can access a double head bound state at low loads, it may be that applying load encourages the binding of this second head. This is perhaps more in keeping with the undocked model of the waiting state (Figure 7.5 (Model 1)), where the tethered head is diffusing and applied tension might bias its binding.

Alternatively, the motor might bind to the MT through a single head, whilst the tethered head fluctuates between a parked and unparked state, and the parking of the tethered head

changing the MT binding properties of the bound head (Figure 7.5 (Model 2)). Again the relative populations of these states could be influenced by the magnitude and direction of applied load. If the parking of one head were to strengthen MT binding by the other head this could be advantageous, as it would stabilise the waiting state in a well-regulated conformation helping to enhance motor processivity.

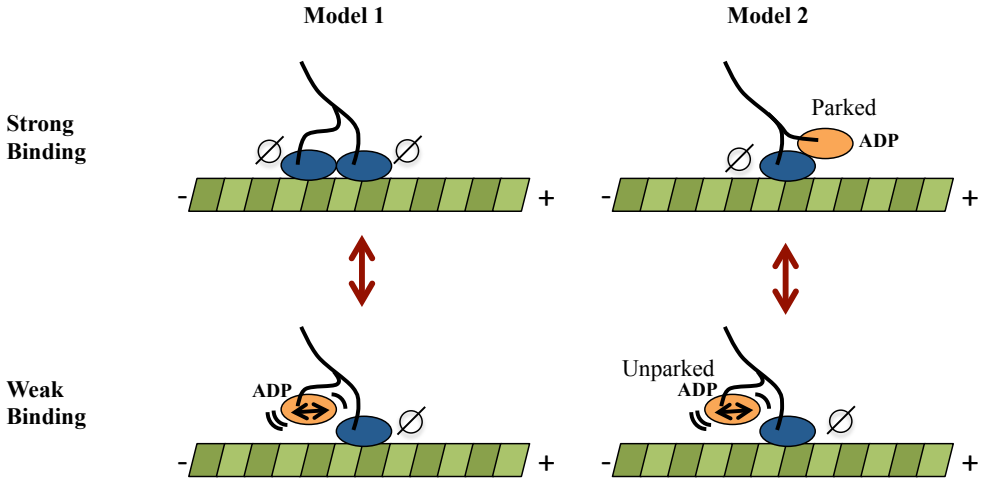

Figure 7.5: Cartoon showing possible double states in the single head bound waiting state. Model 1) The tethered head is diffusive and sits behind the MT bound head. This head can transiently bind the MT in a double headed rigor state, this state may be stabilised by application of load. Model 2) The tethered motor head switches between parked and unparked states. The docking of the tethered head over the MT-bound head increases the MT-binding strength.

At present we cannot distinguish definitively between these two models. The 5 and 1μM ATP conditions have very similar distributions of load-dependent detachment to those in 1mM AMP-PNP. All conditions show a peak at $\sim$20pN, potentially corresponding to the double head bound state in both no nucleotide and AMP-PNP bound motors. In the 5μM ATP conditions this 20pN peak is reduced compared to that in 1μM ATP conditions. If this were a double rigor state with the motor bound to the MT with no nucleotide in either head then this suggests that the binding of ATP (albeit at a slow rate $<$1 per second) reduces the population of this state. This may be reasonable as nucleotide binding to either head might encourage release of this head from the MT. In model 2, in which the 20pN state reflects the

parking of the tethered head, this would also be destabilised by nucleotide binding.

The other slight difference between the two ATP conditions is a shift in the position of the low load peak with 5μM ATP data shifted towards higher loads. This shift could be caused by changing the rate at which the motor moves between the strongly and weakly bound no nucleotide states due to the difference in nucleotide concentration. It would be interesting to collect data at both higher and lower nucleotide conditions in order to start resolving these uncertainties. The application of load in a stepwise manner (1pN steps) could also affect the populations and positions of the two peaks in ATP, this could easily be checked by using a larger step size. Detachment experiments in low ADP concentrations would also be revealing.

7.5.5 FL-Kif15 Tail Inhibition Causes an Increase in the 2 Heads Bound State

The unbinding loads for FL-Kif15 both in 1mM ADP and in 5μM ATP give insights in to the effect of the tail domain of Kif15 on stepping. In low ATP it is not clear what the stepping rate of FL-Kif15 is, as motility is very inconsistent and so an unloaded velocity is difficult to determine. However it is likely that this is a slow stepping rate of less than 30nm/s. In low ATP although the majority of unbinding occurs from the single head bound low load state, the higher load state is more populated for FL-Kif15 than Kif15-1293. This is especially true under assisting loads. In 1mM ADP conditions a second peak is also seen.

Previously we have suggested several possibilities for the mechanism of Kif15 tail inhibition;

1. FL-Kif15 inhibition is caused by an interaction between the tail domain and the motors diffusive region causing this region to bind tightly to the MT opposing stepping motion by the motor domains. It is possible that this also inhibits motor domains from binding the MT
2. The inhibition is caused by binding of the tail regions to the motor heads affecting the rates of nucleotide binding/unbinding.

In the first case the unbinding loads of the motor in 1mM ADP could be easily explained

as a second population of motors bound differently to the MT. In 5μM ATP however the striking similarity of unbinding loads to those of the truncated motor in 1mM AMP-PNP suggests that the inhibition creates a motor bound in a more AMP-PNP like state. If the inhibition acts via the diffusive domain the peak distribution of uninhibited motors would be expected to look more like the 5μM ATP data for Kif15-1293.

In the second case the inhibition of the motor could slow down the ATP hydrolysis rate or P_i release, this would lead to slower stepping and a more AMP-PNP like distribution in low ATP. Unfortunately this does not fit the ADP data. If there is no ATP then hydrolysis wont occur so the inhibition will have no effect. If however the inhibition of Kif15 is due to a decrease in nucleotide binding rates then this can explain the ADP data, the higher peak is the nucleotide free peak. The low ATP data has lower detachment loads for FL-Kif15 than for Kif15-1293 under hindering loads. The inhibited state appears more like the AMP-PNP bound state of Kif15-1293 than the no-nucleotide state. So one possible model for the inhibition mechanism would therefore be that the tail stabilises the motor domain in an ATP-like conformation, even in the absence of nucleotide.

7.6 Updated Models of *in vivo* Function

Our findings confirm those of Sturgill et al. [33], Kif15 steps at a slow rate, has an additional MT binding region and an auto-inhibition mechanism mediated by its tail region. We can add that this second binding region is diffusive on the MT lattice and aids motor processivity. We find that the auto-inhibition mechanism helps Kif15 remain MT bound rather than inhibiting MT binding and suggest a mechanism by which Kif15 auto-inhibition occurs. We report that Kif15 has similar load dependence to Kinesin-1 and has a significant asymmetry to unbinding under assisting over hindering loads. In this Kif15 shows a distinct difference to Eg5. We noted in agreement with Drechsler et al. [34] that Kif15 has longer dwells at MT plus ends and is also inhibited by Tpx2, probably creating a static cross-linker. We found that Tpx2 bound Kif15 could support far greater loads than Kif15 in the absence of Tpx2.

Previous suggestions of Kif15 mechanisms in mitosis are either based on an Eg5 model where

the motor binds MTs in the spindle overlap and creates outward forces in the spindle by walking towards MT plus ends or that Kif15 operates via the K-Fibres increasing stability and creating outwards forces in this way. Our results suggest that Kif15 is not operating as a second Eg5 like motor, it has distinct properties and different load responses. It is still not clear whether Kif15 acts as a tetramer or a dimer or possibly both *in vivo*. Our data suggests that both dimeric and tetrameric Kif15 would be well adapted to operate within K-Fibres, they have the ability to cross-link, diffuse, switch tracks and align parallel MTs.

It is possible that the 'jack-knife' mechanism of Kif15 mediated spindle formation occurs similarly to the mechanism show in Figure 7.4 which also explains the MT 'tiling' seen by Sturgill et al. [33]. In this mechanism Kif15 binds MT plus ends and by walking along MTs towards their plus ends can sort MTs of mixed orientations into two parallel arrays of MTs aligned at their plus tips by clusters of Kif15 motors. If Kif15 were able to modulate MT dynamics this could also have an effect on the mechanism of spindle formation, creating additional forces at the chromosomes. Mis-localisation of Kif15 on to non-K-fibres would allow the motor to fulfil Eg5 like duties as suggested by Sturgill and Ohi [82], however Kif15 would not be as well suited to the cross-link and slide form of spindle separation as Eg5 due to its tendency to slow significantly under load. The effect of Tpx2 regulation appears to be to form strong static cross-links from normally motile motor proteins such as Eg5 and Kif15. This is likely to be spatially regulated, so that Tpx2 affects both Eg5 and Kif15 in regions where MT cross-links require strengthening. The regulation of Kif15 by Ki67 has not been looked in to here but given the antagonistic effects of Kif15 around the chromosomes, both in creating shorter spindles through its interaction with Ki67 and in damping Eg5 based chromosome oscillations it would seem that Kif15 is likely to be regulated so as to make it's behaviour around the chromosomes very different to that of Eg5.

In neuronal cells the effect of Kif15 and Eg5 is to balance dynein dependent axon lengthening, Kif15 is also responsible for aiding the formation of the growth cone and increased axonal branching. Our data shows that Kif15 is likely to be well suited to negotiating arrays of parallel MTs such as those within axons, in its uninhibited state Kif15 should be able to transport MTs back towards the MT plus ends. The branching aspect of Kif15 function not

shared by Eg5 could be due to its ability to bind actin which has not been looked in to here and which might modulate Kif15 behaviour so as to encourage MTs branching away from the main axon.

7.7 Conclusions and Future Work

In conclusion we have progressed in our understanding of Kif15 on a single molecule level. We now know more about its properties under load and its possible states of regulation. Several questions about the single molecule mechanics of Kif15 and how they translate to *in vivo* function still remain. Firstly it would be useful to confirm the diffusive binding region more directly, perhaps through single molecule fluorescence experiments with motor free constructs, these could also test for plus tip binding of the diffusive region. Since Kif15 dwells at MT plus tips it may have an effect on MT dynamics this could be tested through *in vitro* MT dynamics assays.

One of the major issues in interpreting Kif15 *in vitro* and *in vivo* data is the disagreement regarding the oligomerisation state of Kif15. It would be useful to have more structural information on Kif15. If it does tetramerise, is this in a similar manner to Eg5 so that two dimers are aligned in an antiparallel fashion with the tails of one dimer able to influence the head domains of the other? This may not be the case since Eg5 forms a stable tetramer whereas Kif15 is able to dissociate in to dimers at high ionic strengths [34]. Given that Kif15 tetramers are able to dissociate in what form does Kif15 exist *in vivo* and is this another form of Kif15 regulation?

Other questions involve the method of auto-inhibition, we have suggested that this occurs through a reduction in nucleotide binding affinity in the motor domains causing the motor to bind MTs in a tightly bound no nucleotide state. It would be possible to test this by observing the effects of Kif15 tails (both through using the FL motor and by adding tails in solution with truncated Kif15 motors) on values such as the ATP binding rate and the ADP release rate. A further set of experiments would be to test the MT sliding and cross-linking abilities of the truncated Kif15 tetramer *in vitro*. Previous experiments using the full length motor have struggled to find evidence of sliding for longer MTs [34], however it

is possible that this is due to large numbers of inhibited motors opposing the movement in these assays.

In order to test our interpretation of the peak positions in low ATP unbinding experiments it would be necessary to repeat these experiments for Kinesin-1 using different nucleotide concentrations. Along the same lines it would be useful to perform the same experiment with Kif15 in nucleotide free conditions to check whether like Kinesin-1 the MT binding affinities of the AMP-PNP and no nucleotide state are the same, this would help in the interpretation of our Kif15 data. The asymmetry of Kif15 binding to MT plus tips could be an additional experiment, as we believe the plus tip binding to be mediated by the diffusive binding region we would predict that it may display different unbinding load characteristics to lattice bound Kif15. A further set of investigations would be to attempt the same experiments with Eg5, it has been assumed that Eg5 would show less asymmetry than Kinesin-1 and Kif15 based on run length data however this would be interesting to test directly.

The predictions from our asymmetry experiments as to the differences in behaviour of teams of Kif15 and Eg5 motors in the sliding of MTs in bundles could be tested. This could be done by using an optical trap to apply loads to MTs in both surface gliding assays and MT-sliding assays. The aim of these experiments would be to test for directional difference in MT sliding under external loads towards the plus and minus ends of MTs. For Kif15 we would expect easier sliding under loads from the MT plus end, for Eg5 we would expect the behaviour to be the same under both plus and minus ended loads.

Finally despite our increased understanding of Kif15 from a single molecule perspective the *in vivo* picture remains unclear. We now know more about the possible mechanisms by which Kif15 might function but its large variety of MT bound states suggest that it might be extensively regulated within the cell. Because of its functional overlap with Eg5 Kif15 inhibition is a relatively subtle phenotype. In order to test the effect of regulatory regions of Kif15 and Kif15 regulators mitotic cells would need to be sensitised to Kif15 by blocking the function of Eg5. To gain a clearer picture of Kif15 function within the cell the effect on the spindle due to lack of auto-inhibition and Tpx2 binding, lack of motor function and various other qualities need to tested.

Appendix A

A.1 Tether-Lengths

In 1mM AMP-PNP it is possible to collect data on the length of the MT-Bead tether. In these cases the motor is stationary on the MT, initially the stage is offset so that the bead is displaced from the trap. The stage is then moved so that the MT slides past the trap centre bringing the bead back in to the centre of the trap. As the stage continues moving the bead will rotate in the trap centre until the linkage between the bead and the MT is pulled tight. By gathering traces such as those in Figure A.1B the length of the tether can be calculated.

The geometry shown in Figure A.1A gives a tether length T equal to $\sqrt{(d/2)^2 + r^2} - r$. If the velocity of stage movement is known then it is possible to calculate the distance $d = v/t$, the radius of the bead r is already known.

From the tether lengths collected it is clear that Kinesin-1 has a fairly consistent tether length of around 40 nm suggesting that it binds to beads in a consistent way. Kif15 tether lengths are very varied, suggesting that it binds the bead in a variety of conformations Table A.1.

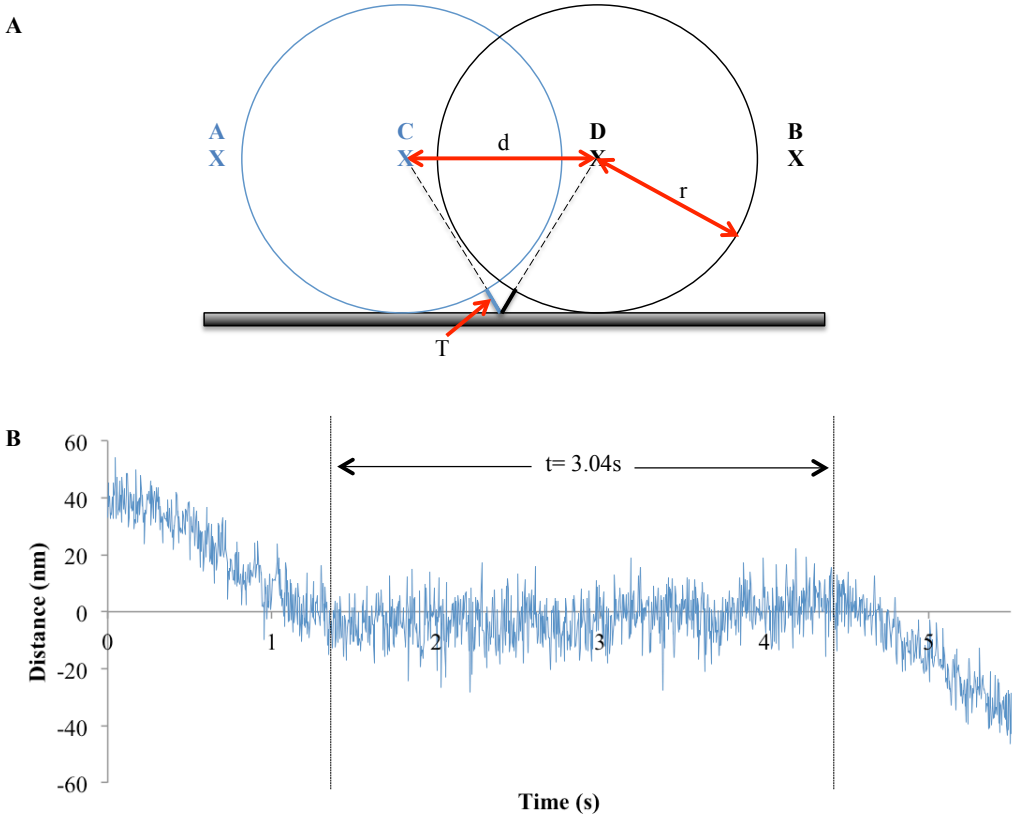

Figure A.1: A)The laser focus is moved from point A to point B at a constant rate of 100nm/s. For a motor of tether length T a bead of radius r will move distance d, whilst the laser focus is within the range of C and D the bead will not appear displaced from the trap centre. B)Example trace for Kinesin-1, time in the trap centre is measured by eye to be 3.04s.

	Time in Trap Centre (s)	**Tether Length (nm)**
Kinesin-1	3.31	45.5
	3.04	38.8
	3.02	38.3
Kinesin-1 Mean	**3.12**	**40.8**
Kif15	5.37	108.0
	3.20	42.5
	2.23	20.5
Kif15 Mean	**3.60**	**57.0**

Table A.1: Data on tether lengths for Kif15 and Kinesin-1.

Bibliography

[1] T Mitchison and M Kirschner. Dynamic instability of microtubule growth. *Nature*, 312(5991):237–42, 1984.

[2] David D Hackney. The kinetic cycles of myosin, kinesin, and dynein. *Annual review of physiology*, 58(1):731–750, 1996.

[3] Steven M Block, Lawrence SB Goldstein, and Bruce J Schnapp. Bead movement by single kinesin molecules studied with optical tweezers. 1990.

[4] J Howard, AJ Hudspeth, and RD Vale. Movement of microtubules by single kinesin molecules. *Nature*, 342(6246):154–158, 1989.

[5] Nobutaka Hirokawa. Organelle transport along microtubules—the role of kifs. *Trends in cell biology*, 6(4):135–141, 1996.

[6] Andrew W Hunter, Michael Caplow, David L Coy, William O Hancock, Stefan Diez, Linda Wordeman, and Jonathon Howard. The kinesin-related protein mcak is a microtubule depolymerase that forms an atp-hydrolyzing complex at microtubule ends. *Molecular cell*, 11(2):445–457, 2003.

[7] Kenneth E Sawin, Katherine LeGuellec, Michel Philippe, and Timothy J Mitchison. Mitotic spindle organization by a plus-end-directed microtubule motor. *Nature*, 359 (6395):540–543, 1992.

[8] Bruce Alberts, Alexander Johnson, Julian Lewis, Martin Raff, Keith Roberts, and Peter Walter. Molecular biology of the cell. new york: Garland science; 2002. *Classic textbook now in its 5th Edition*, 2002.

[9] Mary Ann Jordan and Leslie Wilson. Microtubules as a target for anticancer drugs. *Nature Reviews Cancer*, 4(4):253–265, 2004.

[10] Oliver Rath and Frank Kozielski. Kinesins and cancer. *Nature Reviews Cancer*, 12 (8):527–539, 2012.

[11] Sophie Dumont and Timothy J Mitchison. Force and length in the mitotic spindle. *Current Biology*, 19(17):R749–R761, 2009.

[12] Nicole M Mahoney, Gohta Goshima, Adam D Douglass, and Ronald D Vale. Making microtubules and mitotic spindles in cells without functional centrosomes. *Current Biology*, 16(6):564–569, 2006.

[13] Jody Rosenblatt. Spindle assembly: asters part their separate ways. *Nature cell biology*, 7(3):219–222, 2005.

[14] Sylvain Meunier and Isabelle Vernos. Microtubule assembly during mitosis–from distinct origins to distinct functions? *Journal of cell science*, 125(12):2805–2814, 2012.

[15] Oliver J Gruss, Rafael E Carazo-Salas, Christoph A Schatz, Giulia Guarguaglini, Jürgen Kast, Matthias Wilm, Nathalie Le Bot, Isabelle Vernos, Eric Karsenti, and Iain W Mattaj. Ran induces spindle assembly by reversing the inhibitory effect of importin α on tpx2 activity. *Cell*, 104(1):83–93, 2001.

[16] Thomas A Kufer, Herman HW Silljé, Roman Körner, Oliver J Gruss, Patrick Meraldi, and Erich A Nigg. Human tpx2 is required for targeting aurora-a kinase to the spindle. *The Journal of cell biology*, 158(4):617–623, 2002.

[17] Nan Ma, Janel Titus, Alyssa Gable, Jennifer L Ross, and Patricia Wadsworth. Tpx2 regulates the localization and activity of eg5 in the mammalian mitotic spindle. *The Journal of cell biology*, 195(1):87–98, 2011.

[18] Torsten Wittmann, Haralabia Boleti, Claude Antony, Eric Karsenti, and Isabelle Vernos. Localization of the kinesin-like protein xklp2 to spindle poles requires a leucine zipper, a microtubule-associated protein, and dynein. *The Journal of cell biology*, 143 (3):673–685, 1998.

[19] Marvin E Tanenbaum, Libor Macůrek, Aniek Janssen, Erica F Geers, Mónica Alvarez-Fernández, and René H Medema. Kif15 cooperates with eg5 to promote bipolar spindle assembly. *Curr Biol*, 19(20):1703–11, Nov 2009. doi: 10.1016/j.cub.2009.08.027.

[20] Sachin Kotak, Coralie Busso, and Pierre Gönczy. Cortical dynein is critical for proper spindle positioning in human cells. *The Journal of cell biology*, 199(1):97–110, 2012.

[21] Roy GHP van Heesbeen, Marvin E Tanenbaum, and René H Medema. Balanced activity of three mitotic motors is required for bipolar spindle assembly and chromosome segregation. *Cell reports*, 8(4):948–956, 2014.

[22] Nan Ma, US Tulu, Nick P Ferenz, Carey Fagerstrom, Andrew Wilde, and Patricia Wadsworth. Poleward transport of tpx2 in the mammalian mitotic spindle requires dynein, eg5, and microtubule flux. *Molecular biology of the cell*, 21(6):979–988, 2010.

[23] James Bancroft, Philip Auckland, Catarina P Samora, and Andrew D McAinsh. Chromosome congression is promoted by cenp-q-and cenp-e-dependent pathways. *Journal of cell science*, 128(1):171–184, 2015.

[24] Lukas C Kapitein, Erwin JG Peterman, Benjamin H Kwok, Jeffrey H Kim, Tarun M Kapoor, and Christoph F Schmidt. The bipolar mitotic kinesin eg5 moves on both microtubules that it crosslinks. *Nature*, 435(7038):114–118, 2005.

[25] Susan L Kline-Smith, Alexey Khodjakov, Polla Hergert, and Claire E Walczak. Depletion of centromeric mcak leads to chromosome congression and segregation defects due to improper kinetochore attachments. *Molecular biology of the cell*, 15(3):1146–1159, 2004.

[26] Gernot Neumayer, Camille Belzil, Oliver J Gruss, and Minh Dang Nguyen. Tpx2: of spindle assembly, dna damage response, and cancer. *Cellular and Molecular Life Sciences*, 71(16):3027–3047, 2014.

[27] DG Cole, SW Chinn, KP Wedaman, K Hall, T Vuong, and JM Scholey. Novel heterotrimeric kinesin-related protein purified from sea urchin eggs. *Nature*, 366(6452): 268–270, 1993.

[28] Dawen Cai, Adam D Hoppe, Joel A Swanson, and Kristen J Verhey. Kinesin-1 structural organization and conformational changes revealed by fret stoichiometry in live cells. *The Journal of cell biology*, 176(1):51–63, 2007.

[29] Yumi Kim, John E Heuser, Clare M Waterman, and Don W Cleveland. Cenp-e combines a slow, processive motor and a flexible coiled coil to produce an essential motile kinetochore tether. *The Journal of cell biology*, 181(3):411–419, 2008.

[30] GKT Chan, BT Schaar, and TJ Yen. Characterization of the kinetochore binding domain of cenp-e reveals interactions with the kinetochore proteins cenp-f and hbubr1. *The Journal of cell biology*, 143(1):49–63, 1998.

[31] Julien Espeut, Amaury Gaussen, Peter Bieling, Violeta Morin, Susana Prieto, Didier Fesquet, Thomas Surrey, and Ariane Abrieu. Phosphorylation relieves autoinhibition of the kinetochore motor cenp-e. *Molecular cell*, 29(5):637–643, 2008.

[32] Joshua S Weinger, Minhua Qiu, Ge Yang, and Tarun M Kapoor. A nonmotor microtubule binding site in kinesin-5 is required for filament crosslinking and sliding. *Current Biology*, 21(2):154–160, 2011.

[33] Emma G Sturgill, Dibyendu Kumar Das, Yoshimasa Takizawa, Yongdae Shin, Scott E Collier, Melanie D Ohi, Wonmuk Hwang, Matthew J Lang, and Ryoma Ohi. Kinesin-12 kif15 targets kinetochore fibers through an intrinsic two-step mechanism. *Curr Biol*, 24(19):2307–13, Oct 2014. doi: 10.1016/j.cub.2014.08.022.

[34] Hauke Drechsler, Toni McHugh, Martin R Singleton, Nicholas J Carter, and Andrew D McAinsh. The kinesin-12 kif15 is a processive track-switching tetramer. *Elife*, 3: e01724, 2014.

[35] David Vanneste, Masatoshi Takagi, Naoko Imamoto, and Isabelle Vernos. The role of hklp2 in the stabilization and maintenance of spindle bipolarity. *Current Biology*, 19 (20):1712–1717, 2009.

[36] Daniel W Buster, Douglas H Baird, Wenqian Yu, Joanna M Solowska, Muriel Chauvière, Agnieszka Mazurek, Michel Kress, and Peter W Baas. Expression of the

mitotic kinesin kif15 in postmitotic neurons: implications for neuronal migration and development. *Journal of neurocytology*, 32(1):79–96, 2003.

[37] Tadayuki Ogawa, Ryo Nitta, Yasushi Okada, and Nobutaka Hirokawa. A common mechanism for microtubule destabilizers—m type kinesins stabilize curling of the protofilament using the class-specific neck and loops. *Cell*, 116(4):591–602, 2004.

[38] Kathleen M Hertzer, Stephanie C Ems-McClung, Susan L Kline-Smith, Thomas G Lipkin, Susan P Gilbert, and Claire E Walczak. Full-length dimeric mcak is a more efficient microtubule depolymerase than minimal domain monomeric mcak. *Molecular biology of the cell*, 17(2):700–710, 2006.

[39] F Jon Kull, Elena P Sablin, Rebecca Lau, Robert J Fletterick, and Ronald D Vale. Crystal structure of the kinesin motor domain reveals a structural similarity to myosin. *Nature*, 380(6574):550, 1996.

[40] Jennifer Turner, Robert Anderson, Jun Guo, Christophe Beraud, Robert Fletterick, and Roman Sakowicz. Crystal structure of the mitotic spindle kinesin eg5 reveals a novel conformation of the neck-linker. *Journal of Biological Chemistry*, 276(27): 25496–25502, 2001.

[41] Elena P Sablin, F Jon Kull, Roger Cooke, Ronald D Vale, and Robert J Fletterick. Crystal structure of the motor domain of the kinesin-related motor ncd. *Nature*, 380 (6574):555–559, 1996.

[42] Marta Klejnot, Aditi Falnikar, Venkatasubramanian Ulaganathan, Robert A Cross, Peter W Baas, and Frank Kozielski. The crystal structure and biochemical characterization of kif15: a bifunctional molecular motor involved in bipolar spindle formation and neuronal development. *Acta Crystallographica Section D: Biological Crystallography*, 70(1):123–133, 2013.

[43] F Jon Kull, Ronald D Vale, and Robert J Fletterick. The case for a common ancestor: kinesin and myosin motor proteins and g proteins. *Journal of Muscle Research & Cell Motility*, 19(8):877–886, 1998.

[44] Masahide Kikkawa, Elena P Sablin, Yasushi Okada, Hiroaki Yajima, Robert J Fletterick, and Nobutaka Hirokawa. Switch-based mechanism of kinesin motors. *Nature*, 411(6836):439–445, 2001.

[45] Zhiguo Shang, Kaifeng Zhou, Chen Xu, Roseann Csencsits, Jared C Cochran, and Charles V Sindelar. High-resolution structures of kinesin on microtubules provide a basis for nucleotide-gated force-generation. *Elife*, 3:e04686, 2014.

[46] Megan T Valentine, Polly M Fordyce, Troy C Krzysiak, Susan P Gilbert, and Steven M Block. Individual dimers of the mitotic kinesin motor eg5 step processively and support substantial loads in vitro. *Nature cell biology*, 8(5):470–476, 2006.

[47] Adeline Goulet, William M Behnke-Parks, Charles V Sindelar, Jennifer Major, Steven S Rosenfeld, and Carolyn A Moores. The structural basis of force generation by the mitotic motor kinesin-5. *Journal of Biological Chemistry*, 287(53):44654–44666, 2012.

[48] Jared C Cochran, Joseph E Gatial, Tarun M Kapoor, and Susan P Gilbert. Monastrol inhibition of the mitotic kinesin eg5. *Journal of Biological Chemistry*, 280(13):12658–12667, 2005.

[49] Sarah Rice, Abel W Lin, Daniel Safer, Cynthia L Hart, Nariman Naber, Bridget O Carragher, Shane M Cain, Elena Pechatnikova, Elizabeth M Wilson-Kubalek, Michael Whittaker, et al. A structural change in the kinesin motor protein that drives motility. *Nature*, 402(6763):778–784, 1999.

[50] Nicholas R Guydosh and Steven M Block. Backsteps induced by nucleotide analogs suggest the front head of kinesin is gated by strain. *Proceedings of the National Academy of Sciences*, 103(21):8054–8059, 2006.

[51] Wonmuk Hwang, Matthew J Lang, and Martin Karplus. Force generation in kinesin hinges on cover-neck bundle formation. *Structure*, 16(1):62–71, 2008.

[52] Ahmad S Khalil, David C Appleyard, Anna K Labno, Adrien Georges, Martin Karplus, Angela M Belcher, Wonmuk Hwang, and Matthew J Lang. Kinesin's cover-

neck bundle folds forward to generate force. *Proceedings of the National Academy of Sciences*, 105(49):19247–19252, 2008.

[53] Ahmet Yildiz, Michio Tomishige, Ronald D Vale, and Paul R Selvin. Kinesin walks hand-over-hand. *Science*, 303(5658):676–678, 2004.

[54] Karel Svoboda and Steven M Block. Force and velocity measured for single kinesin molecules. *Cell*, 77(5):773–784, 1994.

[55] N. J. Carter and R. A. Cross. Mechanics of the kinesin step. *Nature*, 435(7040): 308–312, 05 2005. URL `http://dx.doi.org/10.1038/nature03528`.

[56] Steven M Block, Charles L Asbury, Joshua W Shaevitz, and Matthew J Lang. Probing the kinesin reaction cycle with a 2d optical force clamp. *Proceedings of the National Academy of Sciences*, 100(5):2351–2356, 2003.

[57] S Rice, Y Cui, C Sindelar, N Naber, M Matuska, R Vale, and R Cooke. Thermodynamic properties of the kinesin neck-region docking to the catalytic core. *Biophysical journal*, 84(3):1844–1854, 2003.

[58] Steven M Block. Kinesin motor mechanics: binding, stepping, tracking, gating, and limping. *Biophysical journal*, 92(9):2986–2995, 2007.

[59] Mark J Schnitzer and Steven M Block. Kinesin hydrolyses one atp per 8-nm step. *Nature*, 388(6640):386–390, 1997.

[60] Teppei Mori, Ronald D Vale, and Michio Tomishige. How kinesin waits between steps. *Nature*, 450(7168), 2007.

[61] Sotaro Uemura, Kenji Kawaguchi, Junichiro Yajima, Masaki Edamatsu, Yoko Yano Toyoshima, and Shin'ichi Ishiwata. Kinesin–microtubule binding depends on both nucleotide state and loading direction. *Proceedings of the National Academy of Sciences*, 99(9):5977–5981, 2002.

[62] Bojan Milic, Johan OL Andreasson, William O Hancock, and Steven M Block. Kinesin processivity is gated by phosphate release. *Proceedings of the National Academy of Sciences*, 111(39):14136–14140, 2014.

[63] Geng-Yuan Chen, David FJ Arginteanu, and William O Hancock. Processivity of the kinesin-2 kif3a results from rear head gating and not front head gating. *Journal of Biological Chemistry*, 290(16):10274–10294, 2015.

[64] Lisa M Klumpp, Andreas Hoenger, and Susan P Gilbert. Kinesin's second step. *Proceedings of the National Academy of Sciences of the United States of America*, 101 (10):3444–3449, 2004.

[65] Merve Yusra Dogan, Sinan Can, Frank B Cleary, Vedud Purde, and Ahmet Yildiz. Kinesin's front head is gated by the backward orientation of its neck linker. *Cell reports*, 10(12):1967–1973, 2015.

[66] Sotaro Uemura and Shin'ichi Ishiwata. Loading direction regulates the affinity of adp for kinesin. *Nature Structural and Molecular Biology*, 10(4):308–311, 2003.

[67] Ahmet Yildiz, Michio Tomishige, Arne Gennerich, and Ronald D Vale. Intramolecular strain coordinates kinesin stepping behavior along microtubules. *Cell*, 134(6):1030–1041, 2008.

[68] Maria C Alonso, Douglas R Drummond, Susan Kain, Julia Hoeng, Linda Amos, and Robert A Cross. An atp gate controls tubulin binding by the tethered head of kinesin-1. *Science*, 316(5821):120–123, 2007.

[69] Kenji Kawaguchi, Sotaro Uemura, and Shin'ichi Ishiwata. Equilibrium and transition between single-and double-headed binding of kinesin as revealed by single-molecule mechanics. *Biophysical journal*, 84(2):1103–1113, 2003.

[70] Hung Yi Kristal Kaan, David D Hackney, and Frank Kozielski. The structure of the kinesin-1 motor-tail complex reveals the mechanism of autoinhibition. *Science*, 333 (6044):883–885, 2011.

[71] Jessica E Scholey, Stanley Nithianantham, Jonathan M Scholey, and Jawdat Al-Bassam. Structural basis for the assembly of the mitotic motor kinesin-5 into bipolar tetramers. *Elife*, 3:e02217, 2014.

[72] Sai K Balchand, Barbara J Mann, Janel Titus, Jennifer L Ross, and Patricia Wadsworth. Tpx2 inhibits eg5 by interactions with both motor and microtubule. *Journal of Biological Chemistry*, pages jbc–M114, 2015.

[73] Julie Cahu, Aurelien Olichon, Christian Hentrich, Henry Schek, Jovana Drinjakovic, Cunjie Zhang, Amanda Doherty-Kirby, Gilles Lajoie, and Thomas Surrey. Phosphorylation by cdk1 increases the binding of eg5 to microtubules in vitro and in xenopus egg extract spindles. *PLoS One*, 3(12), 2008.

[74] Marvin E Tanenbaum, Libor Macurek, Babet van der Vaart, Matilde Galli, Anna Akhmanova, and René H Medema. A complex of kif18b and mcak promotes microtubule depolymerization and is negatively regulated by aurora kinases. *Current Biology*, 21(16):1356–1365, 2011.

[75] Srinivas Honnappa, Susana Montenegro Gouveia, Anke Weisbrich, Fred F Damberger, Neel S Bhavesh, Hatim Jawhari, Ilya Grigoriev, Frederik JA van Rijssel, Ruben M Buey, Aleksandra Lawera, et al. An eb1-binding motif acts as a microtubule tip localization signal. *Cell*, 138(2):366–376, 2009.

[76] Max E Douglas and Masanori Mishima. Still entangled: assembly of the central spindle by multiple microtubule modulators. In *Seminars in cell and developmental biology*, volume 21, pages 899–908. Elsevier, 2010.

[77] Nick P Ferenz, Alyssa Gable, and Pat Wadsworth. Mitotic functions of kinesin-5. In *Seminars in cell and developmental biology*, volume 21, pages 255–259. Elsevier, 2010.

[78] David J Sharp, Gregory C Rogers, and Jonathan M Scholey. Microtubule motors in mitosis. *Nature*, 407(6800):41–47, 2000.

[79] Marvin E Tanenbaum, Libor Macurek, Liborurek, Niels Galjart, and René H Medema. Dynein, lis1 and clip-170 counteract eg5-dependent centrosome separation during bipolar spindle assembly. *The EMBO Journal*, 27(24):3235–3245, 2008.

[80] Nick P Ferenz, Raja Paul, Carey Fagerstrom, Alex Mogilner, and Patricia Wadsworth. Dynein antagonizes eg5 by crosslinking and sliding antiparallel microtubules. *Current Biology*, 19(21):1833–1838, 2009.

[81] Alexander W Bird and Anthony A Hyman. Building a spindle of the correct length in human cells requires the interaction between tpx2 and aurora a. *The Journal of cell biology*, 182(2):289–300, 2008.

[82] Emma G Sturgill and Ryoma Ohi. Kinesin-12 differentially affects spindle assembly depending on its microtubule substrate. *Curr Biol*, 23(14):1280–90, Jul 2013. doi: 10.1016/j.cub.2013.05.043.

[83] David Vanneste, Vanessa Ferreira, and Isabelle Vernos. Chromokinesins: localization-dependent functions and regulation during cell division. *Biochemical Society Transactions*, 39(5):1154, 2011.

[84] Jonne A Raaijmakers, Roy GHP van Heesbeen, Johnathan L Meaders, Erica F Geers, Belen Fernandez-Garcia, René H Medema, and Marvin E Tanenbaum. Nuclear envelope-associated dynein drives prophase centrosome separation and enables eg5-independent bipolar spindle formation. *The EMBO journal*, 31(21):4179–4190, 2012.

[85] A Sophia Gayek and Ryoma Ohi. Kinetochore-microtubule stability governs the metaphase requirement for eg5. *Molecular biology of the cell*, 25(13):2051–2060, 2014.

[86] Elina Vladimirou, Nunu Mchedlishvili, Ivana Gasic, Jonathan W Armond, Catarina P Samora, Patrick Meraldi, and Andrew D McAinsh. Nonautonomous movement of chromosomes in mitosis. *Developmental cell*, 27(1):60–71, 2013.

[87] Roy GHP van Heesbeen and René H Medema. Kif15: A useful target for anti-cancer therapy? In *Kinesins and Cancer*, pages 77–86. Springer, 2015.

[88] Mei Liu, Vidya C Nadar, Frank Kozielski, Marta Kozlowska, Wenqian Yu, and Peter W Baas. Kinesin-12, a mitotic microtubule-associated motor protein, impacts axonal growth, navigation, and branching. *J Neurosci*, 30(44):14896–906, Nov 2010. doi: 10.1523/JNEUROSCI.3739-10.2010.

[89] Shen Lin, Mei Liu, Young-Jin Son, Barry Timothy Himes, Diane M Snow, Wenqian Yu, and Peter W Baas. Inhibition of kinesin-5, a microtubule-based motor protein, as a strategy for enhancing regeneration of adult axons. *Traffic*, 12(3):269–286, 2011.

[90] Peter W Baas and Andrew J Matamoros. Inhibition of kinesin-5 improves regeneration of injured axons by a novel microtubule-based mechanism. *Neural regeneration research*, 10(6):845, 2015.

[91] Anastasia Eskova, Bettina Knapp, Dorota Matelska, Susanne Reusing, Antti Arjonen, Tautvydas Lisauskas, Rainer Pepperkok, Robert Russell, Roland Eils, Johanna Ivaska, et al. An rnai screen identifies kif15 as a novel regulator of the endocytic trafficking of integrin. *Journal of cell science*, 127(11):2433–2447, 2014.

[92] Megan T Valentine and Steven M Block. Force and premature binding of adp can regulate the processivity of individual eg5 dimers. *Biophysical journal*, 97(6):1671–1677, 2009.

[93] Mikhail J Korneev, Stefan Lakämper, and Christoph F Schmidt. Load-dependent release limits the processive stepping of the tetrameric eg5 motor. *Eur Biophys J*, 36 (6):675–81, Jul 2007. doi: 10.1007/s00249-007-0134-6.

[94] Troy C Krzysiak, Michael Grabe, and Susan P Gilbert. Getting in sync with dimeric eg5 initiation and regulation of the processive run. *Journal of Biological Chemistry*, 283(4):2078–2087, 2008.

[95] Megan T Valentine and Susan P Gilbert. To step or not to step? how biochemistry and mechanics influence processivity in kinesin and eg5. *Current opinion in cell biology*, 19(1):75–81, 2007.

[96] Miho Katsuki, Douglas R Drummond, and Robert A Cross. Ectopic a-lattice seams destabilize microtubules. *Nature communications*, 5, 2014.

[97] Marcus Braun, Douglas R Drummond, Robert A Cross, and Andrew D McAinsh. The kinesin-14 klp2 organizes microtubules into parallel bundles by an atp-dependent sorting mechanism. *Nature cell biology*, 11(6):724–730, 2009.

[98] Keir C Neuman and Steven M Block. Optical trapping. *Review of scientific instruments*, 75(9):2787–2809, 2004.

[99] Takayuki Nishizaka, Hidetake Miyata, Hiroshi Yoshikawa, Shin'ichi Ishiwata, and K Kinosita Jr. Unbinding force of a single motor molecule of muscle measured using optical tweezers. *Nature*, 377(6546):251–254, 1995.

[100] Karel Svoboda, Christoph F Schmidt, Bruce J Schnapp, Steven M Block, et al. Direct observation of kinesin stepping by optical trapping interferometry. *Nature*, 365(6448): 721–727, 1993.

[101] David D Hackney and Maryanne F Stock. Kinesin's iak tail domain inhibits initial microtubule-stimulated adp release. *Nature Cell Biology*, 2(5):257–260, 2000.

[102] Susan P Gilbert and Kenneth A Johnson. Expression, purification, and characterization of the drosophila kinesin motor domain produced in escherichia coli. *Biochemistry*, 32(17):4677–4684, 1993.

[103] William O Hancock and Jonathon Howard. Kinesin's processivity results from mechanical and chemical coordination between the atp hydrolysis cycles of the two motor domains. *Proceedings of the National Academy of Sciences*, 96(23):13147–13152, 1999.

[104] Benjamin H Kwok, Janet G Yang, and Tarun M Kapoor. The rate of bipolar spindle assembly depends on the microtubule-gliding velocity of the mitotic kinesin eg5. *Current biology*, 14(19):1783–1788, 2004.

[105] Nikita Gudimchuk, Benjamin Vitre, Yumi Kim, Anatoly Kiyatkin, Don W Cleveland, Fazly I Ataullakhanov, and Ekaterina L Grishchuk. Kinetochore kinesin cenp-e is a processive bi-directional tracker of dynamic microtubule tips. *Nature cell biology*, 15 (9):1079–1088, 2013.

[106] Lukas C Kapitein, Benjamin H Kwok, Joshua S Weinger, Christoph F Schmidt, Tarun M Kapoor, and Erwin JG Peterman. Microtubule cross-linking triggers the directional motility of kinesin-5. *The Journal of cell biology*, 182(3):421–428, 2008.

[107] Yasushi Okada and Nobutaka Hirokawa. A processive single-headed motor: kinesin superfamily protein kif1a. *Science*, 283(5405):1152–1157, 1999.

[108] Monika Isabelle Mayr, Marko Storch, Jonathon Howard, and Thomas U Mayer. A non-motor microtubule binding site is essential for the high processivity and mitotic function of kinesin-8 kif18a. *PLoS One*, 6(11), 2011.

[109] Jason Stumpff, Yaqing Du, Chauca A English, Zoltan Maliga, Michael Wagenbach, Charles L Asbury, Linda Wordeman, and Ryoma Ohi. A tethering mechanism controls the processivity and kinetochore-microtubule plus-end enrichment of the kinesin-8 kif18a. *Molecular cell*, 43(5):764–775, 2011.

[110] Megan T Valentine, Polly M Fordyce, and Steven M Block. Eg5 steps it up. *Cell Div*, 1(31):31, 2006.

[111] Harjinder S Sardar, Vincent G Luczak, Maria M Lopez, Bradford C Lister, and Susan P Gilbert. Mitotic kinesin cenp-e promotes microtubule plus-end elongation. *Current Biology*, 20(18):1648–1653, 2010.

[112] Hasan Yardimci, Marilyn Van Duffelen, Yinghui Mao, Steven S Rosenfeld, and Paul R Selvin. The mitotic kinesin cenp-e is a processive transport motor. *Proceedings of the National Academy of Sciences*, 105(16):6016–6021, 2008.

[113] Gul Civelekoglu-Scholey and Jonathan M Scholey. Mitotic motors: kinesin-5 takes a brake. *Current biology*, 17(14):R544–R547, 2007.

[114] Jennetta W Hammond, T Lynne Blasius, Virupakshi Soppina, Dawen Cai, and Kristen J Verhey. Autoinhibition of the kinesin-2 motor kif17 via dual intramolecular mechanisms. *The Journal of cell biology*, 189(6):1013–1025, 2010.

[115] Kristen J Verhey and Jennetta W Hammond. Traffic control: regulation of kinesin motors. *Nature Reviews Molecular Cell Biology*, 10(11):765–777, 2009.

[116] David Vanneste, Vanessa Ferreira, and Isabelle Vernos. Chromokinesins: localization-dependent functions and regulation during cell division. *Biochem Soc Trans*, 39(5): 1154–60, Oct 2011. doi: 10.1042/BST0391154.

[117] M-TC Crevel Isabelle, Andrew Lockhart, and Robert A Cross. Weak and strong states of kinesin and ncd. *Journal of molecular biology*, 257(1):66–76, 1996.